Comprehensive and engineering studies of the yeast branched-chain amino acid aminotransferases for improvement of fusel alcohol production

Jirasin Koonthongkaew
Nara Institute of Science and Technology
Division of Biological Sciences

Laboratory of Applied Stress Microbiology
(Prof. Hiroshi Takagi)

Submitted on 2022/08/01

TABLE OF CONTENTS

CHAPTER I: INTRODUCTION 4
1.1. Branched-chain higher alcohols (BCHAs) 4
1.1.1. The importance and industrial usage of BCHAs 5
1.1.2. Microbial production of BCHAs 7
1.2. *Saccharomyces cerevisiae* as a host for BCHA production 9
1.2.1. *S. cerevisiae* in biotechnological application 9
1.2.2. Biosynthesis of BCHAs from *S. cerevisiae* 10
1.3. Branched-chain amino acid aminotransferase (BCAT) 12
1.3.1. BCAT structure and transamination process 12
1.3.2. Mitochondrial (Bat1) and cytosolic (Bat2) isoforms of *S. cerevisiae* BCATs 15
1.3.3. Impact of BCATs on BCHA production 16
1.4. *S. cerevisiae* strain improvement and engineering to overproduce BCHAs 17
1.5. The amino acid substitutions that affect BCAT enzymatic properties or metabolite production and rational design of enzyme 18
CHAPTER II: MATERIALS AND METHODS 20
2.1. Materials 20
2.1.1 Microorganisms 20
2.1.2. Primers 22
2.1.3. Plasmids 23
2.2. Methods 25
2.2.1. Computational simulation and analysis of the Bat1 and Bat2 25
2.2.2. *In silico* engineering of Bat2 27
2.2.3. *In vivo* investigation of BCAT variants 27
2.2.4. *In vitro* investigation of BCATs and variants 31
CHAPTER III: RESULTS 34
3.1. *In silico* investigation of Bat1 and Bat2 34
3.1.1. Structure validation and overlapping analysis of Bat1 and Bat2 34
3.1.2. Pocket analysis of Bat1 and Bat2 37
3.1.3. Modalities of substrate binding with Bat1 and Bat2 41
3.2. *In vitro* investigation of Bat1 and Bat2 56
3.2.1. Construction, expression, and purification of the recombinant yeast Bat1 and Bat2 56
3.2.2. Enzymatic activity of wild-type Bat1 and Bat2 57

3.3. Engineering of BCAT to improve BCHA production 61
3.3.1. *In silico* investigation of BCAT variants 61
3.3.2. *In vivo* investigation of BCAT variants 67
3.3.3. *In vitro* investigation of BCAT variants 75
CHAPTER IV: DISCUSSION.....80
4.1. Bat1 and Bat2 shared a major primary transaminase function with minor differences 80
4.2. Proposed BCHA overproduction mechanism of BCAT variants.....81
4.3. Proposed model for reductive catalytic ability in $Bat1^{G333S}$, $Bat1^{G333W}$, and $Bat2^{G316S}$ 83
4.4. Relationship between growth defected phenotype and catalytic properties of BCAT variants 88
4.5. Argument between *in silico* and *in vitro* investigation of BCAT variants and BCHA productivity from BCAT variants 88
ACKNOWLEDGEMENTS 90
REFERENCES.....91

CHAPTER I: INTRODUCTION

1.1. Branched-chain higher alcohols (BCHAs)

Higher alcohols (also known as fusel alcohols) are alcohols that have more than two carbon atoms and a higher boiling point and molecular weight than ethanol. There are two main categories of higher alcohol: i) aliphatic higher alcohol, including propanol, isobutanol, isoamyl alcohol, and active amyl alcohol; and ii) aromatic higher alcohol, for example, phenylethyl alcohol (1). These compounds are derived from microorganisms' catabolism of amino acids and enriched after the distillation process, called fusel alcohol or fusel oil, a by-product of ethanol fermentation (2). This degradation pathway of amino acids is called the Ehrlich pathway (Fig. 1-1). Generally, amino acids will be converted into α-keto acids by a transamination reaction. Then, α-keto acid will be further converted into fusel aldehyde and fusel alcohol by the decarboxylation and reduction reaction, respectively (2, 3).

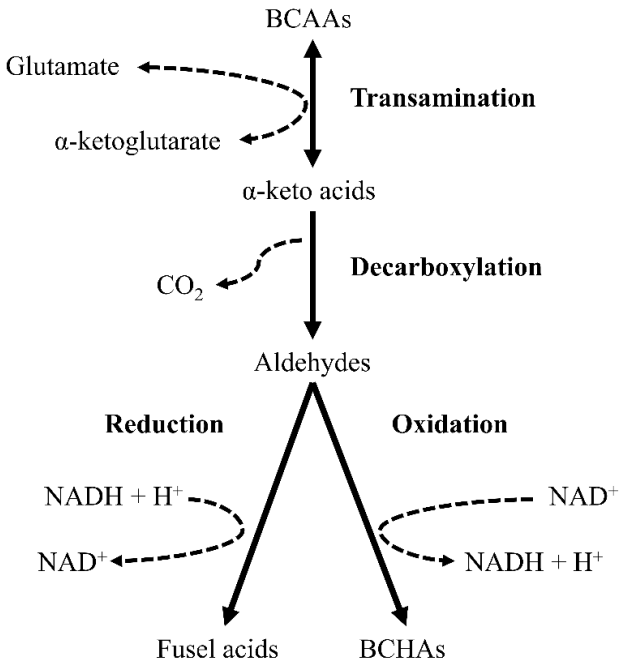

Fig. 1-1 The Ehrlich pathway of BCAAs into BCHAs. In *S. cerevisiae*, transaminase enzymes will drive the transamination reaction to convert BCAAs to the key intermediates in this pathway, α-keto acids. Afterward, α-keto acids will be decarboxylated and oxidated by decarboxylase and dehydrogenase enzymes, respectively, to BCHAs. Abbreviation: BCAAs, branched-chain amino acids; BCHAs, branched-chain higher alcohol [modified from (3)].

Branched-chain higher alcohols (BCHAs): isobutanol (IUPAC: 2-methylpropan-1-ol), isoamyl alcohol (IUPAC: 3-methylbutan-1-ol), and active amyl alcohol (IUPAC: 2-methyl-1-butanol) (Fig. 1-2A) are belonged to an aliphatic higher alcohol group in which specifically the degradation products from branched-chain amino acids (BCAAs) [valine (Val), leucine (Leu), and isoleucine (Ile) into isobutanol, isoamyl alcohol, and active amyl alcohol, respectively] (Fig. 1-2B) (4).

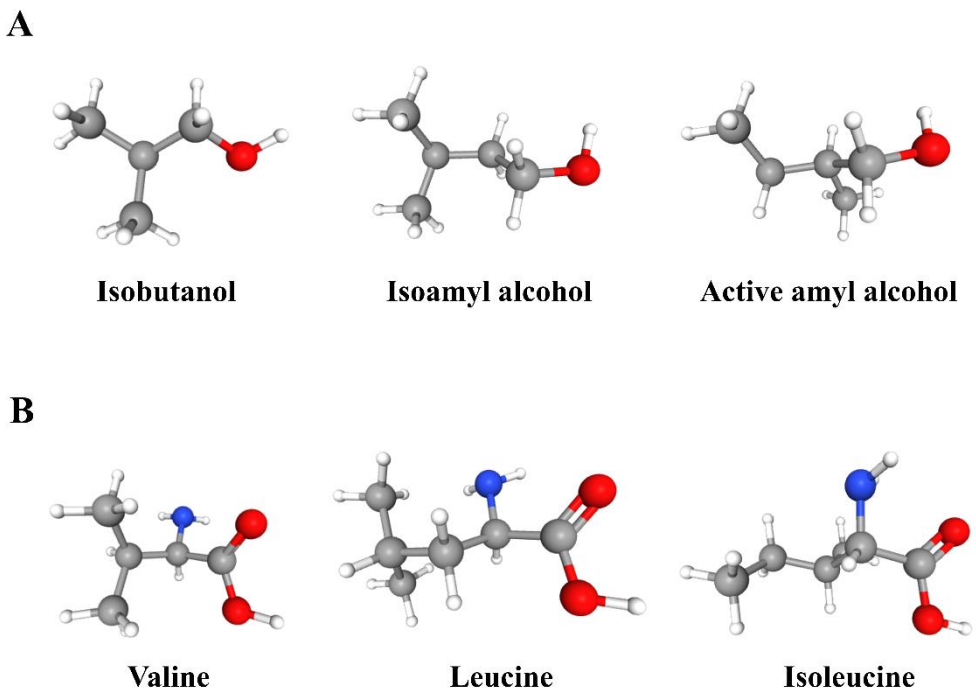

Fig. 1-2 BCHAs (A) and their corresponding BCAAs (B). All chemical structures were obtained from PubChem (5). The gray sphere represents a carbon atom; the red sphere represents an oxygen atom; the blue sphere represents a nitrogen atom; the small white sphere represents a hydrogen atom.

1.1.1. The importance and industrial usage of BCHAs

Recently, BCHAs gained broad interest for being a next-generation biofuel as an ethanol substitute since ethanol has limitations such as less energy density than gasoline (6). Besides, BCHA could be good candidates. They occupy a higher energy density and lower hygroscopicity than ethanol and higher octane numbers than straight-chain alcohol, reducing the engine knocked (7, 8) (Table 1-1). Moreover, blending BCHA with gasoline and diesel fuel can reduce the emission of harmful by-products from combustion, including CO, NO_x, and

SO_x. Therefore, BCHAs are also interested as alternative mixing compounds rather than methyl tertiary butyl ether (MTBE) (9, 10).

Table 1-1 Comparison of characteristics between ethanol and BCHAs [modified from (8)]

	Biofuel compounds			
Physical properties	**Ethanol**	**Isobutanol**	**Isoamyl alcohol**	**Active amyl alcohol**
Molecular weight	46	74	88	88
Density at 20 °C (g/cm^3)	0.794	0.802	0.809	0.805
Boiling point at 1 atm (°C)	78	108	132	132
Energy density (MJ/kg)	29.7	36.1	37.7	37.7
Net heat of combustion (BTU/gal)	80,000	95,000	NA	NA
(R + M)/2[a]	112	103.5	147	147
Blend RVP (psi at 100 °F)	18-22	5.0	NA	NA
Hygroscopicity	High	Low	Low	Low
Compatible with current infrastructure	No	Yes	Yes	Yes

[a]Average of research octane number and motor octane number

Not only as a next-generation biofuel, but BCHAs are also widely used in several industries. Isobutanol is used as the solvent and extractant for organic compounds. Also, the dehydrated isobutanol, butenes, are used as a building block for many polymers synthesis (8, 11). Isoamyl alcohol and active amyl alcohol were traditionally used as flavoring agents for beverages, especially wine, since they have the apple or banana flavor. They are also used for pharmaceutical products as intermediates and solvents (8). Moreover, BCHAs and their acetate derivatives are well known as one of the important flavor compounds in several beverages [wine, beer, Baijiu (one of the traditional Chinese beverages), Japanese sake, and awamori shochu (12–16)], fermented foods [soy sauce, fermented milk, and cheeses (17–19)], and breads (20).

1.1.2. Microbial production of BCHAs

With those benefits in several industries, the demand for BCHAs (China's market: 500,000 tons/year for isobutanol and more than 10,000 tons/year for isoamyl alcohol and active amyl alcohol) is continuously rising. However, the domestic production in China is still far from the demand (81,500 tons/year for isobutanol and around 30,000 tons/year for isoamyl alcohol and active amyl alcohol) (8). Isobutanol is traditionally produced by carbonylation of propylene by either hydroformylation or Reppe carbonylation (8). Meanwhile, isoamyl alcohol and active amyl alcohol are produced from chlorination and hydrolysis of pentane, respectively, or oxo-process (21). Those traditional processes are petrochemical pathways and are primarily concerned with the environment due to the generation of pollution, and the processes are unsustainable (8).

Therefore, microbial production of BCHAs is attractive to be an alternative to BCHA production due to the more environmental affable, higher efficiency, and lower energy consumption than the traditional petrochemical processes (6, 22). Microorganisms like eukaryote, including the yeast *Saccharomyces cerevisiae* or some group of lactic acid bacteria, can naturally produce BCHAs during fermentation from the Ehrlich pathway of BCAAs (as mentioned in the above section, see also Fig. 1-1). Considering BCHA biosynthesis, the branched-chain α-keto acids (BCKAs) [α-ketoisovalerate (KIV), α-ketoisocaproate (KIC), and α-keto-β-methylvalerate (KMV) from Val, Leu, and Ile, respectively] will be decarboxylated to aldehydes (isovaleraldehyde, isoamylaldehyde, and methylvaleraldehyde from KIV, KIC, and KMV, respectively) and dehydrogenated to BCHAs (isobutanol, isoamyl alcohol, and active amyl alcohol from isovaleraldehyde, isoamylaldehyde, and methylvaleraldehyde, respectively) by α-keto acid decarboxylases (KDCs) and alcohol dehydrogenases (ADHs) (Fig 1-3).

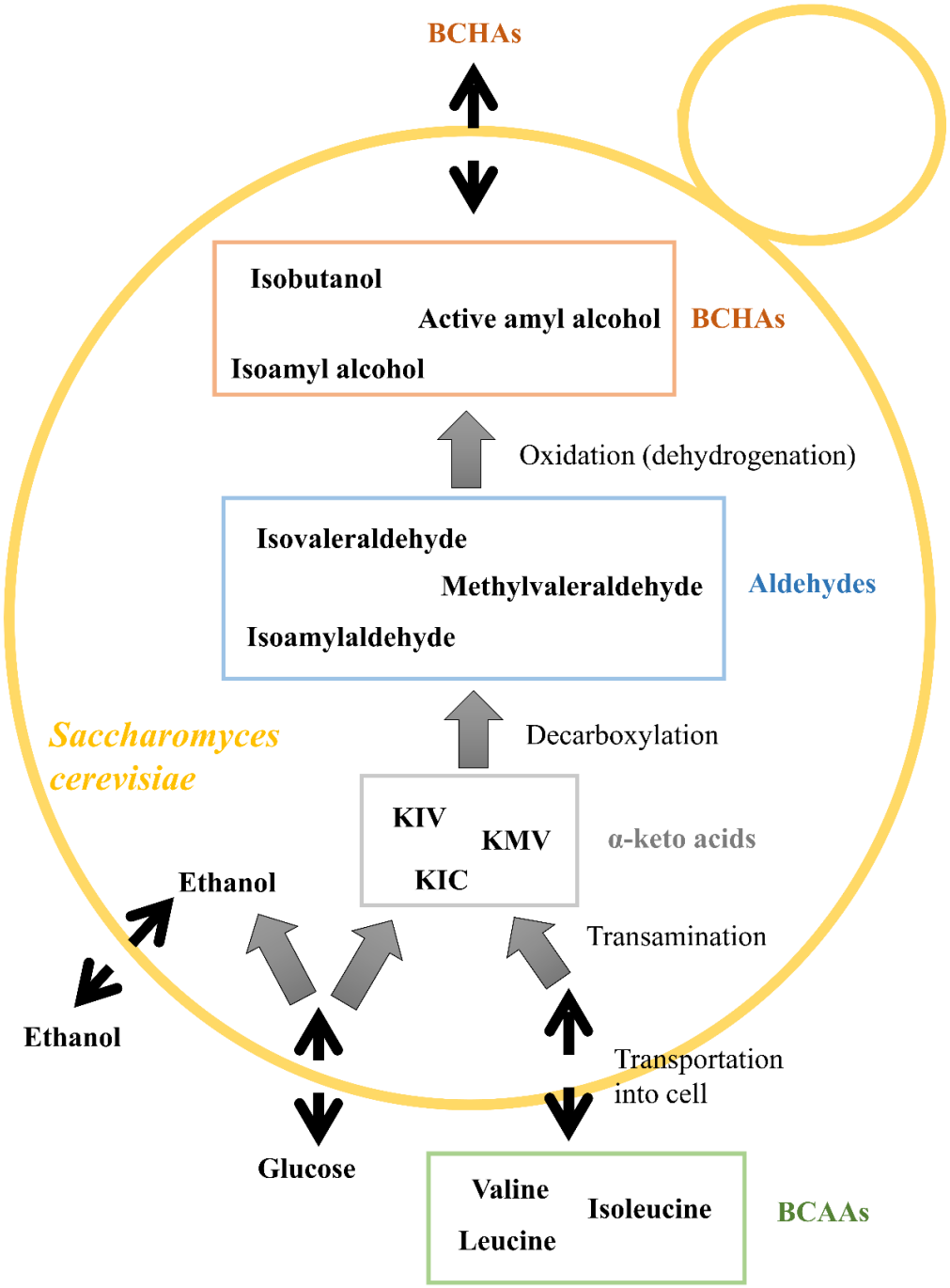

Fig. 1-3 Biosynthesis of BCHAs in *S. cerevisiae*. α-Keto acids, for further conversion to BCHAs, were obtained either from degradation (transamination) of BCAAs or glucose via pyruvate. Carbons from glucose can be converted into pyruvate and α-keto acids, respectively. Alternatively, it can be converted into ethanol and secreted outside the cells. The black-dashed arrows represent transportation into/outside the cells; the gray arrows represent chemical reactions driven by the specific enzymes (not shown). Abbreviations: KIV, α-ketoisovalerate; KIC, α-ketoisocaproate; α-keto-β-methylvalerate, KMV [modified from (16)].

Firstly, the typically industrial-used bacteria, *Escherichia coli* or *Corynebacterium glutamicum*, were engineered to produce BCHAs since they can grow faster than *S. cerevisiae*, and they are facultative anaerobes (6). These bacteria lack KDC for the conversion of α-keto acids into aldehydes. Thus, the common strategy is introducing KDC from other microorganisms, mainly from *Lactococcus lactis*, together with ADH from *S. cerevisiae*, *C. glutamicum*, *E. coli*, or *L. lactis* (6, 23–25). However, the main problem of using bacteria as a host for BCHA production still relies on the toxicity of the products, especially isobutanol, to the host cells (23), which impacts industrial application.

Alternatively, *S. cerevisiae* gains much interest in BCHAs production since it can tolerate up to 20 g/L of isobutanol and can naturally produce a small amount of these compounds during fermentation (3, 26, 27). In *S. cerevisiae*, BCHAs are synthesized from the metabolic pathway of the BCAAs: Val, Leu, and Ile. Practically, there are two primary substrates to produce BCHAs: i) glucose (biosynthesis pathway of BCAAs) and ii) BCAAs (degradation pathway of BCAAs). These two pathways share the same key intermediates, α-keto acids (Fig 1-3).

1.2. *Saccharomyces cerevisiae* as a host for BCHA production

1.2.1. *S. cerevisiae* in biotechnological application

S. cerevisiae, a unicellular fungus, is taxonomy categorized in superkingdom Eukaryota; clade Opisthokonta; kingdom Fungi; subkingdom Dikarya; phylum Ascomycota; clade Saccharomyceta; subphylum Saccharomycotina; class Saccharomycetes; order Saccharomycetales; family Saccharomycetaceae; genus *Saccharomyces* (28). Traditionally, *S. cerevisiae* is also known as a brewer's yeast (since it is widely used for brewing) or a baker's yeast (according to the application for baking bread or other bakery products). It is also known as the budding yeast (because it reproduces by budding) (29, 30). According to many prospects compared to other eukaryotic models, including as single-cell microorganism with a short generation time makes it easy to culture and can control environmental parameters by using defined media for cultured; entire genome sequence was studied; an easy genetic manipulation along with many genetic manipulation protocols were published; many biological processes and structures are conserved among to mammals, make *S. cerevisiae* as a suitable organism for fundamental researches (29, 31, 32).

Unlike the other model organisms, *S. cerevisiae* is also commonly used in industrial and biotechnological applications, such as beverages and food industries (wine, beer, cider, whiskey, sake, bread, sourdough, and cocoa), because it holds the Generally Recognized as Safe (GRAS) status for consumption (33). Importantly, *S. cerevisiae* is a positive crabtree

effect yeast in which the majority of carbon in the cells is utilized into ethanol rather than biomass, even under aerobic conditions (34). Since ethanol is toxic to other competitive microorganisms, this feature gives them an ecological niche over the competitive microorganisms. Moreover, *S. cerevisiae* can consume their produced ethanol to boost its growth after eliminating the competitors (35). Beyond that, *S. cerevisiae* has been used in biofuel production, especially bioethanol owing to its high productivity and high ethanol tolerance (36). They also tolerate harsh industrial conditions and various stresses during fermentation (37). These valuable features also benefit BCHA production and make *S. cerevisiae* an interest as an alternative microorganism for producing BCHAs rather than bacteria (38).

1.2.2. Biosynthesis of BCHAs from *S. cerevisiae*

The biosynthesis of BCAAs mainly occurs in mitochondria. Val and Ile are synthesized from the parallel reaction, starting from two molecules of pyruvate (for Val) or one pyruvate and one α-ketobutyrate, which is synthesized from threonine (Thr) by threonine dehydratase (TD; encoded by the *ILV1* gene), (for Ile). The sequential reactions [catalyzed by acetolactate synthase (AHAS; encoded by the *ILV2* and *ILV6* genes), ketoacid reductoisomerase (KARI; encoded by the *ILV5* gene), and dihydroxyacid dehydratase (DHAD; encoded by the *ILV3* gene), respectively] will occur and convert two pyruvates (for Val)/ one pyruvate and one α-ketobutyrate (for Ile) into the key intermediates, branched-chain α-keto acids (BCKAs): KIV and KMV for Val and Ile, respectively (39). For Leu biosynthesis, KIV undergoes the alternative reaction sequences [catalyzed by α-isopropylmalate synthase (IPMS; mainly encoded by the *LEU4* gene), isopropylmalate isomerase (IPMI, encoded by the *LEU1* gene), and isopropylmalate dehydrogenase (IPMD; encoded by the *LEU2* gene), respectively] together with transportation out of mitochondria into α-ketoisocaproate (KIC) (40). These BCKAs are finally transaminated into BCAAs: Val, Leu, and Ile from KIV, KIC, and KMV, respectively, by branched-chain amino acid aminotransferases (BCATs; encoded by the *BAT1* and *BAT2* genes) (41) (Fig. 1-4).

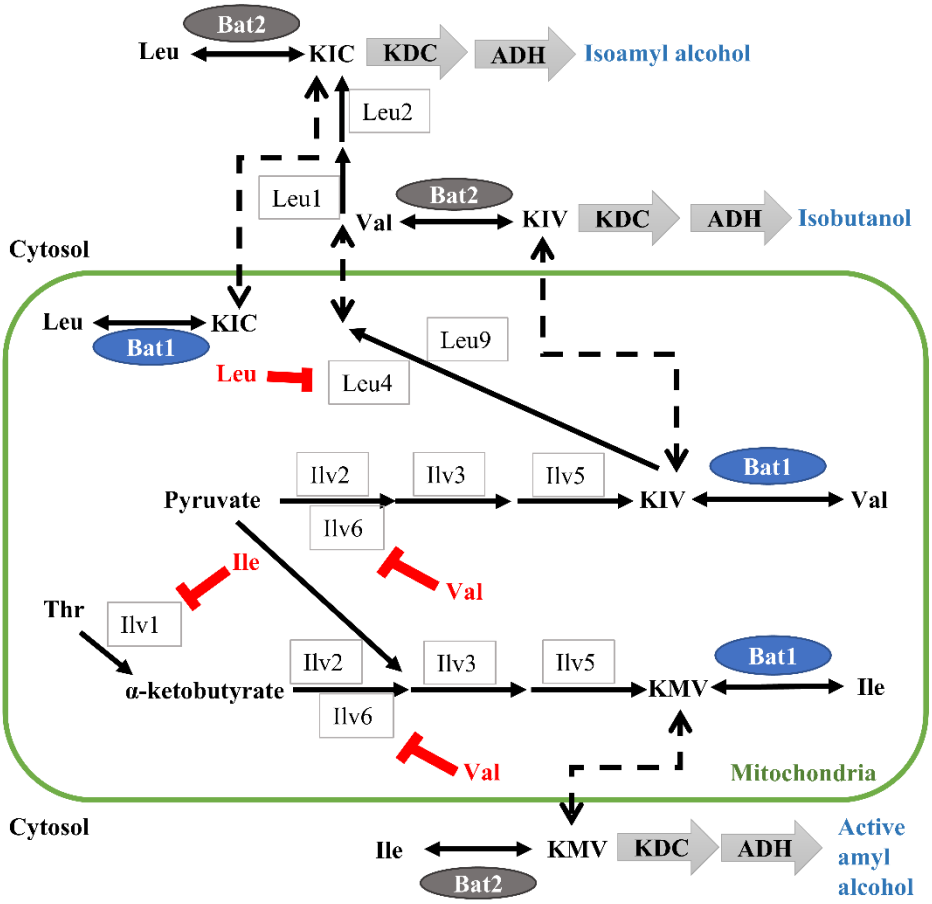

Fig. 1-4 Schematic of BCAA metabolism in *S. cerevisiae*. α-Keto acids, α-ketoisovalerate (KIV), and α-keto-β-methylvalerate (KMV) for valine (Val) and isoleucine (Ile) biosynthesis, respectively, are mainly synthesized in mitochondria from two pyruvates (for KIV) or one pyruvate and α-ketobutyrate (for KMV). On the other hand, α-ketoisocaproate (KIC) for leucine (Leu) biosynthesis is synthesized further from KIV by the reaction occurring in mitochondria and cytosol. The enzymes that participated in synthesizing α-keto acids are shown as the grey-rectangle boxes. Finally, branched-chain amino acid aminotransferases of *S. cerevisiae* (scBCATs): mitochondrial (Bat1) and cytosolic (Bat2) isoforms catalyze transamination from α-keto acids to BCAAs (KIV to Val, KIC to Leu, and KMV to Ile, respectively). Meanwhile, Bat1 and Bat2 can convert BCAAs to α-keto acids to degrade BCAAs. The downstream reactions occurred in the cytosol, for utilizing α-keto acids into branched-chain higher alcohols (BCHAs) are catalyzed by α-keto acid decarboxylases (KDCs) and alcohol dehydrogenases (ADHs); isobutanol from Val (KIV), isoamyl alcohol from Leu (KIC), and active amyl alcohol from Ile (KMV), respectively. Val, Leu, and Ile can feedback-inhibited biosynthetic enzymes (shown as red-marks): Val inhibits Ilv6, Ile inhibits Ilv2, and Leu inhibits Leu4 and Leu9, respectively [modified from (42)].

This BCAA biosynthesis pathway is strictly regulated. The regulatory mechanisms reported are 1) feedback inhibition mechanism from BCAAs. AHAS, which is one of the rate-limiting enzymes, is subject to feedback inhibition by Val; IPMS, another key enzyme for Leu biosynthesis, is also sensitive to feedback inhibition by Leu (39, 40); TD, which is the first-step enzyme for Ile biosynthesis, is subject to feedback inhibition by Ile (Fig. 1-4) (43). 2) Regulation by the transcription factor Gcn4 (as a general amino acid control)], which regulates the *ILV1*, *ILV2*, *ILV3*, *ILV6*, *LEU1*, *LEU4*, *BAT1*, *BAT2*, and *LEU3* genes (44–46).

In contrast, degradation of BCAAs mainly occurs in the cytosol via the Ehrlich pathway of BCAAs (3). In practice, BCAAs can be converted back into BCKAs by BCATs (mainly Bat2, which is a cytosolic isoform in *S. cerevisiae*). BCKAs are further converted by α-keto acid decarboxylases (KDCs) and alcohol dehydrogenases (ADHs) into BCHAs: isobutanol, isoamyl alcohol, and active amyl alcohol from Val, Leu, and Ile, respectively (see also, Fig. 1-3). This pathway is complicated and has many genes involved in the decarboxylation and oxidation step. *S. cerevisiae* has at least four decarboxylases (encoded by *ARO1*, *PDC1*, *PDC5*, and *PDC6*) and 16 dehydrogenases (encoded by *ADH1*, *ADH2*, *ADH3*, *ADH4*, *ADH5*, *ADH6*, *SFA1*, *AAD3*, *AAD4*, *AAD6*, *AAD10*, *AAD14*, *AAD15*, *AAD16*, *YCR105W*, and *YPL088W*) involved in these steps (3). Although no concrete conclusions were reported about the physiological function of this Ehrlich pathway of BCAAs to produce BCHAs, many studies provided an interesting hypothesis. Since two last steps of this pathway are oxidation/reduction, Van Dijken and Scheffers hypothesized that the production of BCHAs helps to maintain redox balance and $NADH/NAD^+$ ratio in yeast cells (47); however, Boulton et al. admitted that yeast cells could produce acetaldehyde in a sufficient amount to achieve this role (48). Another hypothesis relied on an alternative nitrogen source, obtained from the degradation of the BCAAs, for yeast cells while the nitrogen pool in the cells is depleted (49). Alternatively, Ribéreau-Gayon et al. hypothesized that detoxifying intracellular α-keto acids and aldehydes toward the production of BCHAs and amino acid metabolism (50).

1.3. Branched-chain amino acid aminotransferase (BCAT)

1.3.1. BCAT structure and transamination process

The transamination step (the first step) of the Ehrlich pathway was reported to be a rate-limiting step for this pathway (51, 52). The transaminase proteins catalyze this transamination reaction, specifically branched-chain amino acid aminotransferases [or transaminases (BCATs)] (3). In *S. cerevisiae*, there are two isoforms of BCAT: mitochondria BCAT [mBCAT (Bat1); encoded by the *BAT1* gene] and cytosolic BCAT [cBCAT (Bat2); encoded by the *BAT2* gene]. These two isozymes drive the bi-directional transamination reaction between the

corresponding BCKAs and BCAAs: KIV/Val, KIC/Leu, and KMV/Ile, respectively; together with the co-substrates [glutamate (Glu) and α-ketoglutarate (KG)] which acts as the amino group donor and acceptor for Glu and KG, respectively. BCAT was grouped as one of the pyridoxal 5'-phosphate (PLP)-dependent aminotransferase enzymes and belonged to the fold-type IV aminotransferase (D-amino acid aminotransferase family) (53, 54). BCATs of *S. cerevisiae* (scBCATs) have an active dimer form similar to hBCAT (55, 56). However, the primary structural feature of BCATs is conserved among the BCAT family (57).

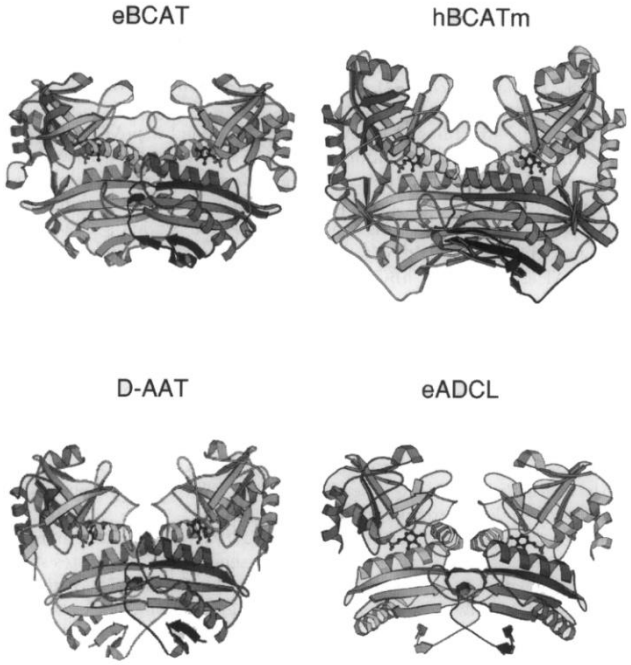

Fig. 1-5 Ribbon representative structures of PLP-dependent fold-type IV proteins. All structures were represented as a dimer. The cofactor PLP is also incorporated in the active site. Abbreviations: eBCAT, *Escherichia coli* BCAT; hBCATm, human BCAT mitochondrial isoform; D-AAT, D-amino acid aminotransferase; eADCL, *E. coli* 4-amino-4-deoxychorismate lyase [orginally from (57)].

Importantly, BCAT requires PLP, as a cofactor, for full function and the binding of PLP induces BCAT's conformational change, allowing substrate binding to the active site (58). PLP is a small organic derivative molecule of vitamin B_6 that plays an important role as a coenzyme for all transamination processes (Fig. 1-6A) (59). In the case of BCATs, PLP was reported to form a Schiff-base linkage with the conserved lysine (Lys) residue (Lys219 and Lys202for Bat1 and Bat2, respectively) in BCATs' active sites (58). During the transamination process, the amino group from amino acids is transferred to PLP, forming pyridoxamine phosphate (PMP) (Fig. 1-6B).

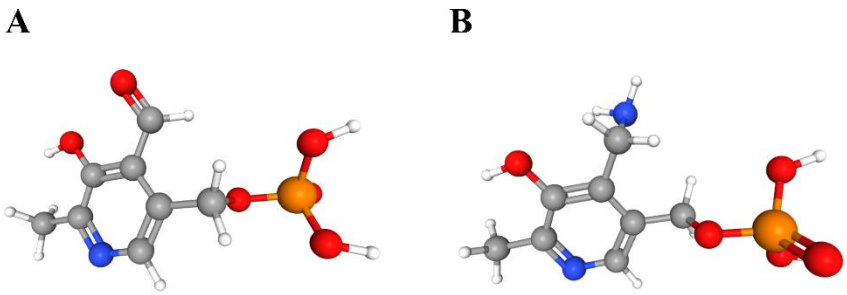

Fig. 1-6 pyridoxal 5'-phosphate (PLP) (A) and pyridoxamine phosphate (PMP) (B). PLP and PMP structures were obtained from PubChem (5). The gray sphere represents a carbon atom; the red sphere represents an oxygen atom; the blue sphere represents a nitrogen atom; the orange sphere represents a phosphorus atom; the small white sphere represents a hydrogen atom.

Hence, the transamination process in BCAT occurs in two steps (or two half-reactions) (Fig. 1-7): 1) Transferring amino group from amino acids [Glu and BCAAs for biosynthesis (Fig. 1-7A) and degradation of BCAAs, respectively (Fig. 1-7B)] to PLP in which leads to PMP formation and 2) Transferring amino group to BCKAs or KG for biosynthesis (Fig. 1-7A) or degradation of BCAAs, respectively (Fig. 1-7B) (60).

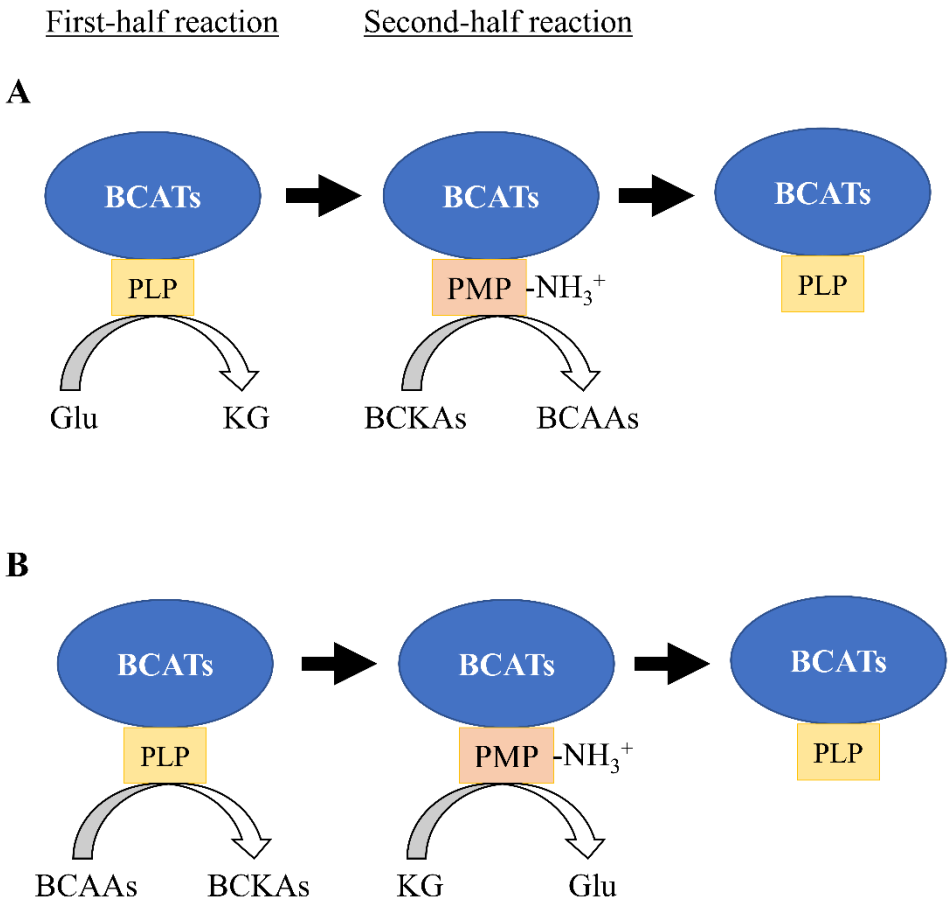

Fig. 1-7 Transamination mechanism occurred in branched-chain amino acid aminotransferase (BCAT). Reactions occur in two-half reactions: 1) first-half, transferring amino group from amino group donors (Glu or BCAAs) to PLP, and 2) second-half, transferring amino group from PMP to amino group receptors (BCKAs or KG). BCAA biosynthesis (A) starts from Glu donates amino group, and BCKAs (KIV, KIC, or KMV) receive amino group. Otherwise, BCAA degradation (B) begins from BCAAs (Val, Leu, or Ile) donate amino group, and KG receives its. Abbreviations: Glu, glutamate; KG, α-ketoglutarate; BCKAs, branched-chain α-keto acids, BCAAs, branched-chain amino acids; KIV, α-ketoisovalerate; KIC, α-ketoisocaproate; KMV, α-keto-β-methylvalerate; Val, valine; Leu, leucine; Ile, isoleucine; PLP, pyridoxal 5'-phosphate; PMP, pyridoxamine phosphate.

1.3.2. Mitochondrial (Bat1) and cytosolic (Bat2) isoforms of *S. cerevisiae* BCATs

The transamination step is involved in both degradations of BCAAs to BCHAs (as a first step) and biosynthesis of BCAAs (as the last step). Therefore, BCATs (Bat1 and Bat2 of *S. cerevisiae*) are one of the key enzymes in the BCAA metabolic pathway, which participates

in both anabolic and catabolic pathways (41, 56, 61). Bat1 (393 amino acid residues, molecular mass 43.6 kDa) and Bat2 (376 amino acid residues, molecular mass 41.6 kDa) proteins have 77% identity in the amino acid sequences. The difference in molecular mass came from the mitochondrial-targeting signal (MTS, amino acid residues 1-17 of Bat1), which is attached to the N-terminus of Bat1 (41, 62). This MTS targets Bat1 in mitochondria. On the other hand, Bat2 is located in the cytosol (41, 61).

Although Bat1 and Bat2 share 77% identity in the amino acid sequences, many studies reported differences in transcriptional regulation, gene expression profile, and metabolic and physiological function between Bat1 and Bat2. Firstly, it was reported that Bat1 and Bat2 have opposite expression profiles. In practice, Bat1 is highly expressed during the logarithmic growth phase and down-regulated during the stationary phase; otherwise, Bat2 is repressed during the logarithmic growth phase but up-regulated during the stationary phase (61). Later, Colón et al. clarified the differences in expression patterns between Bat1 and Bat2. They also found that under respiro-fermentative conditions (yeast cells were cultivated in fermentable carbon source), the *BAT1* gene expressed higher than the *BAT2* gene in the yeast cells grown on glucose when using ammonia as a sole-nitrogen source; the *BAT2* gene was up-regulated when BCAAs presented as a sole-nitrogen source. Oppositely, under respiratory conditions (yeast cells were cultivated in non-fermentable carbons source), the *BAT2* gene was up-regulated, but an expression of the *BAT1* gene was reduced (63). This expression pattern of the *BAT1* gene (induced when BCAAs are absent with primary nitrogen source, i.e., ammonium; repressed when BCAAs are present in the media) and the *BAT2* gene (induced when BCAAs are present; repressed when primary nitrogen source, i.e., ammonium is present in the media) demonstrated the biosynthetic expression profile and catabolic expression profile, respectively for the *BAT1* and *BAT2* gene (63). González et al. implemented this finding by clarifying the difference in the transcriptional regulation system between the *BAT1* and *BAT2* genes, affecting the difference between the *BAT1* and *BAT2* genes (64). Indeed, the *BAT1* gene is activated by Leu3-α-IPM, whereas Gln3 and Gcn4 activate the *BAT2* gene to respond to the metabolic status in yeast cells (64).

Interestingly, as one of the metabolic enzymes in the cells, Bat1 and Bat2 were reported to have different metabolic roles in the cells: Bat1 prefers BCAA biosynthesis (anabolic role), but Bat2 prefers BCAA degradation (catabolic role) (62, 63, 65, 66).

1.3.3. Impact of BCATs on BCHA production

More importantly, BCATs are highly impacted BCHA production in *S. cerevisiae*. As mentioned previously, the transamination step driven by Bat1 and Bat2 is the rate-limiting step for the degradation of BCAAs. Many recent studies investigated the effect of Bat1 and Bat2,

whether deletion or overexpression of these two genes on BCHAs, especially isobutanol production (38, 51, 65, 67–70). Most of the results were in the same way that overexpression of either Bat1 or Bat2 could increase isobutanol production (51, 70). Interestingly, they reported an opposite effect of Bat1 and Bat2 deletion on isobutanol production: deletion of Bat1 showed increasing in isobutanol content, but deletion of Bat2 led to a decrease in isobutanol production (38, 51, 69). However, some studies reported contradictory results that deletion of Bat1 also decreased the isobutanol production (68). Hammer and Avalos clarified these conflict results with the finding that the medium condition, in practice, nitrogen-source (Val) in the culture medium also affected isobutanol production (65). The deletion of Bat1 and an absence of Val in the fermentation medium can highly increase isobutanol (up to around 8-folded) together with the other BCHA production, which is consistent with my previous study (65, 71).

Interestingly, Hammer and Avalos also proposed two possible pathways for isobutanol production: KIVC-dependent and ValC-dependent. They also found that in a culture medium without Val, the KIVC-dependent pathway was more productive than the ValC-dependent pathway. This pathway mainly produces isobutanol from BCKA, KIV, which is generated from glucose (65).

1.4. *S. cerevisiae* strain improvement and engineering to overproduce BCHAs

As mentioned in the previous section, scBCATs (Bat1 and Bat2) highly impact BCHA production. However, the other enzymes in the BCAA metabolic pathway also gained much interest, especially AHAS, a rate-limiting step for BCAA biosynthesis by acting as the bottleneck metabolic flux control of carbon from glucose (65, 72). AHAS is composed of two-subunit: a catalytic subunit (Ilv2) and a regulatory subunit (Ilv6) (73). Ilv2 is subject to feedback inhibition by Val (73) (see also, Fig. 1-4). The previous study from my lab also identified the feedback inhibition-insensitive Ilv6 variants. The yeast transformants carrying these Ilv6 variants also showed increased intracellular Val content (74). Additionally, using valine-insensitive Ilv6 also enhanced isobutanol production (65). To further increase the metabolic flux of carbon into the metabolism of BCAAs, the *ILV* genes (*ILV2*, *ILV3*, and *ILV5*) involved in KIV and KMV biosynthesis were overexpressed together with the deletion of the *BAT1* gene. As a result, both isobutanol and isoamyl alcohol contents were significantly increased from the parent strain (65). In the case of isoamyl alcohol, produced from the Leu metabolic pathway, KIC is the downstream intermediate of KIV. Similar to Val, Leu also feedback inhibits IPMS (the *LEU4* gene) (75) (see also, Fig. 4). Hence, to improve isoamyl alcohol production, the Leu4 insensitive variant was also used previously together with increased carbon flux by overexpression upstream biosynthetic genes of KIV (the *ILV2*, *ILV3*,

and *ILV5* genes), along with downstream biosynthetic genes of KIC from KIV (the *LEU4*, *LEU1*, and *LEU2* genes) and deletion of the *BAT1* gene (76).

Due to the separation between upstream engines for the biosynthesis of BCKAs and downstream for utilizing BCKAs into BCHAs, most BCKA biosynthetic enzymes are located in mitochondria, including Ilv2, Ilv3, and Ilv5 (for KIV and KMV) and Ilv2, Ilv5, and Leu4 (for KIC). In contrast, KDC and ADH (BCHA biosynthesis) are located in the cytosol. Hence, transportation of intermediated across mitochondria by unknown transporter is required. Even though increasing carbon flux through the BCAA biosynthetic pathway is one of the most effective pathways for the production of BCHAs, these intermediates for BCHA production still face transportation limitations (65). Many previous studies performed the compartmentalization of BCHA biosynthetic engines into mitochondria and increased carbon flux through the BCAA metabolic pathway to overcoming transportation limitations (65, 76, 77). Hammer and Avalos obtained the highest isobutanol producer using this approach (65).

1.5. The amino acid substitutions that affect enzymatic properties or metabolite production and rational design of enzyme

Several amino acid substitutions that alter enzymatic activity have been identified and studied in human BCATs since these amino acid substitutions are related to human diseases, i.e., R170Q/E264K and V182G/R341T heterogeneous amino acid substitutions in hBCATm were reported to have an impact on substrate recognition; eventually, the patients showed high concentrations of BCAAs in plasma (78, 79). Otherwise, amino acid substitution in scBCATs was not widely studied. My previous study clarified the amino substitution (Ala to Asp at position 234 of Bat1; A234D), which benefits BCHA production. However, this amino acid substitution precedes a Bat1 dysfunction (71). Hence, no functional amino acid substitutions on scBCAT that change the enzymatic activity or substrate specificity and benefit the production of BCHA have been reported.

As described above, the traditional strategies to increase the production of BCHAs in *S. cerevisiae* are overexpression of BCKA biosynthetic genes (*ILV* genes; *ILV2*, *ILV3*, and *ILV5*) along with deletion of *BAT1*; this strategy leads to an enhancement of BCKAs (the key intermediates) (65, 77). However, the transamination step of the Ehrlich pathway for BCHA biosynthesis (catalyzed by Bat1 and Bat2) is still the rate-limiting step. The previous study on hBCAT showed that hBCATs prefer to synthesize BCAAs from BCKAs rather than degrade them (BCKAs had lower in apparent K_m; higher in apparent k_{cat} and k_{cat}/K_m than BCAAs) (55). A similar trend was obtained in scBCAT while using crude extract (56). Therefore, I hypothesized that amino acid substitution on scBCATs (Bat1 and Bat2) that change/alter the

enzymatic activity, or substrate-specificity would benefit the productivity of BCHAs by increasing the availability of BCKAs.

Recently, the rational design of protein has gained much interest as one of the efficient approaches for protein engineering since it provides more specific detail of the targeted protein than the traditional method, including random mutagenesis (80). This approach is based on computational or *in silico* analysis of a protein's three-dimensional (3D) structure. Many studies applied the rational design to enhance the productivity of designed products by creating variant enzymes that improve enzymatic properties, i.e., enantioselectivity (81), thermostability (82), catalytic activity, and stability (83). A recent study from my laboratory applied molecular docking simulation to reduce the feedback inhibition effect of lysine on homocitrate synthase (HCS), resulting in the higher productivity of lysine (84). Notably, molecular docking is an extensively used computational method for analyzing the binding positions and energies between ligands and receptors (85). In the present study, I applied *in silico* computational analysis (rational design) to study substrates binding on scBCATs using molecular docking simulation. Then, I screened for the appropriate amino acid substitutions around the active site or substrate-binding site of scBCAT that are likely to change/alter their activity or catalytic preference.

Research objectives

(1) Improvement of BCHA productivity in *S. cerevisiae* by engineering the rate-limiting enzymes, Bat1 and Bat2

(2) Clarifying Bat1 and Bat2 fundamental structure and function

(3) Investigation of BCHA overproduction mechanism from Bat1 and Bat2 variants

CHAPTER II: MATERIALS AND METHODS

2.1. Materials

2.1.1 Microorganisms

Saccharomyces cerevisiae and *Escherichia coli* strains used in this study are shown in Table 2-1.

Table 2-1 Strains used in this study

Strains	Description	Sources
***S. cerevisiae* BY4741**	*MATa his3Δ1 leu2Δ0 met15Δ0 ura3Δ0*	Possessed in the laboratory
BY4741 (EV)	BY4741 harboring pRS416 and pRS415-Cg*HIS3MET15*	This work
BY4741*bat1*Δ*bat2*Δ	BY4741*Δbat1::hphNT1Δbat2::kanMX6*	Possessed in the laboratory
BY4741*bat1*Δ*bat2*Δ (Bat1)	BY4741*Δbat1::hphNT1Δbat2::kanMX6* harboring pRS416 with Bat1 and pRS415-Cg*HIS3MET15*	This work
BY4741*bat1*Δ*bat2*Δ (Bat1^{G333S})	BY4741*Δbat1::hphNT1Δbat2::kanMX6* harboring pRS416 with Bat1 (Gly333Ser) and pRS415-Cg*HIS3MET15*	This work
BY4741*bat1*Δ*bat2*Δ (Bat1^{G333W})	BY4741*Δbat1::hphNT1Δbat2::kanMX6* harboring pRS416 with Bat1 (Gly333Trp) and pRS415-Cg*HIS3MET15*	This work
BY4741*bat1*Δ*bat2*Δ (Bat2)	BY4741*Δbat1::hphNT1Δbat2::kanMX6* harboring pRS416 with Bat2 and pRS415-Cg*HIS3MET15*	This work

BY4741*bat1*Δ*bat2*Δ (Bat2^{G316S})	BY4741*Δbat1::hphNT1Δbat2::kanMX6* harboring pRS416 with Bat2 (Gly316Ser) and pRS415-Cg*HIS3MET15*	This work
BY4741*bat1*Δ*bat2*Δ (Bat2^{G316W})	BY4741*Δbat1::hphNT1Δbat2::kanMX6* harboring pRS416 with Bat2 (Gly316Trp) and pRS415-Cg*HIS3MET15*	This work
BY4741*bat1*Δ*bat2*Δ (Bat1-GFP)	BY4741*Δbat1::hphNT1Δbat2::kanMX6* harboring pRS416 with Bat1-GFP tag and pRS415	This work
BY4741*bat1*Δ*bat2*Δ (Bat2-GFP)	BY4741*Δbat1::hphNT1Δbat2::kanMX6* harboring pRS416 and pRS415 with Bat2-GFP tag	This work
BY4741*bat1*Δ*bat2*Δ (Bat1^{G333S}-GFP)	BY4741*Δbat1::hphNT1Δbat2::kanMX6* harboring pRS416 with Bat1 (Gly333Ser)-GFP tag and pRS415	This work
BY4741*bat1*Δ*bat2*Δ (Bat1^{G333W}-GFP)	BY4741*Δbat1::hphNT1Δbat2::kanMX6* harboring pRS416 with Bat1 (Gly333Trp)-GFP tag and pRS415	This work
BY4741*bat1*Δ*bat2*Δ (Bat2^{G316S}-GFP)	BY4741*Δbat1::hphNT1Δbat2::kanMX6* harboring pRS416 and pRS415 with Bat2 (Gly316Ser)-GFP tag	This work
***Escherichia coli* DH5α**	*F-, φ80dlacZΔM15, Δ(lacZYA-argF)U169, deoR, recA1, endA1, hdR17 (r_k^-, m_k^+), phoA, supE44, λ^-, thi-1, gyrA96, relA1*	Possessed in the laboratory
***E. coli* DH5α for plasmid multimerization**	*E. coli* DH5α harboring all constructed pRS416 and pRS415 plasmids	This work
***E. coli* BL21 (DE3)**	BL21 (DE3) harboring all constructed pET53 plasmids	This work

2.1.2. Primers

Primers used in this study are shown in Table 2-2.

Table 2-2 Primers used in this study (double-underlined nucleotides reveal the corresponding amino acid substitution in Bat1 and Bat2).

Primer	Sequences (5'-3')
F-*BAT1*-Si1	5'-GATCCATATTGCCTTCTTATGA-3'
R-*BAT1*-Si1	5'-AGAATATTATTTATTTGAGTTGTCC-3'
F-*BAT1*-Si2	5'-ATACTATCACCATGTTCCGTC-3'
R-*BAT1*-Si2	5'-TAAGGAAGAACGGTCACTGA-3'
F-*BAT1*-Si3	5'-AAGAAGGAATTGGTTACCG-3'
R-*BAT1*-Si3	5'-GTCTTGAGGAGTTTTATGATAGTG-3'
F-*BAT2*-Si1	5'-GATATTCGACTATTTCCTGGG-3'
R-*BAT2*-Si2	5'-GGTCGTTCTATTCACGAATCAAG-3'
F-*BAT2*-Si2	5'-GAACTAAGCACTTATCTTGCTGG-3'
R-*BAT2*-Si4	5'-GGAAACTGTAACATATATACTTAAGGACCT-3'
F-*BAT2*-Si3	5'-ACTTCACTATAGGCGAAGTTACTG-3'
R-*BAT2*-Si1	5'-ATGAAGTGATATCCGCTTCAATGAC-3'
G333S_F	5'-GCCTTCGGTTCTAGTGCTGCTGTC-3'
G333S_R	5'-GAC AGC AGC AGT ACT AGA ACC GAA GGC-3'
G333W_F	5'-GCCTTCGGTTCTTGGACTGCTGCTGTC-3'
G333W_R	5'-GACAGCAGCAGTCCAAGAACCGAAGGC-3'
G316S_F	5'- GCCTTTGGTTCTAGTACTGCTGCGATT-3'
G316S_R	5'-AATCGCAGCAGTACTAGAACCAAAGGC-3'
G316W_F	5'-GCCTTTGGTTCTTGGACTGCTGCGATT-3'
G316W_R	5'- AATCGCAGCAGTCCAAGAACCAAAGGC-3'
F-*BAT1*N16-attB1	5'-GGGGACAAGTTTGTACAAAAAAGCAGGCTTACTCGC
R-*BAT1*-attB2	TACTGGTGCCCCATT-3'
	5'-GGGGACCACTTTGTACAAGAAAGCTGGGTTGTTCAA
	GTCGGCAACAGTTT-3'

F-*BAT2*-attB1 **R-*BAT2*-attB2**	5’-GGGGACAAGTTTGTACAAAAAAGCAGGCTTAATGACCTTGGCACCCCTAGA-3’ 5’-GGGGACCACTTTGTACAAGAAAGCTGGGTTGTTCAAATCAGTAACAACCCT-3’

2.1.3. Plasmids

The plasmids used in this study are shown in Table 2-3.

Table 2-3 Plasmids used in this study

Plasmids	Description	Sources
pRS415-Cg*HIS3MET15*	yeast centromere vector pRS415-*LEU2HIS3MET15*	Possessed in the laboratory
pRS416	yeast centromere vector pRS416-*URA3*	Possessed in the laboratory
pRS416-*BAT1*	pRS416 harboring *BAT1*	Possessed in the laboratory
pRS416-*BAT1*^{G333S}	pRS416 harboring *BAT1* point mutation (Gly333Ser)	This work
pRS416-*BAT1*^{G333W}	pRS416 harboring *BAT1* point mutation (Gly333Trp)	This work
pRS416-*BAT2*	pRS416 harboring *BAT2*	Possessed in the laboratory
pRS416-*BAT2*^{G316S}	pRS416 harboring *BAT2* point mutation (Gly316Ser)	This work
pRS416-*BAT2*^{G316W}	pRS416 harboring *BAT2* point mutation (Gly316Trp)	This work
pRS416-*BAT1* with GFP tag	pRS416 harboring *BAT1* with GFP tag	This work
pRS416-*BAT1*^{G333S} with GFP tag	pRS416 harboring *BAT1* point mutation (Gly333Ser) with GFP tag	This work

pRS416-*BAT1*^{G333W} with GFP tag	pRS416 harboring *BAT1* point mutation (Gly333Trp) with GFP tag	This work
pRS415-*BAT2* with GFP tag	pRS415 harboring *BAT2* with GFP tag	This work
pRS415-*BAT2*^{G316S} with GFP tag	pRS415 harboring *BAT2* point mutation (Gly316Ser) with GFP tag	This work
pDONR221	Gateway® donor vector with attP1 and attP2 sties, *KAN*^{R}	Gateway®
pET-53-DEST	Gateway® bacterial destination vector for expressing proteins with 6X-His affinity tagged	Gateway®
pDONR221-*BAT1*	pDONR221 harboring *BAT1* without stop codon	This work
pDONR221-*BAT1ΔN16*	pDONR221 harboring *BAT1-MTS* without stop codon	This work
pDONR221-*BAT1ΔN16*^{G333S}	pDONR221 harboring *BAT1-MTS* (Gly333Ser) without stop codon	This work
pDONR221-*BAT2*	pDONR221 harboring *BAT2* without stop codon	This work
pDONR221-*BAT2*^{G316S}	pDONR221 harboring *BAT2* (Gly316Ser) without stop codon	This work
pET-53-DEST-*BAT1*	pET-53-DEST harboring *BAT1* without stop codon	This work
pET-53-DEST-*BAT1ΔN16*	pET-53-DEST harboring *BAT1-MTS* without stop codon	This work
pET-53-DEST-*BAT1ΔN16*^{G333S}	pET-53-DEST harboring *BAT1-MTS* (Gly333Ser) without stop codon	This work
pET-53-DEST-*BAT2*	pET-53-DEST harboring *BAT2* without stop codon	This work
pET-53-DEST-*BAT2*^{G316S}	pET-53-DEST harboring *BAT2* (Gly316Ser) without stop codon	This work

2.2. Methods

2.2.1. Computational simulation and analysis of the Bat1 and Bat2

2.2.1.1. Homology modeling and quality validation of the Bat1 and Bat2 homologous structures with and without PLP

Homologous structures of Bat1 and Bat2 with and without PLP were modeled as a homodimeric enzyme based on the previous study by employing the SWISS-MODEL (86). Bat1 and Bat2 without PLP (named Bat1 and Bat2, respectively) were modeled using human mitochondrial branched-chain amino acid aminotransferase (hBCATm) with the SWISS-MODEL template library (SMTL) ID: 2hdk.1 (chain A) as a template. Bat1 and Bat2 with PLP (named Bat1-PLP and Bat2-PLP, respectively) were modeled using human cytosolic branched-chain amino acid aminotransferase (hBCATc) with the SMTL ID: 2abj.1 (chain A) as a template. All the homologous structures were saved as PDB files for further simulation and analysis.

Structural qualities of Bat1, Bat2, Bat1-PLP, and Bat2-PLP were validated by the SWISS-MODEL quality estimation (QSQE, GMQE, and QMEAN) connecting with the SWISS-MODEL web-server (86) and the PROCHECK analysis (Ramachandran plots and G-factors) (87) connecting with the PDBsum database (88).

2.2.1.2. Pocket, cavity, and structural comparison analysis

The PDB files of Bat1 and Bat2 obtained from the UniProt database were used for determining the possible pockets on each homo-dimeric subunit using the CavityPlus (89) with default parameters. The amino acid residues involved in each pocket formation were also predicted from the CavityPlus. The cavities of the Bat1 and Bat2 were analyzed on the possible pockets for substrate binding using the CavityPlus. The potential pockets for substrates binding were demonstrated as the pKd value (ligandability, using KIC as a ligand). The potential pockets for ligand binding were further analyzed more precisely by the PARS web-server (90), using a normal mode analysis (NMA) approach with default parameters. The potential pockets obtained from the PARS are the pockets that can change protein flexibility while the substrate (KIC) is bound. The binding of a substrate (KIC) to each pocket was scored as a pFlex (p-value), and the ranking of pockets was based on descended of pocket size. It is noteworthy that

the PARS software is particularly used for allosteric site prediction. However, this software can apply to find the catalytic pocket (91).

The PDB files of Bat1, Bat2, Bat1-PLP, and Bat2-PLP from the SWISS-MODEL were also used for superimposition structural analysis between Bat1/Bat2, Bat1-PLP/Bat2-PLP, Bat1/Bat1-PLP, and Bat2/Bat2-PLP. The superimposition structural analysis was also analyzed by the MatchMarker tool connecting with the UCSF Chimera software (92) with the default parameters.

2.2.1.3. Molecular docking simulation

DFT-optimized structures of the BCAAs (Val, Leu, and Ile), BCKAs (KIV, KIC, and KMV), and the reaction pairwise ligands or co-substrates (KG and Glu) were obtained using the Gaussian 09 program package (93) at the B3LYP/6-311+G(d,p) level of theory (94–96). All the B3LYP/6-311+G (d, p)-optimized structures were converted to the protein data bank (PDB) format for employment in the molecular docking. The most robust binding, based on each docking simulation's binding affinity or binding energy, was considered the most stable configuration. The docking simulations were performed using the AutoDock Vina v.1.1.2 (97). Docking simulations and analyses were performed using the ADT/PMV/Viewer v.1.5.6 software (98).

2.2.1.4. Alignment of protein and interaction configurations of ligand-protein

The interaction configurations between the Bat1-PLP and Bat2-PLP proteins with all substrates were analyzed and visualized using the LigPlot+ v. 2.2 software using an academic-free license (99). Conservative scores of interactive residues in Bat1-PLP and Bat2-PLP catalytic pockets were calculated and analyzed from the ConSurf server using the ConSurf method (100). The conservative scores were calculated using specific multiple sequences alignment (MSA).

The amino acid sequences of the BCATs were obtained directly from the UniProt database with UniProtKB: BCA1_YEAST for Bat1, BCA2_YEAST for Bat2, BCAT2_HUMAN for human BCAT mitochondrial isoform (hBCATm), BCAT1_HUMAN for human BCAT cytosolic isoform (hBCATc), and ILVE_ECOLI for eBCAT. The amino acid alignment of the BCATs was performed using the Clustal Omega program (101), connecting with the UniProt database (Uniprot C). The % identity of each amino acid sequence was calculated using GENETYX ver. 15 (Genetyx Corp., Osaka, Japan).

2.2.2. *In silico* engineering of Bat2

2.2.2.1. Construction of Bat2 variant homology structures

The Bat2 variant's structures were constructed by the Rotamers tool, connecting with UCSF Chimera (92), using Dunbrack 2010 Rotamer library (102). Structural minimization of wild-type and variants Bat2 were performed in UCSF Chimera to remove atomic clashes and contacts using 1000 steepest descent steps (step size = 0.02 Å). The net charge of PLP (-2) was computed using ANTECHAMBER (103). Interatomic interaction of wild-type and variants Bat2 structures were analyzed and visualized by the Arpeggio web-server (104).

2.2.2.2. Design and *in silico* analysis of Bat2 variants

Preliminary screening of amino acid substitution to Bat2 was performed using the CUPSAT web-server (105). The mutations which affect protein stability were quantified as the change in folding free energy (ΔΔG). CUPSAT estimates ΔΔG upon mutation using mean force atom pair and torsion angle potential. The amino acid substitutions that stabilize the folding stability of protein structure were selected for further analysis. An effect of mutations on protein-small molecule affinity was further investigated by the mCSM-lig web-server (106). mCSM-lig can predict the change in binding affinity upon mutation compared to the wild-type using a graph-based signature. Hence, the amino acid substitutions to Bat2 that stabilize substrate-binding affinity were selected for the study.

2.2.3. *In vivo* investigation of BCAT variants

2.2.3.1. Strains and culture media

The yeast *S. cerevisiae* strain BY4741*bat1*Δ*bat2*Δ, constructed from the previous study (62), was used as a host strain for the construction of transformants in this study. *S. cerevisiae* strain BY4741 was also used as an original wild-type strain in this study. An *Escherichia coli* DH5α strain was used as a host for constructing and extracting plasmids. Yeast strains were cultured in a nutrient-rich YPD medium {10 g/L yeast extract [Becton, Dickinson, and Company (BD), Franklin Lakes, NJ], 20 g/L peptone (BD), and 20 g/L glucose (Nacalai

Tesque, Kyoto, Japan)} or a synthetic dextrose (SD) minimal medium [1.7 g/L yeast nitrogen base without amino acid (BD), 5 g/L ammonium sulfate (Nacalai Tesque) and 20 g/L glucose at pH 6.0]. The antibiotics, geneticin (150 μg/mL) and hygromycin B (50 μg/mL), were appropriately supplemented to maintain the gene disrupted status. SD medium supplemented with 20 mg/L of histidine and methionine (SD+His/Met) was used as a cultured medium for checking the expression of BCATs in yeast cells.

An *E. coli* DH5α strain was cultivated in Luria-Bertani (LB) complete medium [5 g/L yeast extract, 10 g/L tryptone (BD), and 10 g/L NaCl (Nacalai Tesque)]. Ampicillin (100 μg/mL) was supplemented to maintain the transformant status. For the bacterial cells harboring pDONR221, 50 μg/mL of kanamycin was added to LB media. Otherwise, the bacterial cells harboring pET53 were cultured in LB with an addition of 100 μg/mL ampicillin. In case of BCAT proteins expression in *E. coli* BL21 (DE3) cells, bacterial cells were cultured in M9 [4 g/L glucose, 246 mg/L $MgSO_4 \cdot 7H_2O$ (Nacalai Tesque), 6 g/L Na_2HPO_4 (Nacalai Tesque), 3 g/L KH_2PO_4 (Nacalai Tesque), 0.5 g/L NaCl, and 1 g/L NH_4Cl (Nacalai Tesque)] + 20 g/L casamino acid (Nacalai Tesque) (M9CA) with the supplementation of ampicillin (100 μg/mL). If necessary, all media were solidified by adding 2% agar.

2.2.3.2. Construction of the expression plasmids and transformants

BCAT proteins were expressed in *S. cerevisiae* BY4741*bat1*Δ*bat2*Δ using pRS416-*BAT1* and pRS416-*BAT2*, which were used in the previous study (62). Site-directed mutagenesis was performed using those pRS416-*BAT1* and pRS416-*BAT2* as a template. The mutagenesis primer lists (Table 2-2) were used to introduce mutation in the *BAT1* gene (from Gly333 to Ser333 and Gly333 to Trp333) and *BAT2* gene (from Gly316 to Ser316 and Gly316 to Trp316). The subsequently PCR products were cut with DpnI and transformed into *E. coli* DH5α cells (107). After obtaining PCR products and designing plasmid, the DNA sequences of the products were verified using a DNA sequencer (ABI PRISM 3130 Genetic Analyzer, Applied Biosystems, Waltham, MA). Corresponding Bat1 variants (G333S and G333W) and Bat2 variants (G316S and G316W) in pRS416-series [(pRS416-$BAT1^{G333S}$ and pRS416-$BAT1^{G333W}$) and (pRS416-$BAT2^{G316S}$ and pRS416-$BAT2^{G316W}$), respectively for Bat1 and Bat2] were co-transformed with plasmid pRS415-Cg*HIS3MET15* [used in the previous study (62)] using high-efficiency transformation method (108) to complement the auxotrophic phenotype of BY4741 strain. SD agar plates were used to select the transformant colonies for corresponding experiments. Meanwhile, pRS416-*BAT1*-GFP and pRS415-*BAT2*-GFP, which were also used in the previous study (62), were used to confirm an expression of BCATs in the yeast cells. Site-directed mutagenesis was performed using previously mentioned primers to introduce the same mutation in *BAT1* and *BAT2* genes, resulting in pRS416-$BAT1^{G333S}$-GFP, pRS416-$BAT1^{G333W}$-GFP, and pRS415-$BAT2^{G316S}$-GFP. All designed plasmids were verified

DNA sequences and transformed to BY4741 strain using the previously mentioned method. SD+His/Met agar plates were used to select the transformant colonies for further experiments.

For expression of BCATs using *E. coli* BL21 (DE3) cells, *BAT1* and *BAT1ΔN16* genes were amplified from genomic DNA of *S. cerevisiae* BY4741 using the following primers, F-*BAT1*ΔN16-attB1 and R-*BAT1*-attB2 (Table 2-2). The resultant PCR fragments of *BAT1* and *BAT1ΔN16* were introduced into the pDONR221 vector (Thermo Scientific) using BP clonase II (Thermo Scientific), resulting in pDONR221-*BAT1* and pDONR221-*BAT1ΔN16*. Site-directed mutagenesis was performed using the pDONR221-*BAT1ΔN16* as a template by using the same primers as in pRS416-*BAT1* variants construction (Table 2-2), resulting in pDONR221-*BAT1ΔN16*^{G333S} and pDONR221-*BAT1ΔN16*^{G333W}. For the construction of pDONR221-*BAT2* and pDONR221-*BAT2* variant, both *BAT2* gene and *BAT2* mutant gene were directly amplified from pRS416-*BAT2* and pRS416-*BAT2*^{G316S} using the following primers, F-*BAT2*-attB1 and R-*BAT2*-attB2 (Table 2-2). The following resultant PCR fragments of the *BAT2*-series were also introduced into the pDONR221 vector using BP clonase II, resulting in pDONR221-*BAT2* and pDONR221-*BAT2*^{G316S}. DNA sequences of *BAT1* and *BAT2* series in pDONR221 were confirmed and transferred into the pET53-DEST expression vector (Thermo Scientific) using LR clonase II (Thermo Scienctific). Finally, the corresponding *E. coli* expression vectors with BCATs: pET53-*BAT1*, pET53-*BAT1ΔN16*, pET53-*BAT1ΔN16*^{G333S}, pET53-*BAT1ΔN16*^{G333W}, pET53-*BAT2*, and pET53-*BAT2*^{G316S} were obtained.

2.2.3.3. Growth phenotype measurement

Yeast cells were pre-cultured in 5 mL of SD medium at 30 °C for 18 h. Then, the cell suspensions were transferred to 50 mL of SD medium with an initial OD_{600} of 0.1 per mL. OD_{600} was measured every four h until the cultured reached 24 h. After 24 h, OD_{600} was measured every 6 h until the cultured reached 48 h to trigger the growth phenotype.

2.2.3.4. Measurement of BCAT metabolites

Yeast cells were pre-cultured in 5 mL of SD medium at 30 °C for 18 h. Then, the cell suspensions were transferred to 50 mL of SD medium with an initial OD_{600} of 0.1 per mL. After 48 h incubation, the yeast cells were collected and adjusted OD_{600} to 10 per mL. Amino acid contents were quantified using the same method as the previous study (71).

To quantify branched-chain higher alcohol (BCHA) content, the supernatants obtained from yeast cells cultured in an SD medium with shaking for 3 days were collected. BCHA contents were also quantified by GC-MS with a similar method as in the previous study (71).

2.2.3.5. Western blot analysis of the BCATs

The yeast proteins were extracted using the alkaline extraction method. *S. cerevisiae* strains were pre-incubated in 5 mL of SD+His/Met medium at 30 ºC for 72 h. The yeast cells were harvested with OD_{600} = 1.0 per mL, and the supernatant was removed by centrifugation at 13,000 rpm at 4 ºC for 5 min. The cell pellets were resuspended in 0.8 mL of 2 M lithium-acetate and kept on ice for 5 min. The supernatants were removed, and the cell pellets were resuspended in 0.8 mL of 0.4 M NaOH. After keeping the cell suspension on ice for 5 min, the supernatants were removed and the cell pellets were resuspended in 50 µL of HU buffer (200 mM phosphate buffer, pH 6.8, 8 M urea, 5% (w/v) SDS, 1 mM EDTA, 100 mM DTT, bromophenol blue). The samples were heated at 70 ºC for 10 min and centrifuged at 13000 rpm for 1 min. Resultant 10 µL of samples were applied to SDS-polyacrylamide gel electrophoresis (SDS-PAGE).

Aliquot 10 µL of samples were loaded to the gel. Electrophoresis was performed at 0.02 A for 30 min and continuously altered the current and running time amounts to 0.04 A and 90 min, respectively. The gel was transferred to Polyvinylidene Difluoride (PVDF) membrane using wet protein transfer: PVDF membrane and gel were clamped and soaked in 1X blotting buffer (methanol: 5X blotting buffer [29 g/L Tris, 145 g/L Glycine, and 5 g/L SDS]: MilliQ H_2O = 1:1:3). The transformation was performed at 80V and 400 mA for 2 h.

After finishing the transferring step, the PVDF membrane was used to perform a western blot. The membrane was soaked in 5% (w/v) skim milk in 1X TBS-T (10X TBS [30 g/L Tris, 80 g/L NaCl, 2 g/L KCl, pH = 8.0]: 30% (v/v) TWEEN20: MilliQ water = 1:0.1:9.9) at 4 ºC with shaking (55 rpm) for overnight. Primary antibody reaction was performed using α-GFP (Proteintech, USA), α-Pgk1 antibody (Invitrogen, USA), and α-Porin (Abcam, Japan) [at dilution rates of 1:5,000 (for α-GFP and α-Pgk1 antibodies) and 1:1000 (for α-Porin antibody) at 25 ºC with shaking (55 rpm) for 1 h. The membrane was washed by 1X TBS-T 3 times at 25 ºC with shaking (55 rpm) for 5 min (at the first and second washing steps) and 15 min (at the third washing step), respectively. A secondary antibody reaction was performed using an Anti-mouse antibody (Promega, Japan), with a dilution rate of 1:2,000, at 25 ºC with shaking (55 rpm) for 1 h, and the membrane was washed by the method mentioned above. The signal was detected by the chemiluminescence method.

2.2.4. *In vitro* study of BCATs and their variants

2.2.4.1. Expression and purification of the recombinant BCATs

N-terminal His-tagged recombinant BCATs were expressed using *E. coli* BL21 (DE3) cells harboring pET53-*BAT1ΔN16*, pET53-*BAT1ΔN16*^{G333S}, pET53-*BAT2*, and pET53-*BAT2*^{G316S}. DE3 cells were pre-culture in an LB medium containing ampicillin at 37 °C for 18 h. Then, the cell suspensions were transferred to 50 mL M9CA with the initial OD_{600} 0.05 per mL. The cells were cultured at 37 °C until OD_{600} reached 0.6-0.8 per mL. Isopropyl β-D-1-thiogalactopyranoside (IPTG) with 0.25 mM and 0.5 mM concentrations, respectively, for the Bat1 and Bat2 series, was added to induce protein expression. After cultivation at 18 °C for 20 h, the cells were harvested by centrifugation and re-suspended in 5 mL of buffer A [50 mM Tris-HCl (pH 8) and 300 mM NaCl]. The cell suspensions were homogenized and removed insoluble fractions by centrifugation undercooling. The supernatants were loaded onto the nickel affinity column (Ni SepharoseTM 6 Fast flow, GE Healthcare Life Sciences). After washing the column with buffer A containing 20 mM and 40 mM imidazole, buffer A with 500 mM imidazole was applied to the column to elution the recombinant BCATs. Dialysis was performed to remove imidazole together with exchanging the buffer from Tris-HCl to potassium phosphate and addition of dithiothreitol (DTT) to maintain and maximize the recombinant BCATs activity (55) using buffer B, which contained 50 mM potassium phosphate buffer (pH 8.0), 300 mM NaCl, and 1 mM DTT.

2.2.4.2. BCAT enzymatic activity assay

The recombinant BCATs activity was measured by triggering the production or extermination of NADH by coupling the transamination reaction with NAD-dependent glutamate dehydrogenase (GTD-211, Toyobo) as in previous studies with some modification (56, 63, 109) (Fig. 2-1). The NADH level was monitored by measuring the absorbance at 340 nm using a DU-800 spectrophotometer (Bechman Coulter). All reactions were maintained at 30 °C for 15 min, with pre-equilibrated the reaction mixture for 2 min at 30 °C. The forward reaction of BCAT was defined as a conversion of BCKAs (KIV, KIC, and KMV) to BCAAs (Val, Leu, and Ile) monitored by NADH production. Oppositely, the reverse reaction of BCAT was defined as a conversion of BCAAs (Val, Leu, and Ile) to BCKAs (KIV, KIC, and KMV), which was monitored by the extermination of NADH. Amino acid group donor (Glutamate, Glu) and receptor (α-ketoglutarate, KG) was added to forward (Glu was added) and reverse (KG was added) reaction with the appropriate concentration.

The specific activity of wild-type Bat1 and Bat2 ($Bat1\Delta N16^{WT}$ and $Bat2^{WT}$) were assayed in conditions containing the excess amount of each substrate (BCKAs and BCAAs) and co-substrates (KG and Glu). Forward reaction assay mixtures contained: 200 mM potassium phosphate buffer (pH 8.0), 0.25 mM NADH, 100 mM NH_4Cl, 50 μM PLP, 20 mM Glu, 1.5 mM of each BCKA, 12 U of GDH, and 2 μg of purified BCATs. Each BCKA was added to initiate the reaction. Reverse reaction assay mixtures contained: 200 mM potassium phosphate buffer (pH 8.5), 5 mM NAD^+, 50 μM PLP, 1 mM KG, 15 mM of each BCAA, 20 U of GDH, and 2 μg of purified BCATs. KG was added to initiate the reaction. Both forward and reverse reactions were maintained at 30°C for 15 min.

Steady-state kinetics of the recombinant BCATs were assayed for both forward and reverse reactions of BCAT. Steady-state kinetics for forward-reaction assay, the concentration of Glu was kept at 100 mM for both wild-type and variant recombinant BCATs. Meanwhile, the concentration of BCKAs was varied [(0.075-2.5 mM) and (0.15-10 mM) for wild-type ($Bat1\Delta N16^{WT}$ and $Bat2^{WT}$) and variants ($Bat1\Delta N16^{G333S}$ and $Bat2^{G316S}$) BCATs, respectively]. The other mixtures component of steady-state kinetics for forward-reaction assay contained: 200 mM of potassium phosphate buffer (pH 8.0), 0.25 mM of NADH, 100 mM of NH_4Cl, 50 μM of PLP, 100 mM of Glu, 12 U of GDH, and 2 μg of purified recombinant BCATs. Each BCKA at a certain concentration was added to initiate the forward reaction. Otherwise, for steady-state kinetics for reverse-reaction assay, the concentration of KG was kept at 2 mM for both wild-type and variant recombinant BCATs. The concentration of BCAAs was varied [(0.25-20 mM) and (5-125 mM), respectively for wild-type ($Bat1\Delta N16^{WT}$ and $Bat2^{WT}$) and variant ($Bat1\Delta N16^{G333S}$ and $Bat2^{G316S}$) BCATs]. 2 mM of KG was added to initiate the reverse reaction. The other mixtures component of steady-state kinetics for reverse-reaction assay contained: 200 mM potassium phosphate buffer (pH 8.5), 5 mM NAD^+, 50 μM PLP, 24 U of GDH, and 2 μg of purified recombinant BCATs. One unit of BCAT activity was defined as the amount of enzyme required to produce 1 μmol of KG per min (for forward-reaction) or the amount of enzyme required to produce 1 μmol of Glu per min (for reverse-reaction). Kinetic parameters of each enzyme were calculated with GraphPad Prism version 9 (GraphPad Software) using nonlinear regression analysis.

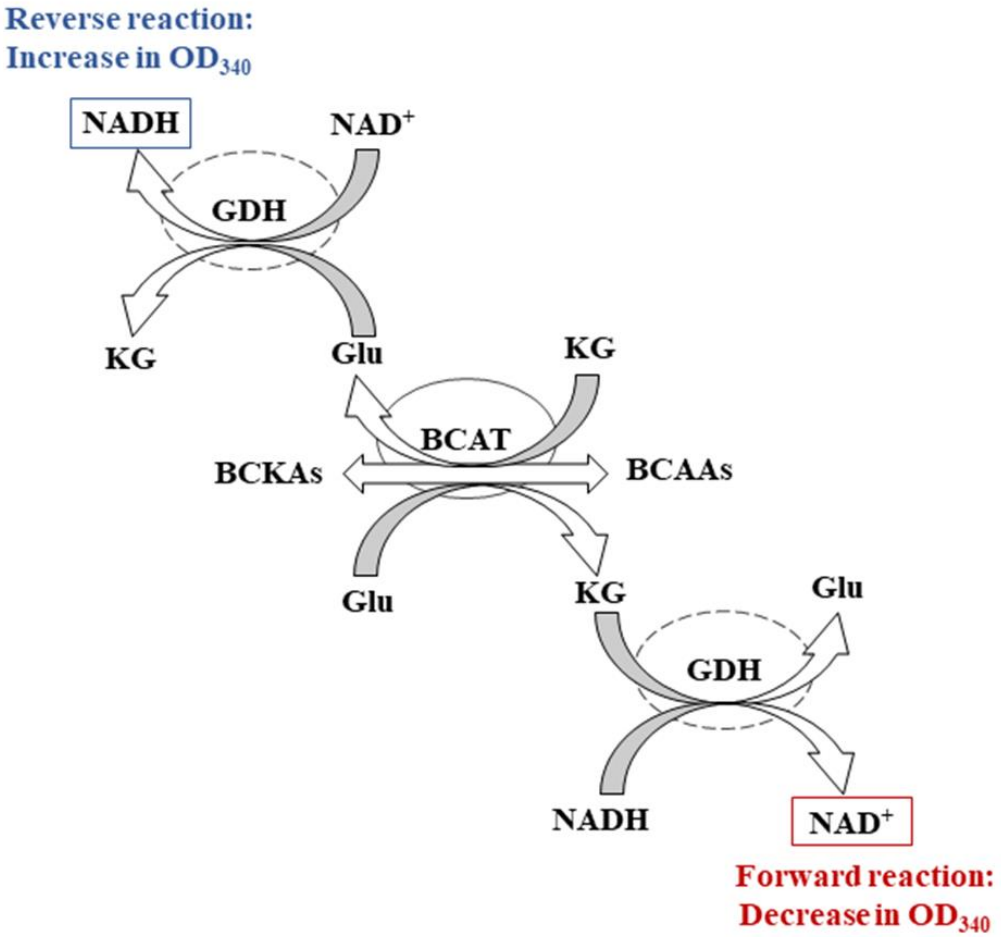

Fig. 2-1 Schematic branched-chain amino acid aminotransferase (BCATs) assay. Glutamate dehydrogenase (GDH) couples the bi-directional transamination reaction of the yeast Bat1 and Bat2. GDH can utilize the product from forward-reaction (α-ketoglutarate, KG) and reverse-reaction (glutamate, Glu), which leads to degradation of NADH to NAD^+ (forward-reaction) or generation of NADH from NAD+ (reverse-reaction). The changing of NADH level was measured at an absorbance of 340 nm [originally from (42)].

CHAPTER III: RESULTS

3.1. *In silico* investigation of Bat1 and Bat2

3.1.1. Structure validation and overlapping analysis of Bat1 and Bat2

Even though branched-chain amino acid aminotransferases of *Saccharomyces cerevisiae* (scBCATs) were known to impact branched-chain amino acid (BCAA) metabolism dynamically, the crystal structure of Bat1 and Bat2 has not been studied yet. Hence, I modeled the homology structure of Bat1 and Bat2 from SWISS-MODEL (Fig. 3-1). SWISS-MODEL quality estimation and PROCHECK analysis (section 2.4.) (Table 3-1) were used to confirm the reliability and validate the quality of the homodimer structures of the BCATs.

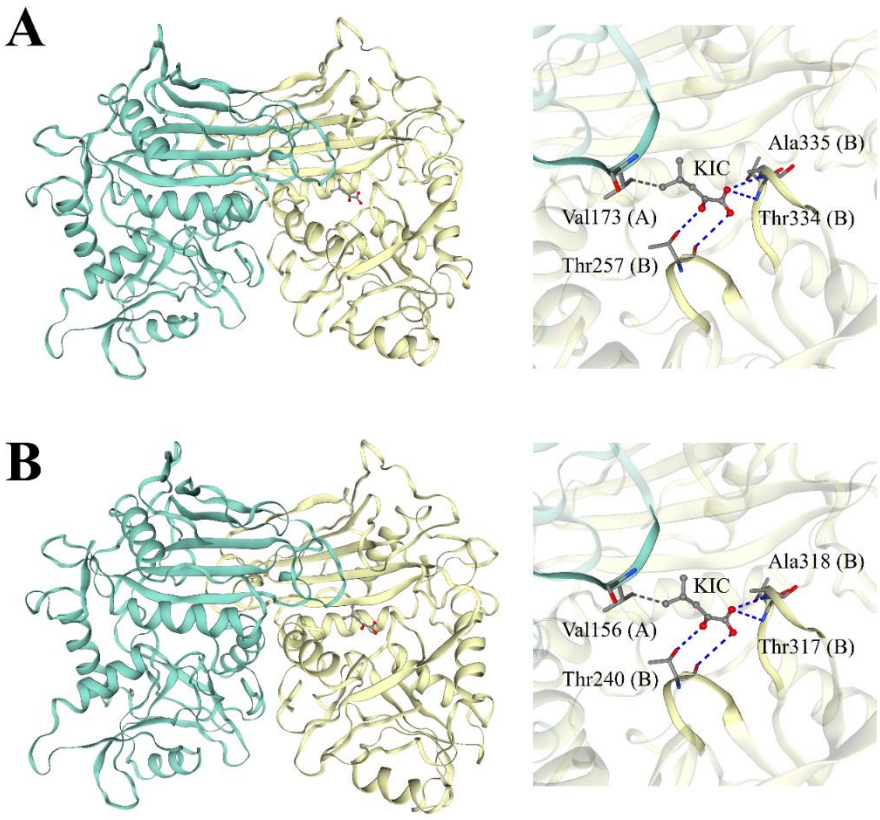

Fig. 3-1 Matching-predicted homodimer of Bat1 (A) and Bat2 (B), modeled from SWISS-MODEL, shown as a front view structure (left) and binding of KIC (right).

Table 3-1 Structural validation of Bat1, Bat2, Bat1-PLP, and Bat2-PLP homology structures that were modeled from SWISS-MODEL

Proteins			Bat1	Bat2	Bat1-PLP	Bat2-PLP
Quality check parameters	SWISS-MODEL parameters	Template	2hdk.1.A	2hdk.1.A	2abj.1.A	2abj.1.A
		Sequence Identity (%)	44.04	46.41	45.25	47.77
		QSQE	0.95	0.99	0.9	0.92
		GMQE	0.73	0.76	0.72	0.76
		QMEAN (Z-score)	-1.83	-1.9	-1.31	-0.96
	Ramachandran Plot statistics	Most favored regions [A, B, L] (%)	88.2	88.7	90.1	90.5
		Additional allowed regions [a, b, l, p] (%)	10.4	9.7	9.2	8.9
		Generously allowed regions [~a, ~b, ~l, ~p] (%)	0.5	0.6	0.2	0.2
		Disallowed region (%)	1	1	0.5	0.5
	G-Factors	Dihedral angles	-0.27	-0.24	-0.34	-0.32
		Main-chain covalent forces	-0.06	-0.06	-0.03	-0.01
		Overall average	-0.17	-0.15	-0.2	-0.18

The results revealed that the amino acid sequences of Bat1 and Bat2 showed 44.04% and 46.41% identity with the template (2hdk.1), respectively. The scores of the quaternary structure quality estimate (QSQE) were 0.95 for Bat1 and 0.99 for Bat2 (higher than 0.7), respectively; the scores of the qualitative model energy analysis (QMEAN) of Bat1 and Bat2 were -1.83 and -1.90 (not below -4.0), respectively. Additionally, the results of PROCHECK analysis by Ramachandran Plot statistics showed that Bat1 and Bat2 contain 88.2% and 88.7% of the most favored regions [A, B, L]. Meanwhile, overall G-Factors scores were -0.17 for Bat1 and -0.15 for Bat2 (higher than -0.5). These results indicated that the SWISS-MODEL was adequate for the *in silico* analysis of BCATs. The superimposed structures of Bat1 and Bat2 showed high identity, with a low root mean square deviation (RMSD) of 0.199 Å (Fig. 3-2A). These results indicate that the differences in primary structures between Bat1 and Bat2 do not affect their structural conformations.

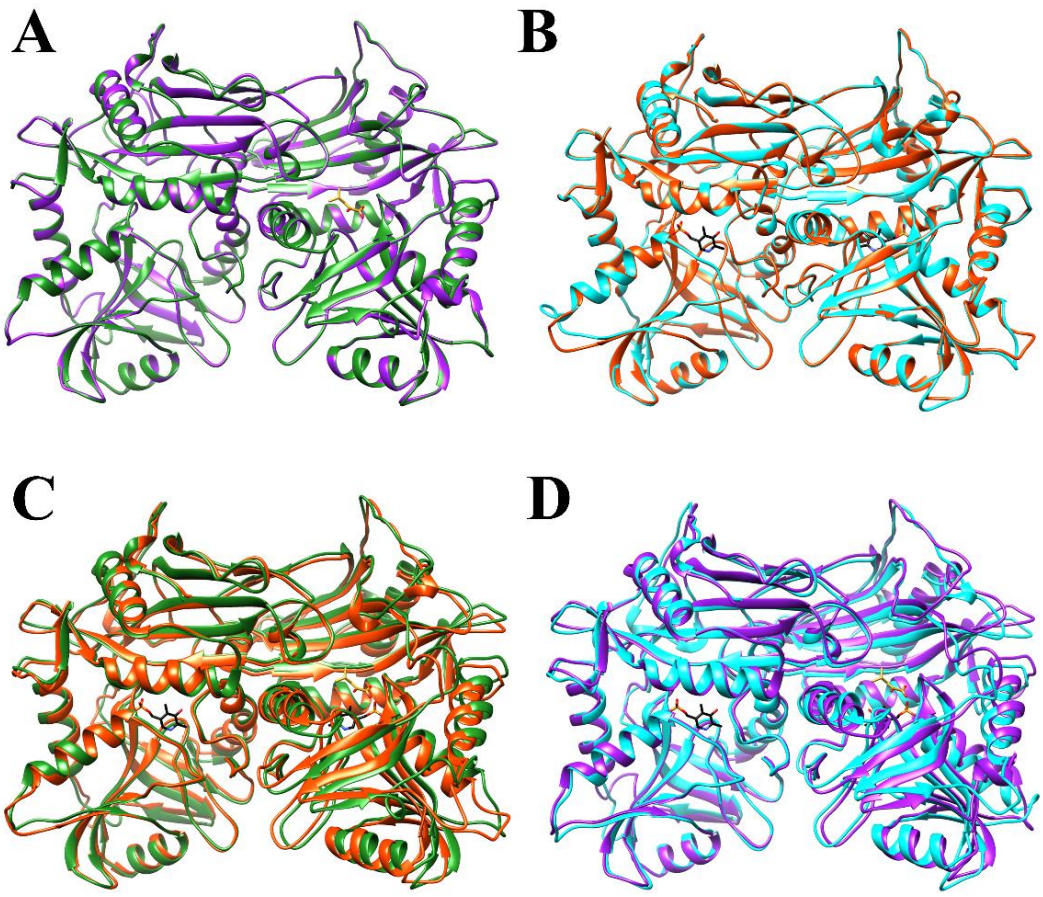

Fig. 3-2 Superimposition structures between Bat1/Bat2 (A), Bat1-PLP/Bat2-PLP (B), Bat1/Bat1-PLP (C), and Bat2/Bat2-PLP (D). The root means square deviation (RMSD) between each pruned atom pairs of the superimposition structure are 0.199 Å (with 359 pruned atom pairs) in Bat1/Bat2, 0.203 Å (with 366 pruned atom pairs) in Bat1-PLP/Bat2-PLP, 0.793 Å (with 359 pruned atom pairs) in Bat1/Bat1-PLP, and 0.733 Å (with 359 pruned atom pairs) in Bat2/Bat2-PLP, respectively. The

representative colors indicate Bat1 (forest-green), Bat2 (purple), Bat1-PLP (orange-red), Bat2-PLP (gray), KIC (golden-rod), and PLP (black), respectively.

3.1.2. Pocket analysis of Bat1 and Bat2

Although several studies have revealed the enzymatic properties of yeast BCATs through *in vitro* assays (41, 56, 63), few studies have attempted to clarify the relationships between the high-dimensional structures and the functions of individual yeast BCATs (57). Moreover, BCATs physically interact with several proteins in yeast cells (110). Based on these findings, I considered that the structures of BCATs might include a pocket conformation related to the active site or BCAT regulation. Thus, I first attempted to determine whether the Bat1 or Bat2 structure included a pocket(s) that could bind with a ligand. The analysis revealed nine potential pockets on both Bat1 and Bat2, of which four were on equivalent subunits (α, α', β, β', γ, γ', δ, and δ'), and the other five were on the overlapping region between two subunits (ε and ε') (Fig. 3-3). Notably, almost the pockets without γ and γ' on Bat1 and Bat2 were located at similar positions on both BCATs. The levels of pKd were nearly equivalent to each other on the pockets located in equivalent positions on individual BCAT (Table 3-2). The highest pKd values in Bat1 and Bat2 are shown in pockets α and α'. The pKd values of pockets α and α' were 6.87 and 6.97 in Bat1 and 6.90 and 6.98 in Bat2, respectively. Focusing on the pKd values in Bat1 and Bat2, pockets δ, δ', and ε showed differences in ligandability. Therefore, it can be presumed that Bat1 and Bat2 have partially different conformations despite their high similarity in structure.

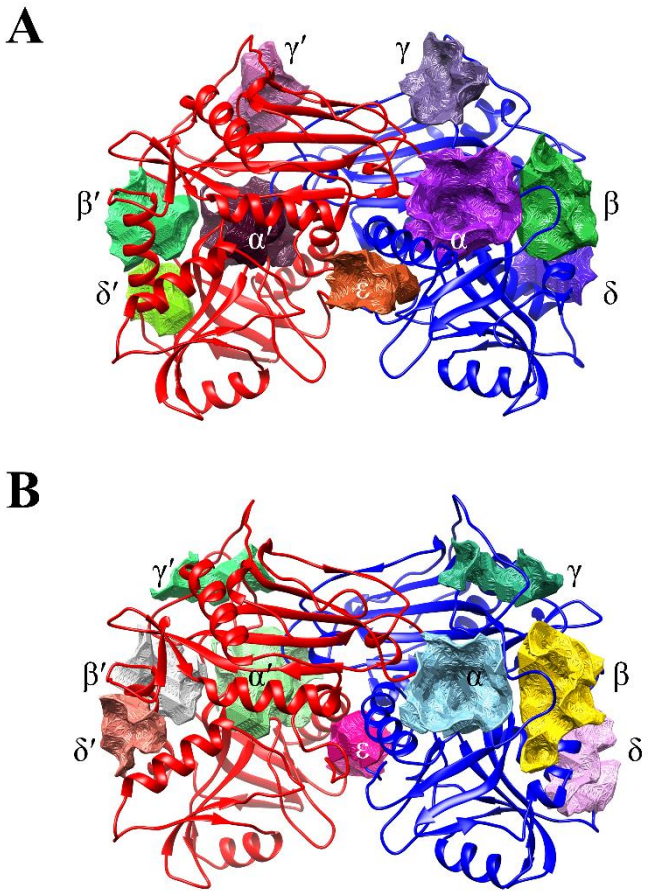

Fig. 3-3 The predicted potential pockets in Bat1 (A) and Bat2 (B). The pocket surfaces were shown as a different color for each pocket. The pockets that have pKd more than or around 6 correspond to be a potential pocket for substrate binding. Red and blue ribbons indicate the chain A and B of Bat1 and Bat2, respectively.

Table 3-2 The predicted potential pockets of the Bat1 and Bat2

Assigned types[a]	Average of pKd[b]					
	Bat1			Bat2		
	Bat1/B	Bat1/A	Bat1 (A/B)[c]	Bat2/B	Bat2/A	Bat2 (A/B)[c]
α, α'	6.87	6.97	–	6.90	6.98	–

β, β'	6.44	6.58	–	6.01	6.18	–
γ, γ'	6.00	5.95	–	5.15	5.07	–
δ, δ'	6.00	5.65	–	5.68	5.54	–
ε	–	–	6.21	–	–	5.52

[a] N and N' indicate labels of potential pockets presented in the B and A chains of the Bat1 and Bat2 proteins, respectively.
[b] The pKd values are defined as the ligandability of each pocket. The values above 6.0 suggest that this binding site is considered a possible ligand-binding pocket.
[c] Pocket ε exists overlapping regions between the B and A chains of the Bat1 or Bat2 proteins, respectively.

I performed a PARS analysis to investigate further the potential binding ability of the putative pockets in BCATs (Fig. 3-4 and Table 3-3). PARS uses normal mode analysis (NMA), a useful approach to investigate protein dynamics, to determine the protein flexibility change upon ligand binding.

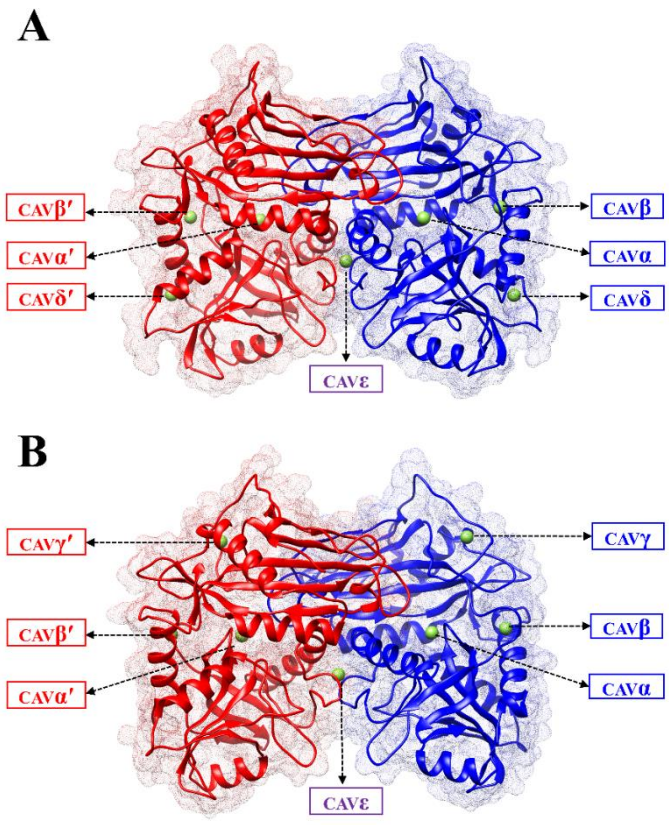

Fig. 3-4 Caves of the Bat1 (A) and Bat2 (B) from PARS. The green spheres represent the substrates' binding position in each cave. The surfaces of Bat1 and Bat2 were analyzed and showed as watermarked red- or blue colors, respectively, for chains A and B using UCSF Chimera.

The results strongly suggested that the two largest pockets (CAVα and CAVα') in BCATs were potential binding sites based on their pFlex value (0.03 and 0.06, respectively), which indicated their highest compatibility with those of the other pockets (0.43 and 0.92). The location of the CAVα in BCATs was consistent with previous studies of human BCAT (hBCAT) crystallized structures (111, 112). Additionally, some distinct residues were found in the amino acid cluster that composed catalytic pockets (Table 3-4) and related to substrate binding directly in human BCAT (mitochondrial isoform, hBCATm), such as Val173, Thr257, Thr334, and Ala335 in Bat1 (112). Considering the results of the pocket analysis by CavityPlus (Fig. 3-3 and Table 3-2) and PARS (Fig. 3-4 and Table 3-3), I confidently concluded that the two largest pockets (CAVα and CAVα') were the catalytic pockets of BCATs.

Table 3-3 The impact of each pocket on protein flexibility by the occupancy of substrates

Bat1	pFlex			Bat2	pFlex		
cavities	Bat1/B	Bat1/A	Bat2 (A/B)	cavities	Bat2/B	Bat2/A	Bat2 (A/B)
CAVα, CAVα'	0.03*	0.06*	–	CAVα, CAVα'	0.04*	0.03*	–
CAVβ, CAVβ'	0.43	0.58	–	CAVβ, CAVβ'	0.52	0.56	–
CAVε	–	–	0.32	CAVε	–	–	0.34
CAVδ, CAVδ'	0.66	0.67	–	CAVγ, CAVγ'	0.92	0.88	–

Descended orders of the row in cavity items represent the decrease of protein pocket size (the rank order of cavity sizes are α, α′ > β, β′ > ε > δ, δ′ and α, α′ > β, β′ > ε > γ, γ′ in Bat1 and Bat2, respectively).
*indicates a significant difference in protein flexibility between with and without ligand on the enzyme.

Table 3-4 The predicted amino acid residues involved in the catalytic pocket formation of the Bat1 and Bat2, obtained from CavityPlus.

Enzyme	Amino acid residues
Bat1	Chain A:
	Cys84, His87, Tyr88, Ser168, Lys169, Gly170, Leu171, Gly172, Val173, Gly174, Thr175, Pro176

	Chain B: Glu44, Leu45, Val46, Phe47, Gly48, Gln49, Phe93, Glu94, Gly95, Leu96, Lys97, Asn114, Arg117, Tyr159, Arg161, Val188, Gly189, Pro190, Tyr191, Tyr192, Lys193, Gly195, Phe196, Lys197, Ala198, Val199, Arg200, Leu201, Lys219, Tyr224, Cys227, Ile228, Leu229, Pro230, Gln231, Leu232, Ala234, Ala235, Gly238, Tyr239, Gln240, Gln241, Asn242, Trp244, Glu254, Val255, Gly256, Thr257, Met258, Asn259, Leu284, Glu285, Gly286, Val287, Thr288, Arg289, Ser332, Gly333, Thr334, Ala335, Ala336, Val337, Val338, Ser339, Pro340
Bat2	Chain A: Val67, His70, Tyr71, Thr151, Ala152, Gly153, Leu154, Gly155, Vsl156, Ser157, Thr158 Chain B: Glu27, Leu28, Val29, Phe30, Gly31, Lys32, Phe76, Glu77, Gly78, Met79, Lys80, Asn97, Arg100, Tyr142, Arg144, Val171, Gly172, Pro173, Tyr174, Tyr175, Lys176, Phe179, Lys180, Ala181, Val182, Arg183, Leu184, Lys202, Tyr207, Cys210, Val211, Leu212, Pro213, Gln214, Leu215, Ala217, Ala218, Gly221, Tyr222, Gln223, Gln224, Asn225, Trp227, Glu237, Val238, Gly239, Thr240, Met241, Asn242, Leu267, Glu268, Gly269, Val270, Thr271, Arg272, Ser315, Gly316, Thr317, Ala318, Ala319, Ile320, Val321, Ser322, Pro323

3.1.3. Modalities of substrate binding with Bat1 and Bat2

3.1.3.1. Verification of the BCAT structures containing pyridoxal 5'-phosphate (PLP)

BCAT can catalyze a mutual transamination between BCAAs (Val, Leu, and Ile) and BCKAs (KIV, KIC, and KMV). Previous studies have proved that the yeast BCATs have substrate specificity (56, 63). Moreover, many studies have been conducted to elucidate the complex structures of hBCATs with substrates to analyze drug resistance or the catalysis mechanism of hBCATs (111–113). These findings have contributed to our understanding of the basic functions of hBCATs. On the other hand, no serious attempt has been made to examine the differences in substrate specificities between yeast Bat1 and Bat2 from a comprehensive perspective. Thus, I attempted to perform such an examination by analyzing the binding behavior of all substrates (BCAAs and BCKAs) and co-substrates [glutamate (Glu) and α-ketoglutarate (KG)] to Bat1 and Bat2 by molecular docking simulation. BCAT is a PLP-

dependent enzyme, and PLP is essential for the catalytic reaction of Bat1 and Bat2 (114). Homology structures of Bat1 and Bat2 with PLP (named Bat1-PLP and Bat2-PLP, respectively) were constructed from SWISS-MODEL using hBCAT (cytosolic isoform, hBCATc) (SWTL ID: 2abj.1) as a template (Fig. 3-5). Structure validation of these homology structures was performed as described above (Table 3-1).

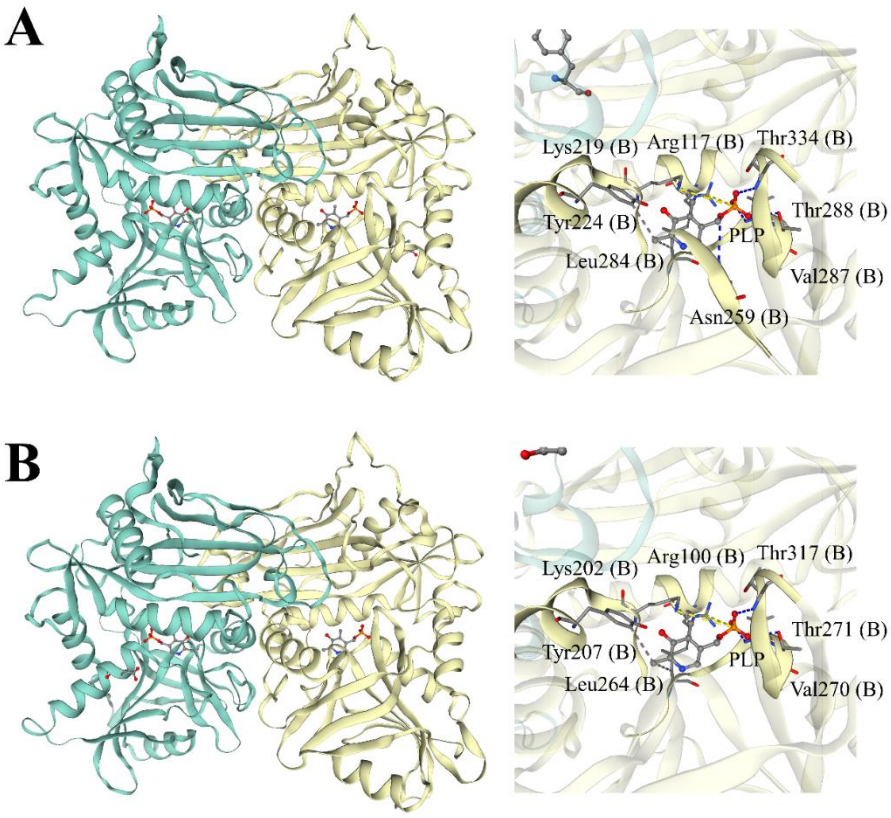

Fig. 3-5 Matching-predicted homodimer of Bat1-PLP (A) and Bat2-PLP (B), modeled from SWISS-MODEL, shown as a front view structure (left) and binding of PLP (right).

As a result, the structures of Bat1-PLP and Bat2-PLP showed higher QMEAN values (-1.31 in Bat1-PLP and -0.96 in Bat2-PLP, respectively). The Ramachandran Plot statistics levels of most favored regions also showed higher values (90.1% in Bat1-PLP and 90.5% in Bat2-PLP, respectively). Superimposition structures of Bat1/Bat2 and Bat1-PLP/Bat2-PLP showed high identity (Fig. 3-2A and B) with low root mean square (RMSD) values (0.199 Å and 0.203 Å, respectively). On the other hand, a comparison of the superimposition structure between BCATs and BCATs with PLP indicated a difference in structural conformation (Fig. 3-2C and D). The RMSD values of Bat1/Bat1-PLP and Bat2/Bat2-PLP were higher (0.793 Å and 0.733 Å, respectively) than those of Bat1/Bat2 and Bat1-PLP/Bat2-PLP. However, a

previous study also reported a conformational change of p-protein with or without PLP (115). Moreover, the validation results suggest that Bat1-PLP and Bat2-PLP are better-quality structures for *in silico* study than Bat1 and Bat2 structures without PLP (Table 3-1). For these reasons, it can safely conclude that the conformational change of BCATs with PLP can be used to analyze the structures in this study.

3.1.3.2. Identification of amino acid residues involved in substrate-binding on BCATs

Based on the pocket analysis results, the pockets α and α' of Bat1 and Bat2 are the catalytic pockets. Thus, pocket α was selected for elucidating the substrate-binding manner by a molecular docking simulation. The AutoDock Vina program was chosen for the docking simulation due to improved binding accuracy prediction (97). With respect to the binding interactions and orientation among Bat1-PLP/Bat2-PLP and substrate species in the active centers, both the whole-substrates and co-substrates bound in almost the same position and showed a clustered-binding trend in both the BCATs (Fig. 3-6). Next, I analyzed the molecular interactions between substrates and BCATs in the active center in more detail (Table 3-5 and Fig. 3-7 to 3-10). In Bat1, the bindings of substrates (BCAAs or BCKAs) were constituted by a combination of 14 residues (Phe47, Tyr88, Phe93, Tyr159, Arg161, Leu171, Gly172, Val173, Tyr191, Lys219, Tyr224, Thr257, Thr334, and Ala335) and PLP. Among them, Phe93, Tyr159, and Ala335 were involved in the binding of all substrates. In particular, Tyr159 formed hydrogen bonds with several substrates as well as hydrophobic interactions. Phe47, Tyr88, Arg161, Val173, Tyr224, and Thr257 were also used as residues for a high-frequency substrate binding. Notably, four substrates interacted with Arg161 by hydrophobic interaction, and three of these four substrates formed hydrogen bonds. On the other hand, some residues were utilized for substrate-binding with low frequency, such as Leu171, Gly172, Tyr191, and Thr334. Interestingly, those residues participated only in the binding of BCAAs.

The active center of Bat2, BCKAs and BCAAs was found by the effects of hydrophobic interactions, which were attributed to a combination of 14 residues: Phe30, Tyr71, Phe76, Gly78, Tyr142, Leu154, Val156, Arg161, Tyr174, Lys202, Tyr207, Thr240, Gly316, and Ala318, and PLP. Among those residues, Phe30, Tyr71, Phe76, Tyr142, Val156, Lys202, Thr240, and Ala318 were commonly used for substrate-binding. Remarkably, almost all Tyr142 formed hydrogen bonds as well as hydrophobic interactions with the substrates. Similarly, Arg144 also interacted with several substrates by hydrogen bonding and hydrophobic interactions but participated only in bonding BCKAs.

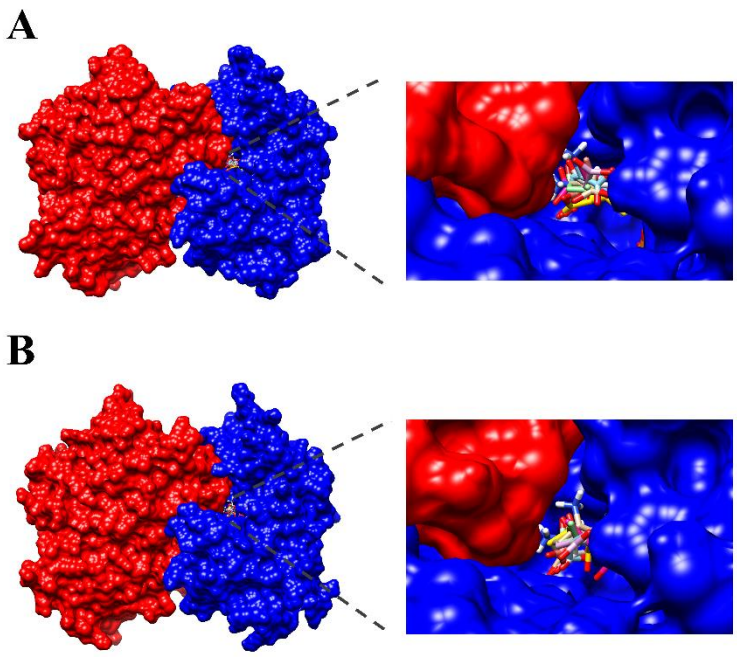

Fig. 3-6 Binding of substrates to the active site in Bat1-PLP (A) and Bat2-PLP (B). Red and blue colors represent the surfaces of chains A and B, respectively. The sticks with different colors represent each substrate that binds to Bat1-PLP and Bat2-PLP catalytic site (KIV, hot pink stick; KIC, green stick; KMV, gray stick; Val, yellow stick; Leu, magenta stick; Ile, cyan stick; KG, purple stick; and Glu, gold stick).

Surprisingly, virtually all substrates and co-substrates interacted with PLP and Lys residues (Lys219 in Bat1 and Lys202 in Bat2), known as a cofactor and catalytic residues of BCATs, respectively. In BCATs, transamination between BCAAs and BCKAs is processed by forming Schiff-base intermediates with PLP and Lys (58). As is well known, hydrogen bonds play an important role in enzyme-substrate interaction (116). Regarding the contribution of the cofactor in the substrate binding, guanosine-5'-monophosphate reductase (GMPR) forms the complex of GMPR-substrate-$NADPH^+$ (117), and those factors are linked in intricate, reaction-specific, dynamic networks for the exertion of enzyme catalysis (118). Like GMPR, PLP and a Lys residue in BCATs might also be essential for substrate binding and catalytic activity. To further verify the results, a continuous study of the structure of BCATs would demonstrate the catalysis mechanisms in detail by combining them with biochemical analysis.

Table 3-5 Interactive amino acid residues for substrate-binding on Bat1 and Bat2 [modified from (42)]

Substrate Species	Amino acid residues involved in substrate-binding	
BCKAs	**Bat1**	**Bat2**
KIV	Phe47, Tyr88, Phe93, Tyr159, Val173, Lys219, Tyr224, Thr257, Ala335, **PLP**	Phe30, Tyr71, Phe76, **Tyr142, Arg144,** Val156, **Lys202,** Thr240, Ala318, PLP
KIC	Phe47, Tyr88, Phe93, **Tyr159**, **Arg161**, Val173, Lys219, Tyr224, Thr257, Ala335, **PLP**	Phe30, Tyr71, Phe76, **Tyr142**, **Arg144**, Val156, Lys202, Tyr207, Thr240, Ala318, **PLP**
KMV	Tyr88, Phe93, Tyr159, **Arg161**, Val173, **Lys219**, Ala335, PLP	Phe76, **Tyr142**, **Arg144**, Tyr174, Lys202, Thr240, Ala318, PLP
BCAAs		
Val	Phe93, **Tyr159**, **Lys219**, Tyr224, Thr257, Thr334, Ala335, **PLP**	Phe30, Tyr71, Phe76, Gly78, **Tyr142**, Val156, **Lys202**, Ala318, PLP
Leu	Phe47, Tyr88, Phe93, **Tyr159**, **Arg161**, Leu171, Val173, Tyr191, Thr257, Ala335	Phe30, Tyr71, **Tyr142**, Leu154, Val156, Tyr174, Thr240, Gly316, **Ala318**, PLP
Ile	Phe47, **Tyr88**, Phe93, Tyr159, Arg161, **Leu171**, Gly172, Val173, Tyr191, Ala335	Phe30, **Tyr71**, Phe76, Tyr142, Val156, Tyr174, Lys202, Tyr207, Thr240, Ala318, **PLP**

These residues were retrieved from the docking configurations of the ligand-protein interactions (Table S3), which were analyzed as 2D-interaction plots between substrates and catalytic sites of Bat1-PLP and Bat2-PLP from LigPlot^{+}. Residues represented by bold indicate hydrogen formation residues to each substrate.

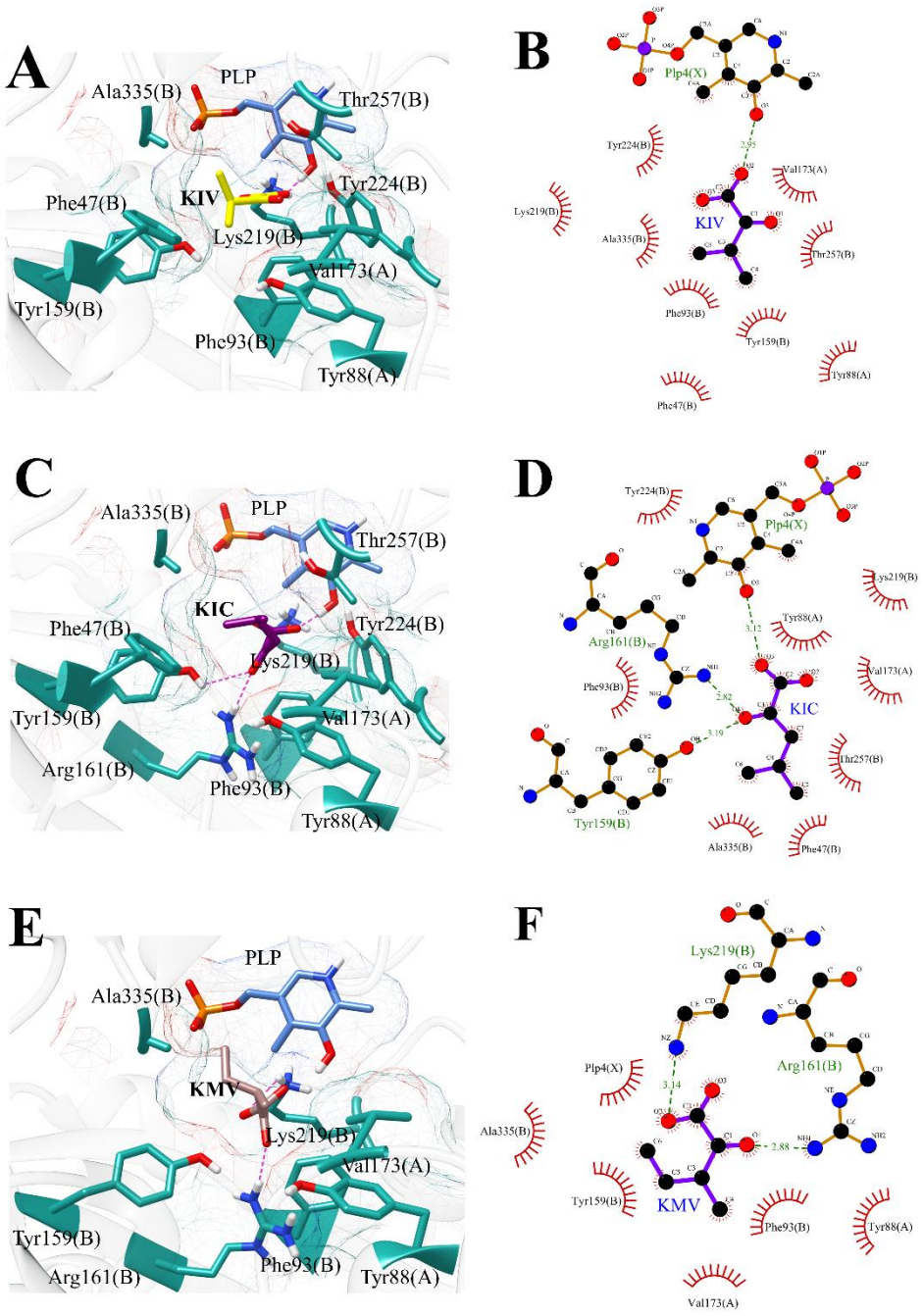

Fig. 3-7 Docking of BCKAs in the active site of Bat1 and interactive residues (cofactor) to each substrate. Three-dimensional binding conformations of KIV (A), KIC (C), and KMV (E) in the active site of Bat1 are shown. Two-dimensional plots between BCKAs and active sites in Bat1 are also shown in B (KIV), D (KIC), and F (KMV), respectively. The hot-pink dashed in the 3D-plot represents the hydrogen bond between substrates atom and amino acid residues at the catalytic pocket, which matches with the green-dashed (H-bond) in the 2D-plot [with the atomic distance in Å]. The red-semi circle dashed in the 2D-plot represents hydrophobic interaction between substrates and amino acid residues at the catalytic pocket matching the stick residues in 3D-plot. Each red-, blue-, and white-labeled atom on sticks represents the

molecule's O-, N-, and H-atom. The hydrophobic surface analysis shows and determines each substrate's binding manner, especially the hydrophobic interaction network with the side chain of each substrate.

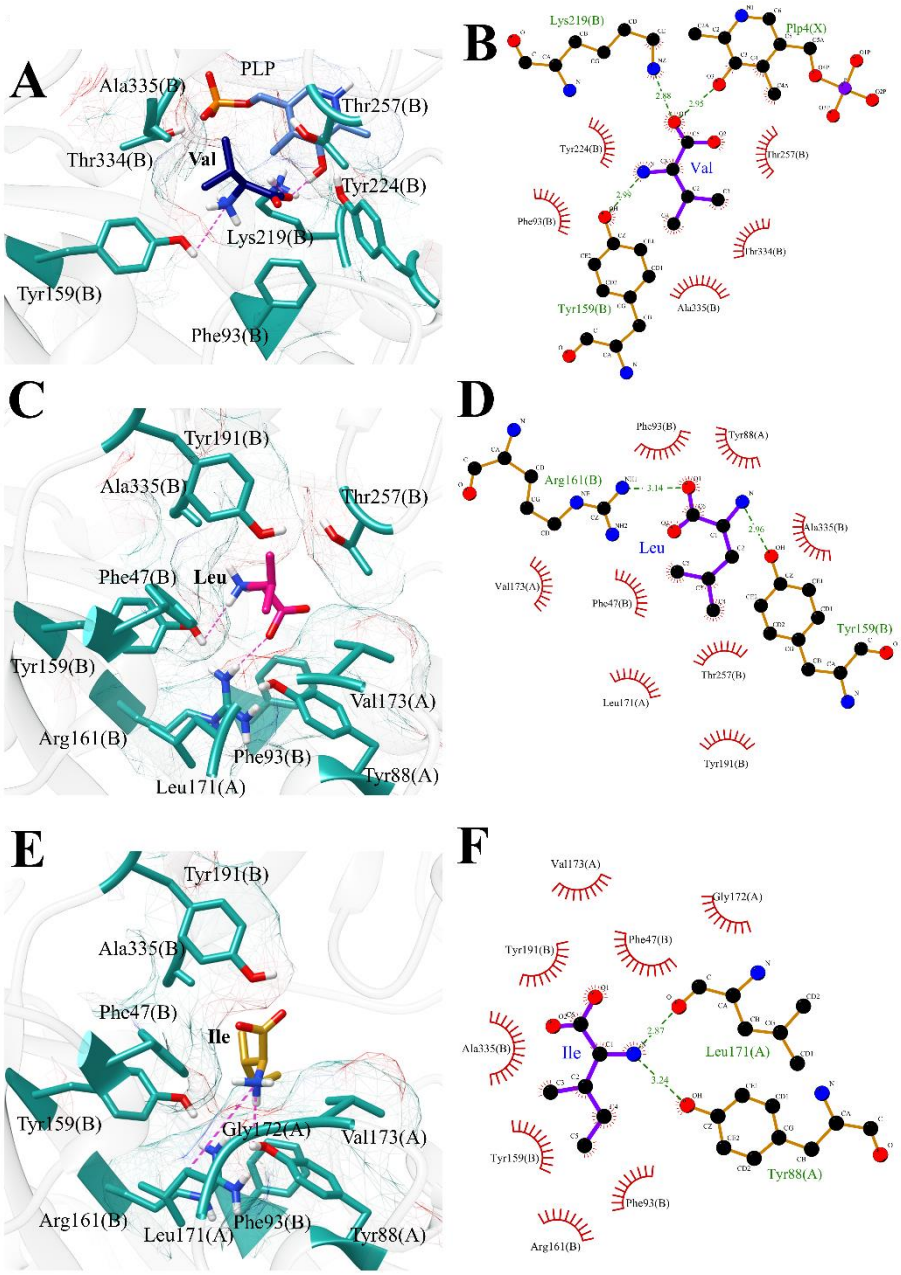

Fig. 3-8 Docking of BCAAs in the active site of Bat1 and interactive residues (cofactor) to each substrate. Three-dimensional binding conformations of Val (A), Leu (C), and Ile (E) in the active site of Bat1 are shown. Two-dimensional plots between BCAAs and active sites in Bat1 are also shown in B (Val), D (Leu), and F (Ile), respectively. The hot-pink dashed in the 3D-plot represents the hydrogen bond between substrates atom and amino acid residues at the catalytic pocket, which

matches with the green-dashed (H-bond) in the 2D-plot [with the atomic distance in Å]. The red-semi circle dashed in the 2D-plot represents hydrophobic interaction between substrates and amino acid residues at the catalytic pocket matching the stick residues in 3D-plot. Each red-, blue-, and white-labeled atom on sticks represents the molecule's O-, N-, and H-atom. The hydrophobic surface analysis shows and determines each substrate-binding manner, especially the hydrophobic interaction network with the side chain of each substrate.

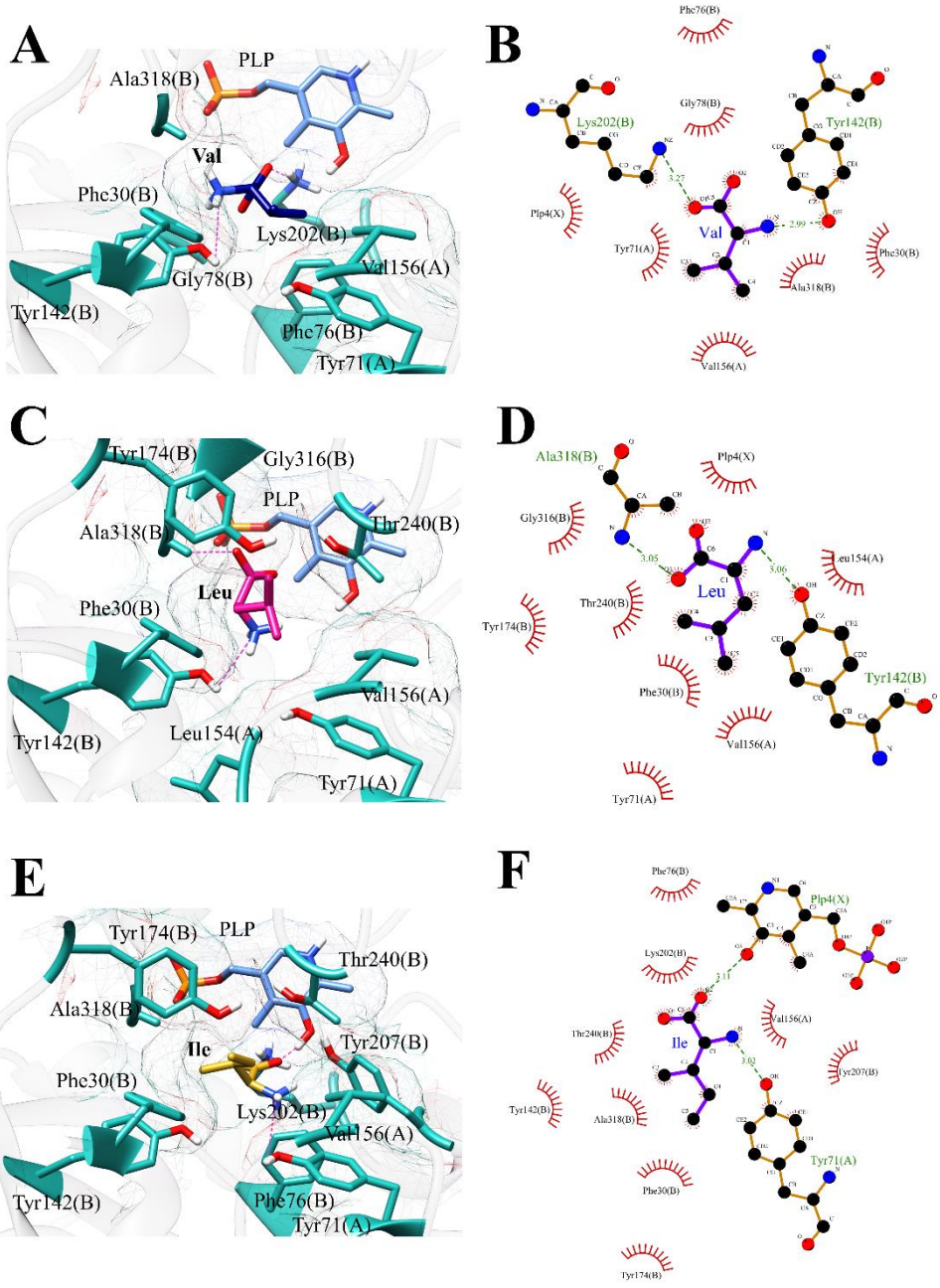

Fig. 3-9 Docking of BCKAs in the active site of Bat2 and interactive residues (cofactor) to each substrate. Three-dimensional binding conformations of KIV (A),

KIC (C), and KMV (E) in the active site of Bat2 are shown. Two-dimensional plots between BCKAs and active sites in Bat2 are also shown in B (KIV), D (KIC), and F (KMV), respectively. The hot-pink dashed in the 3D-plot represents the hydrogen bond between substrates atom and amino acid residues at the catalytic pocket, which matches with the green-dashed (H-bond) in the 2D-plot [with the atomic distance in Å]. The red-semi circle dashed in the 2D-plot represents hydrophobic interaction between substrates and amino acid residues at the catalytic pocket matching the stick residues in 3D-plot. Each red-, blue-, and white-labeled atom on sticks represents the molecule's O-, N-, and H-atom. The hydrophobic surface analysis shows and determines each substrate's binding manner, especially the hydrophobic interaction network with the side chain of each substrate [originally from (42)].

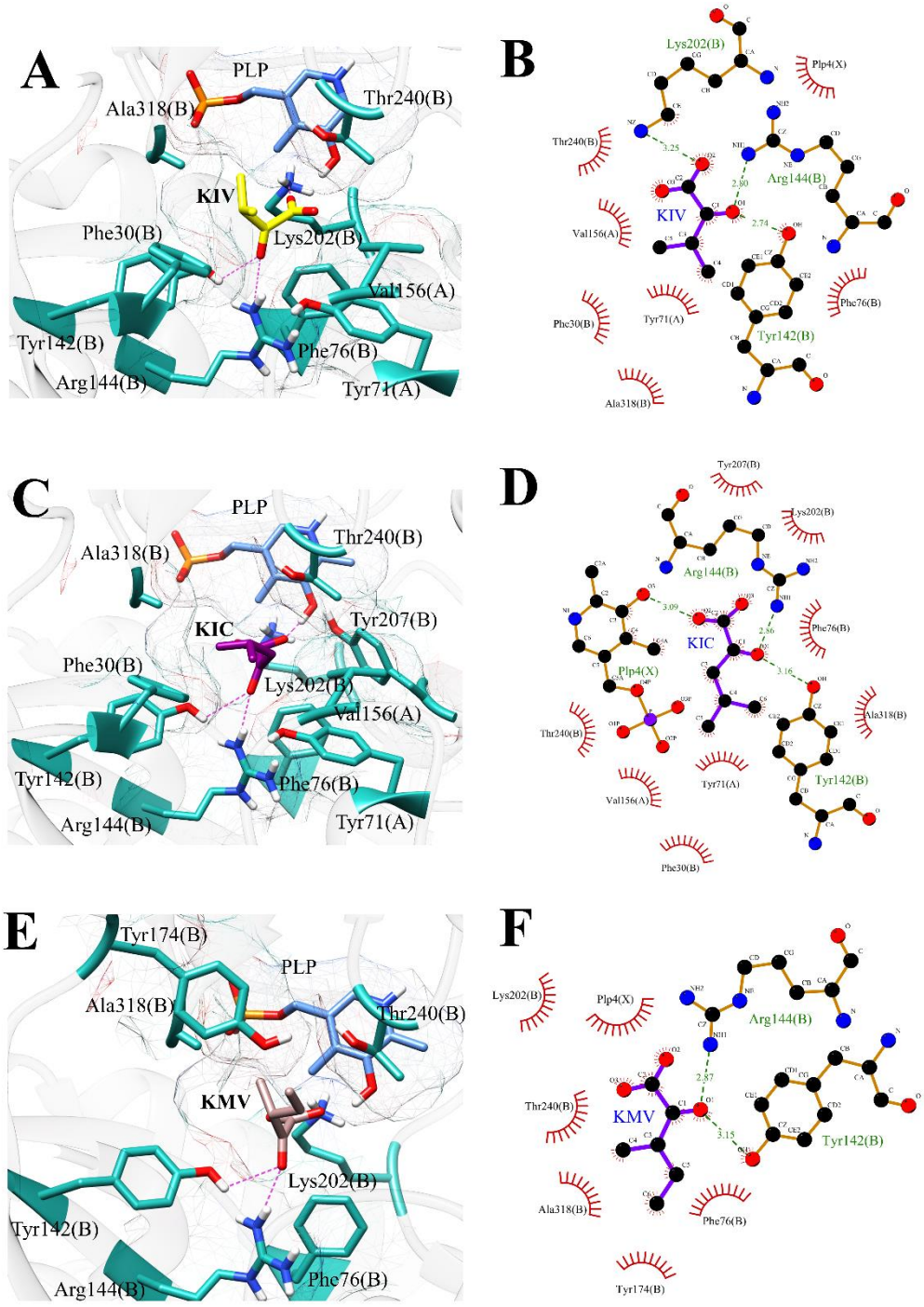

Fig. 3-10 Docking of BCKAs in the active site of Bat2 and interactive residue (cofactor) to each substrate. Three-dimensional binding conformations of KIV (A), KIC (C), and KMV (E) in the active site of Bat2 are shown. Two-dimensional plots between BCKAs and active sites in Bat2 are also shown in B (KIV), D (KIC), and F (KMV), respectively. The hot-pink dashed in the 3D-plot represents the hydrogen bond between substrates atom and amino acid residues at the catalytic pocket, which

matches with the green-dashed (H-bond) in the 2D-plot [with the atomic distance in Å]. The red-semi circle dashed in the 2D-plot represents hydrophobic interaction between substrates and amino acid residues at the catalytic pocket matching the stick residues in 3D-plot. Each red-, blue-, and white-labeled atom on sticks represents the molecule's O-, N-, and H-atom. The hydrophobic surface analysis shows and determines each substrate's binding manner, especially the hydrophobic interaction network with the side chain of each substrate [originally from (42)].

3.1.3.3. Similarities and differences in the substrates-binding mechanisms between Bat1 and Bat2

To elucidate the differences in the substrate-binding mechanisms between Bat1 and Bat2 in more detail, I analyzed each of the 14 residues in BCATs by confirming a conformational binding state in BCATs and sequence alignments. As a result, 12 residues in Bat1 (Phe47, Tyr88, Phe93, Tyr159, Arg161, Leu171, Val173, Tyr191, Lys219, Tyr224, Thr257, and Ala335) were found to correspond with Phe30, Tyr71, Phe76, Tyr142, Arg144, Leu154, Val156, Tyr174, Lys202, Tyr207, Thr240, and Ala318 in Bat2, respectively (Table 3-4). Moreover, all the residues involved in substrate-binding on BCATs were highly conserved among all biological species (Table 3-6). These results strongly indicated that those residues might contribute to the binding or recognition of substrates on BCATs present in other species.

Meanwhile, several residues showed distinctive dissimilarities between Bat1 and Bat2 as follows. (1) Arg residues in BCATs were suspected to be important for substrate-binding because of their hydrogen bond formation with several substrates. However, Arg144 in Bat2 formed a hydrogen bond only with all BCKAs, in contrast with Agr161 in Bat1, which formed a hydrogen bond or hydrophobic interaction with KIC, KMV, Leu, and Ile. (2) Tyr142 in Bat2 formed hydrogen bonds with most of the substrates except Ile, whereas Tyr159 in Bat1 formed hydrogen bonds with KIC, Val, and Leu. (3) Tyr207 (hydrophobic interaction) and PLP (hydrogen bond) in Bat2 participated in the binding of both co-substrates (KG and Glu), while only a hydrophobic interaction with co-substrates was observed on PLP in Bat1. Additionally, some residues were used with low frequency for substrate-binding in BCATs – namely, Leu171, Gly172, The334 (in Bat1), Gly154, Leu154, and Gly316 (in Bat2) were involved only in the bindings of BCAAs. These results suggested that the recognition or binding mechanism of substrates is highly generalized in BCATs, while minimal differences in substrate-binding exist between Bat1 and Bat2, which might derive from the differences of amino acid sequences in their primary structure.

Table 3-6 Correspondance of residues involved in substrate-binding between Bat1 and Bat2 and amino acid conservation scores among the other BCAT families

Chain	Bat1	Bat2	Conservative
	Residues		scores
A	Tyr88	Tyr71	9
	Val173	Val156	8
	Leu171	Leu154	7
	Gly172		7
B	Phe47	Phe30	9
	Phe93	Phe76	9
		Gly78	9
	Tyr159	Tyr142	9
	Arg161	Arg144	9
	Tyr191	Tyr174	8 - 9
	Lys219	Lys202	9
	Tyr224	Tyr207	9
	Thr257	Thr240	7
		Gly316	9
	Thr334		9
	Ala335	Ala318	9

In the conservative score, a higher value indicates that the corresponding residue is highly conserved among the other BCATs derived from other species (nine is highest and one is lowest).

3.1.3.4. Identification of the important residues for substrate recognition and stabilization

The substrate interactions on BCATs indicated that the carboxy groups, i.e., α-carbonyls and α-amino in BCKAs and BCAAs, formed hydrogen bonds with BCATs (Fig. 3-7 to 3-10). Tyr residues, such as Tyr88, Tyr159 (both are in Bat1), Tyr71, or Tyr142 (both are in Bat2), bore a hydrogen bond to α-carbonyls in BCKAs or α-amino in BCAAs. Additionally,

Arg residues such as Arg161 in Bat1 and Arg144 in Bat2 are also bound to α-carbonyls in BCKAs. Likewise, in co-substrates, Tyr88, Arg161 (both in Bat1), Tyr71, and Tyr142 (both in Bat2) showed a strong interaction with α-carbonyls and α-amino in KG and Glu, respectively (Fig. 3-11).

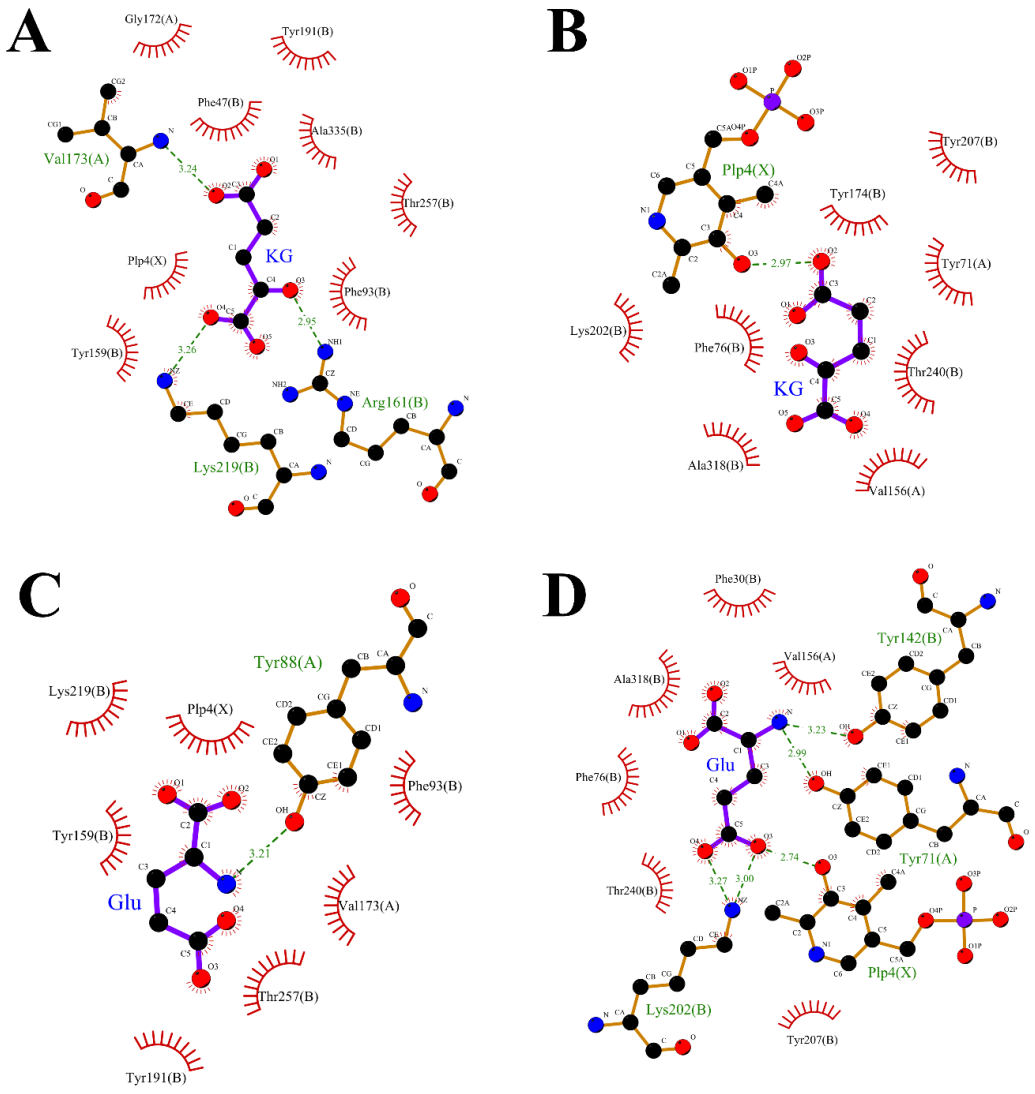

Fig. 3-11 Schematic interaction (2D-plots) between co-substrates (KG and Glu) around the catalytic pocket of the Bat1-PLP (A and C, respectively) and Bat2-PLP (B and D, respectively).

A previous study based on a crystalized structure analysis has revealed that Tyr31, Tyr97, and Arg99 in *Escherichia coli* BCAT (eBCAT) form hydrogen bonds with Glu (113). Arg143 (with Tyr141 and Tyr70) in hBCATm helps define the optimal substrate-binding pocket's optimal size and suitable substrate binding orientation through its hydrogen bond

interactions (119). It should be noted that the residues mentioned above in eBCAT and hBCATs correspond to Tyr88 (Tyr71), Tyr159 (Tyr142), and Asp161 (Asp144) in Bat1 (Bat2), respectively (Fig. 3-12). Taking these results into account, it appears that Tyr and Arg residues [(Tyr88, Tyr159, Arg161) of Bat1, which is corresponded to (Tyr71, Tyr142, and Arg166) of Bat2] in BCATs are essential for recognizing and binding substrates and co-substrates. Another study reported that a patient with hypervalinemia and hyperleucine-isoleucinemia had amino acid substitutions (Arg170Gln and Glu264Lys) in hBCATm (78). Arg170 is identical to Arg143 in hBCATm, which we described above; we confirmed the identities of these residues by sequence alignment (Fig. 3-12), so I describe them according to their descriptions in the original papers. Perhaps, the conversion of the Tyr and Arg residues described above to other amino acids leads to a negative effect on BCAT function because of their crucial role in substrate-binding in BCATs, based on the previous findings and the results of this study.

Tyr31, Phe36, Arg97, Val109, Y129, and Y164 in eBCAT are identified as the residues involved in the dual recognition mechanism of hydrophobic side-chain substrates (BCKAs and BCAAs) and co-substrates that contain carboxylate groups in their side chain (KG and Glu) (113). These residues are also conserved in BCATs (Fig. 3-12). Together with the interaction with PLP and Lys159 (identical to Lys219 and Lys202 in Bat1 and Bat2, respectively) upon the transamination reaction processing, these results suggest that the yeast BCATs might have a similar recognition mechanism to eBCAT. Further investigation is needed to clarify substrates' recognition and binding mechanisms in BCATs.

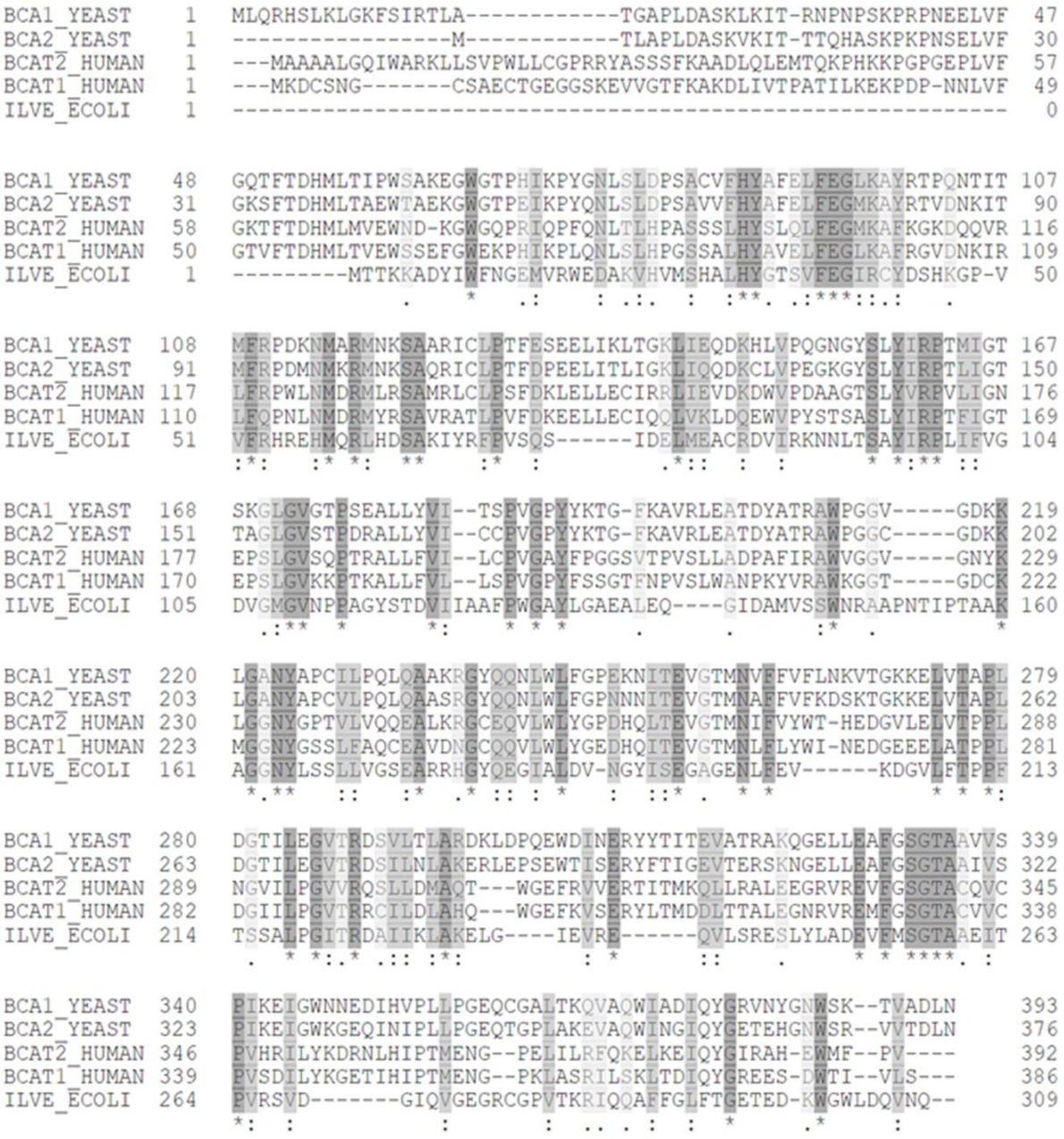

Fig. 3-12 Amino acid sequences alignment of BCATs from *S. cerevisiae*, human, and *E. coli*. The alignment was performed using the Clustal Omega program by alignment tool in the Uniprot database. BCA1_YEAST, BCA2_YEAST, BCAT2_HUMAN, BCAT1_HUMAN, and ILVE_ECOLI indicate Bat1, Bat2, hBCATm, hBCATc, and eBCAT, respectively. Grey boxes represent the similarity of amino acid residues between each BCAT. The percent identities of Bat1/mBCAT, Bat1/eBCAT, Bat2/cBCAT, Bat2/eBCAT, and Bat1/Bat2 are 43, 24, 48, 26, and 77%, respectively. * indicates a fully conserved residue position. : indicates conservation between groups of strongly similar properties (scoring > 0.5 in the Gonnet PAM 250 matrix). . indicates conservation between groups of weakly similar properties (scoring

=< 0.5 in the Gonnet PAM 250 matrix). - indicates the absence of corresponding amino acid residues at the positions.

Considering substrate specificity on BCATs, it is appropriate to consider the contribution of a side chain (the branched-aliphatic carbon chain) in substrates for recognizing BCAAs and BCKAs as a substrate. To identify the residues which contribute to being aware of an aliphatic side chain of substrates, I analyzed the residues that stabilize those aliphatic side chains of substrates bound to BCATs-PLP by confirming the distances (< 4Å) to the side-chain of each substrate (Fig. 3-7 to 3-10). As a result, I found some residues which had a hydrophobic side chain, such as Phe47 (aromatic), Tyr88, Tyr159 (aromatic), Val173 (aliphatic), Thr257 (polar neutral), and Ala335 (aliphatic) in Bat1 (which were corresponding to Phe30, Tyr71, Tyr142, Val156, Thr240, and Ala318 in Bat2, respectively). Notably, almost every Phe, Thr, and Ala residue involved in binding substrates was located within the range of 4Å from the aliphatic side chain of substrates. In fact, the patient with neurodevelopmental disorders, who also revealed elevated BCAA concentrations in plasma, had a paternally inherited hBCATm Val182Gly and a maternally inherited hBCATm Ala341Thr variant in the proband (79). These residues in hBCATm are corresponding to those in Bat1 and Bat2 (Fig. 3-12). Reasoning from the matters, a group of the residues is probably involved in recognizing and fixing an aliphatic side chain of substrates in BCATs by forming a hydrophobic interaction network.

3.2. *In vitro* investigation of Bat1 and Bat2

3.2.1. Construction, expression, and purification of the yeast recombinant Bat1 and Bat2

The previous study successfully declared the differences between transaminase activity of Bat1 and Bat2 using yeast cells extract with Bat1 or Bat2 disrupted (63). However, yeast cells still have the other transaminase enzymes, which are likely to disturb the enzymatic activity assay of Bat1 and Bat2. Instead, I used the recombinant purified scBCATs for enzymatic activity assay. The recombinant Bat1 and Bat2, tagged with N-terminal histidine, were expressed in *E. coli* BL21 (DE3) cells (Fig. 3-13). The result demonstrated that recombinant $Bat2^{WT}$ was wealthily purified by elution with 500 mM of imidazole. Concurrently, most recombinant $Bat1^{WT}$ appeared in the insoluble fraction and cannot be purified from Ni Sepharose 6 Fast Flow column (data not shown). In fact, a similar phenomenon was also reported to form the previous study while attempting to purify hBCATm (55).

To address the Bat1 expression and purification problem, I constructed the truncated Bat1^{WT} by removing the first 16 amino acid residues at N-terminus, named Bat1ΔN16^{WT}. Those 16 amino acids are encoded as a mitochondrial-targeting signal (MTS) (62). Then, the expression and purification of Bat1ΔN16^{WT} were operated (Fig. 3-13). By removing MTS at the N-terminus from Bat1, Bat1ΔN16^{WT} was predominantly expressed in the soluble fraction and was able to purify by elution with 500 mM imidazole, similar to Bat2^{WT} (Fig. 3-13). Noteworthy, the previous study also successfully purified the truncated Bat1 that lacked the amino acid residues 1-16, and this truncated Bat1 can measure the enzymatic activity (56).

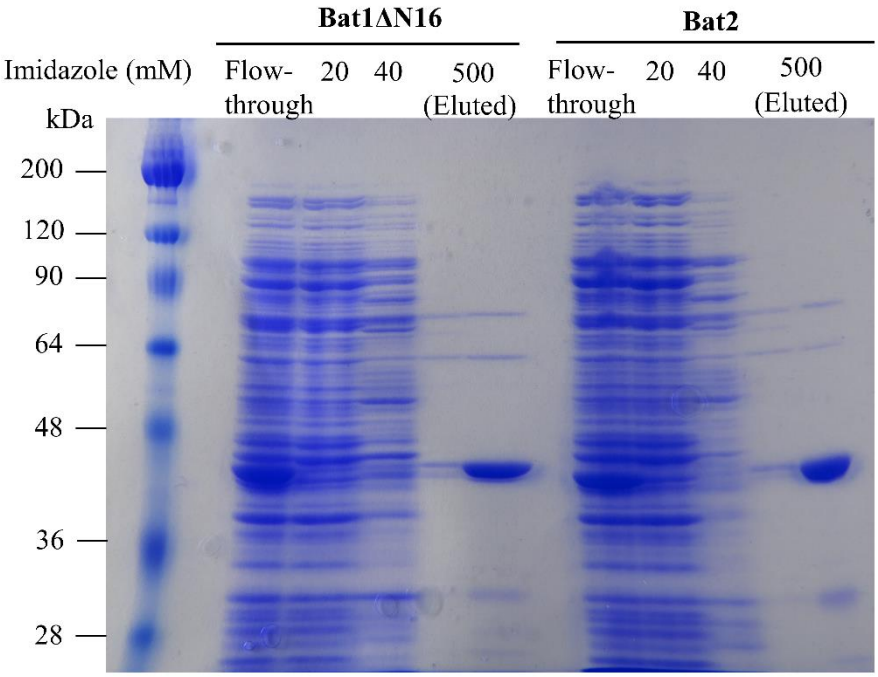

Fig. 3-13 Purification of Bat1ΔN16^{WT} and Bat2^{WT}. Bat1ΔN16^{WT} and Bat2^{WT} sizes were around 41.6 kDa. Ten µL of each sample were loaded to SDS-PAGE. BL21 (DE3) cells containing expression vectors that expressed Bat1ΔN16^{WT} and Bat2^{WT} were grown in M9 + 2% CAS amino acids. The target proteins' expression was induced by the addition of IPTG, incubated overnight at 18°C. The target proteins' expression was induced by adding 0.1 mM and 0.5 mM of IPTG, respectively, for Bat1ΔN16^{WT} and Bat2^{WT} and incubated at 18°C overnight.

3.2.2. Enzymatic activity of wild-type Bat1 and Bat2

As previously mentioned, no studies reported or investigated the enzymatic activity of scBCATs for transamination in both directions using the purified enzyme. Therefore, I

constructed and optimized an enzymatic activity assay system (data not shown). In practice, the optimized condition for forward-reaction assay of scBCATs is 20 mM of Glu, 1.5 mM of BCKAs, and 12 U of GDH at pH 8.0. On the other hand, reverse-reaction assay of scBCATs requires 1 mM of KG, 15 mM of BCAAs, and 24 U of GDH at pH 8.5.

Then, I examined the enzymatic activity of these two scBCAT isoforms (Fig. 3-14). The specific activity results of Bat1ΔN16^{WT} and Bat2^{WT} revealed a similar trend for each substrate. In practice, KIC exhibited the highest specific activity (14.7 ± 0.5 and 11.0 ± 0.2 U/mg, respectively, for Bat1ΔN16^{WT} and Bat2^{WT}) among the other BCKAs, followed by KIV (10.1 ± 0.5 and 9.6 ± 0.3 U/mg, respectively for Bat1ΔN16^{WT} and Bat2^{WT}) and KMV (7.8 ± 0.7 and 6.6 ± 0.9 U/mg, respectively for Bat1ΔN16^{WT} and Bat2^{WT}). On the other hand, the specific activity of all BCAAs exhibited a similar level for each of Bat1ΔN16^{WT} and Bat2^{WT} without the outstanding: 6.6 ± 1.0 U/mg for Bat1ΔN16^{WT} and 4.2 ± 0.1 Bat2^{WT} U/mg, 7.0 ± 0.5 U/mg for Bat1ΔN16^{WT} and 4.2 ± 0.1 Bat2^{WT} U/mg, and 6.4 ± 0.5 U/mg for Bat1ΔN16^{WT} and 4.0 ± 0.1 Bat2^{WT} U/mg, respectively for Val, Leu, and Ile. Interestingly, the specific activity of all BCKAs was higher than those of BCAAs for both Bat1ΔN16^{WT} and Bat2^{WT}, indicating that BCKAs are a better substrate for scBCATs than BCAAs. These results agree with the previously reported enzymatic activity for hBCATm and hBCATc. BCKAs exhibited a higher k_{cat}/K_m value than BCAAs, and KIC is the best substrate for hBCATm and hBCATc (55). Even though Bat1ΔN16^{WT} and Bat2^{WT} exhibited a similar specific activity trend for all substrates, the higher than those of Bat2^{WT}, some substrates demonstrated the different specific activity levels between Bat1ΔN16^{WT} and Bat2^{WT}; Bat1ΔN16^{WT} exhibited a higher level of specific activities for KIC and all BCAAs than Bat2^{WT}.

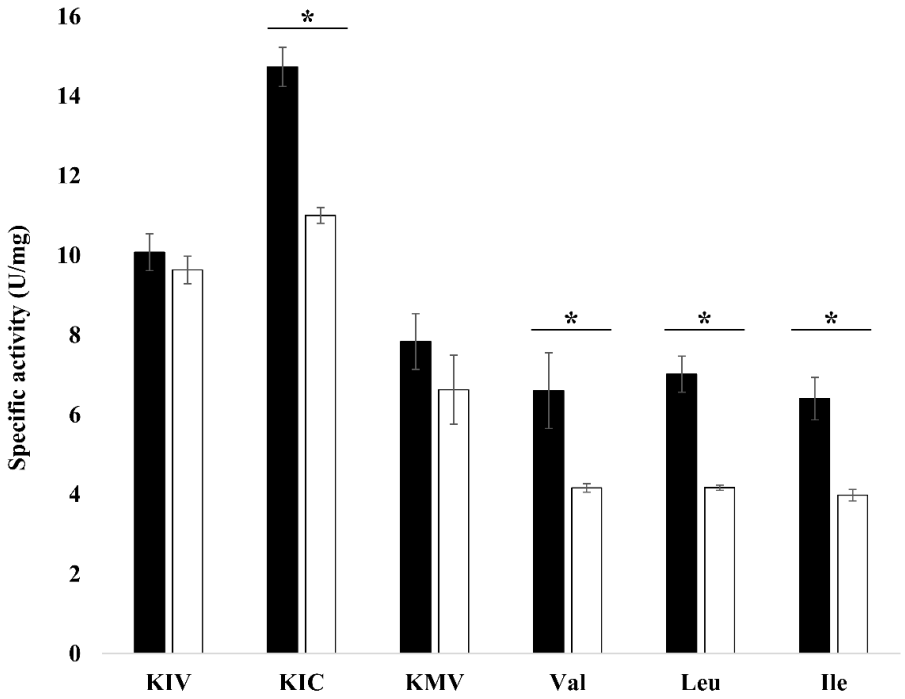

Fig. 3-14 Specific activity of Bat1ΔN16^{WT} (filled bar) and Bat2^{WT} (open bar). 2 µg of each purified Bat1ΔN16^{WT} and Bat2^{WT} were used in the assay. Specific activities were expressed as enzyme units per mg of the purified enzymes. The values are the mean and standard deviation values of three independent experiments. Differences in specific activity values toward each substrate where $p < 0.05$ (*) between Bat1ΔN16^{WT} versus Bat2^{WT} were verified by Student's T-test.

According to the specific activity of Bat1ΔN16^{WT} and Bat2^{WT} (Fig. 3-14), Bat1ΔN16^{WT} and Bat2^{WT} showed higher enzymatic activity toward BCKAs than BCAAs, which suggests that Bat1ΔN16^{WT} and Bat2^{WT} have substrates specificity. To further investigate the substrate specificity of Bat1ΔN16^{WT} and Bat2^{WT}, the specific activity of Bat1ΔN16^{WT} and Bat2^{WT} toward the non-native substrates of Bat1ΔN16^{WT} and Bat2^{WT} were analyzed (Tables 3-7 and 3-8). The highest specific activity of Bat1ΔN16^{WT} was obtained using Leu as a substrate. Otherwise, Val is the amino acid substrate with the highest specific activity for Bat2^{WT} (115 ± 0.3 % relative rate, compared to Leu). For Ile, Bat2^{WT} (95 ± 0.6 % relative rate, compared to Leu) can utilize Ile with a higher relative rate than Bat1ΔN16^{WT} (99 ± 0.3 % relative rate, compared to Leu). Interestingly, Bat1ΔN16^{WT} and Bat2^{WT} show differences in substrate specificity toward non-native amino acid substrates (Table 3-5). Bat2^{WT} can utilize Norleucine (69 ± 0.2 % relative rate, compared to Leu), Norvaline (7 ± 0.1 % relative rate, compared to Leu), and Methionine (73 ± 0.1 % relative rate, compared to Leu) with a higher rate than Bat1ΔN16^{WT} (64 ± 1, 5 ± 0.1, and 52 ± 0.3 % relative rate, compared to Leu, respectively for Norleucine, Norvaline, and Methionine). Otherwise, Bat1ΔN16^{WT} can utilize aspartate (12 ± 0.1 % relative rate, compared to Leu) with a higher rate than Bat2^{WT} (7 ± 0.1 % relative rate, compared to Leu). Moreover, Bat2^{WT} (94 ± 0.5 % relative rate, compared to KIC) can also utilize α-ketocaproate with a higher relative rate than Bat1ΔN16^{WT} (72 ± 1 % relative rate, compared to KIC) (Table 3-6).

Table 3-7 Substrate specificity of Bat1 and Bat2 toward amino acids

Amino acids	Relative rate (%)	
	Bat1ΔN16^{WT}	**Bat2^{WT}**
Leucine	100	100
Valine	91 ± 0.2	115 ± 0.3
Isoleucine	95 ± 0.6	99 ± 0.3
Norleucine	64 ± 1	69 ± 0.2
Norvaline	5 ± 0.1	7 ± 0.1
Aspartate	0	0
Methionine	52 ± 0.3	73 ± 0.1
Phenylalanine	12 ± 0.1	7 ± 0.1
Tryptophan	0	0

Table 3-8 Substrate specificity of Bat1 and Bat2 toward keto acids

Keto acids	Relative rate (%)	
	Bat1ΔN16^{WT}	**Bat2^{WT}**
KIC	100	100
KIV	68 ± 0.7	79 ± 0.7
KMV	54 ± 0.3	53 ± 0.4
α-ketocaproate	72 ± 1	94 ± 0.5

3.3. Engineering of BCAT to improve BCHA production

3.3.1. *In silico* investigation of BCAT variants

3.3.1.1. Screening for candidate amino acid residues for engineering

The transamination step of the Ehrlich degradation pathway is well-known as a rate-limiting step (51, 52). In *S. cerevisiae*, this transamination process is catalyzed by Bat1 (mitochondrial isoform) and Bat2 (cytosolic isoform). These two isozymes have compatibility in their function and impact on BCHA production (51, 62, 65). However, many studies suggested that Bat2 is likely to have more physiological impact on branched-chain higher alcohol (BCHA) production than Bat1: 1) deletion of *BAT2* gene together with other flavor compound production-genes leads to a significantly reduce in flavor compounds productivity (52), 2) Bat2 is necessary for the production of BCHAs when the yeast cells were cultivated in non-fermentable carbon source, i.e., ethanol (120), and 3) deletion of Bat2 shows decreasing in isobutanol and isoamyl alcohol contents (16, 51, 69). However, the natively or artificially constructed sBCAT variants that impact BCHA production or alter the enzymatic activity have not been widely reported. To design the specific and appropriate amino acid substitutions for this study, I selected the candidate residues of Bat2 based on the molecular docking results of Bat2 (section 3.1.2.2). I analyzed all residues within 5 angstroms surrounded by all substrates (Fig. 3-15).

As a result, 18 residues, located nearby substrates, were identified: Phe30, Tyr71, Phe76, Glu77, Gly78, Tyr142, Arg144, Leu154, Gly155, Val156, Tyr174, Lys202, Tyr207, Thr240, Gly316, Thr317, Ala318, and Ala319. Of which 18 residues, three residues (Tyr71, Tyr142, and Arg144) which are involved in hydrogen bond formation with substrates, as mentioned in the previous section (see also section 3.1.2.2), were omitted, together with the other three residues (Lys202, Tyr207, and Thr317) that involved in binding of PLP (121). In total, 12 residues of Bat2 (Phe30, Phe76, Glu77, Gly78, Leu154, Gly155, Val156, Tyr174, Thr240, Gly316, Ala318, and Ala319) were selected as candidate residues for *in silico* mutagenesis.

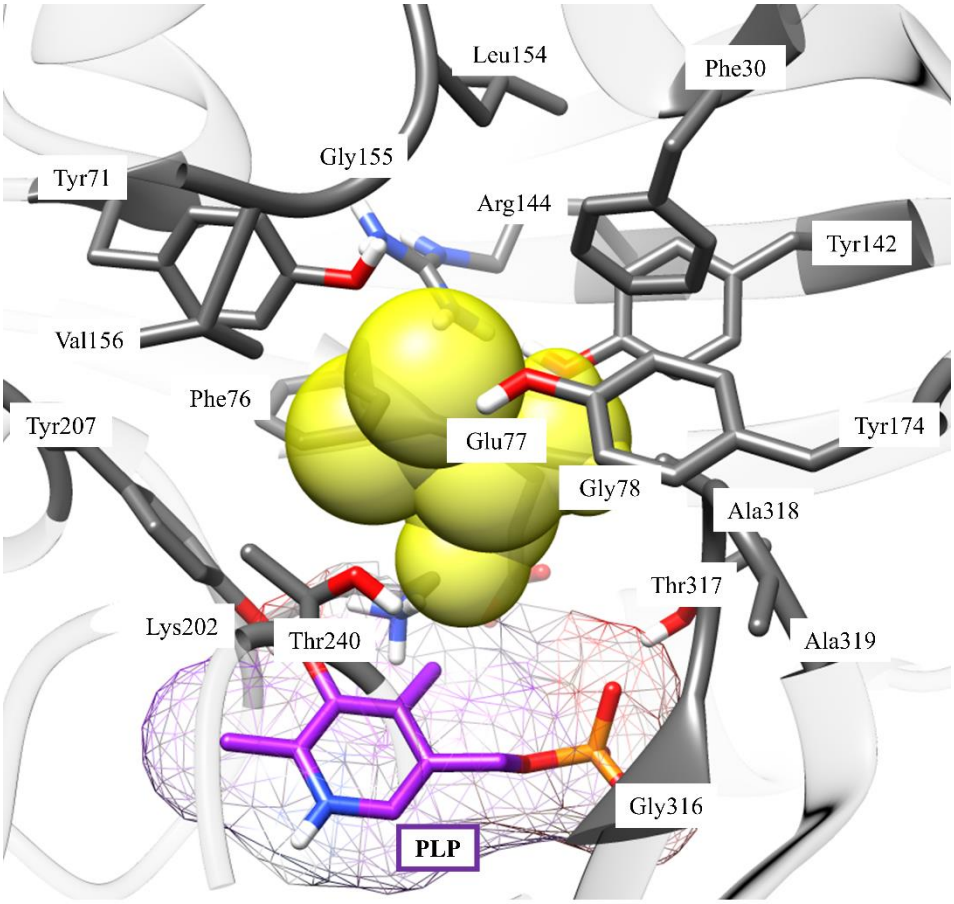

Fig. 3-15 Amino acid residues interacted with substrates at the Bat2 active site. The yellow sphere represents substrates that bind to the Bat2 active site. PLP was shown as a purple stick. Amino acid residues in the Bat2 active site that interact or surround substrates (5 angstroms) are shown as grey sticks [originally from (42)].

3.3.1.2. *In silico* screening the candidate amino acid substitutions on Bat2

Firstly, I screened for the amino acid substitutions that improve protein stability using CUPSAT (105). This web-server will automatically perform mutation from the original amino acid to all other amino acids, along with calculating the ΔΔG value for protein stability determination of each amino acid substitution. 82 amino acid substitutions {[Phe30 (F30C)], [Phe76 (F76C)], [Glu77 (E77T, E77Q, E77K, E77D, and E77H)], [Gly78 (G78V, G78L, G78I, G78M, G78T, G78F, G78K, G78N, G78E, G78R, and G78H)], [Leu154 (L154G, L154M, L154T, L154Q, L154K, L154E, L154R, and L154H)], [Gly155 (G155A, G155P, G155T, G155F, G155Q, and G155C)], [Tyr174 (Y174G, Y174A, Y174V, Y174L, Y174I, Y174M, Y174P, Y174S, Y174T, Y174Q, Y174K, Y174N, Y174C, Y174E, Y174D, Y174R, and Y174H)], [Thr240 (T240P, T240W, T240S, T240F, T240Q, and T240C)], [Gly316 (G316L,

G316I, G316W, G316S, G316T, G316Q, G316K, G316Y, G316N, G316E, G316D, G316R, and G316H)], [Ala318 (A318V, A318L, A318I, A318P, A318W, A318Q, A318Y, A318C, and A318H)], and [Ala319 (A319V, A319P, A319W, A319T, and A319R)]} in which increasing protein stability (showing positive in ΔΔG value) were selected for further analysis (Table 3-9).

Table 3-9 Predicted the effect of amino acid substitutions on protein stability. ΔΔG was calculated from CUPSAT. The positive and negative ΔΔG value indicates an increase and decrease in protein stability, respectively [originally from (42)].

Original amino acid	Mutated amino acid	Overall Stability	Torsion	Predicted ΔΔG (kcal/mol)
Phe30	Cys	Stabilizing	Unfavorable	0.06
Phe76	Cys	Stabilizing	Favorable	2.89
Glu77	Thr	Stabilizing	Favorable	2.43
	Gln	Stabilizing	Unfavorable	1.66
	Lys	Stabilizing	Unfavorable	4.85
	Asp	Stabilizing	Unfavorable	1.73
	His	Stabilizing	Favorable	3.93
Gly78	Val	Stabilizing	Unfavorable	0.53
	Leu	Stabilizing	Unfavorable	4.17
	Ile	Stabilizing	Unfavorable	1.31
	Met	Stabilizing	Unfavorable	1.95
	Thr	Stabilizing	Unfavorable	1.72
	Phe	Stabilizing	Favorable	1.33
	Lys	Stabilizing	Unfavorable	1.58
	Asn	Stabilizing	Favorable	1.65
	Glu	Stabilizing	Unfavorable	5.54
	Arg	Stabilizing	Unfavorable	3.06
	His	Stabilizing	Favorable	4.66

Leu154	Gly	Stabilizing	Unfavorable	0.76
	Met	Stabilizing	Unfavorable	1.97
	Thr	Stabilizing	Unfavorable	0.84
	Gln	Stabilizing	Favorable	0.94
	Lys	Stabilizing	Unfavorable	5.79
	Glu	Stabilizing	Unfavorable	2.39
	Arg	Stabilizing	Unfavorable	4.92
	His	Stabilizing	Favorable	3.21
Gly155	Ala	Stabilizing	Favorable	0.08
	Pro	Stabilizing	Favorable	1.21
	Thr	Stabilizing	Unfavorable	0.59
	Phe	Stabilizing	Unfavorable	0.79
	Gln	Stabilizing	Unfavorable	0.74
	Cys	Stabilizing	Unfavorable	0.62
Tyr174	Gly	Stabilizing	Unfavorable	1.14
	Ala	Stabilizing	Unfavorable	1.21
	Val	Stabilizing	Unfavorable	0.69
	Leu	Stabilizing	Favorable	0.74
	Ile	Stabilizing	Unfavorable	2.84
	Met	Stabilizing	Favorable	2.72
	Pro	Stabilizing	Unfavorable	0.01
	Ser	Stabilizing	Favorable	1.23
	Thr	Stabilizing	Favorable	1.37
	Gln	Stabilizing	Favorable	0.98
	Lys	Stabilizing	Favorable	1.67
	Asn	Stabilizing	Favorable	1.44

	Cys	Stabilizing	Unfavorable	3.13
	Glu	Stabilizing	Unfavorable	2.25
	Asp	Stabilizing	Favorable	2.0
	Arg	Stabilizing	Unfavorable	0.05
	His	Stabilizing	Favorable	0.53
Thr240	Pro	Stabilizing	Unfavorable	0.74
	Trp	Stabilizing	Unfavorable	0.4
	Ser	Stabilizing	Unfavorable	0.62
	Phe	Stabilizing	Favorable	0.1
	Gln	Stabilizing	Unfavorable	0.06
	Cys	Stabilizing	No change	1.34
Gly316	Leu	Stabilizing	Unfavorable	0.04
	Ile	Stabilizing	Unfavorable	0.87
	Trp	Stabilizing	Unfavorable	3.44
	Ser	Stabilizing	Favorable	0.44
	Thr	Stabilizing	Unfavorable	1.4
	Gln	Stabilizing	Unfavorable	3.03
	Lys	Stabilizing	Unfavorable	2.35
	Tyr	Stabilizing	Favorable	1.02
	Asn	Stabilizing	Unfavorable	2.31
	Glu	Stabilizing	Unfavorable	2.49
	Asp	Stabilizing	Unfavorable	4.0
	Arg	Stabilizing	Unfavorable	3.09
	His	Stabilizing	Favorable	1.17
Ala318	Val	Stabilizing	Favorable	0.95
	Leu	Stabilizing	Favorable	0.09

	Ile	Stabilizing	Favorable	0.75
	Pro	Stabilizing	Unfavorable	1.37
	Trp	Stabilizing	Favorable	1.63
	Gln	Stabilizing	Favorable	0.15
	Tyr	Stabilizing	Favorable	0.02
	Cys	Stabilizing	Unfavorable	0.38
	His	Stabilizing	Unfavorable	0.17
Ala319	Val	Stabilizing	Unfavorable	0.1
	Pro	Stabilizing	Unfavorable	0.59
	Trp	Stabilizing	Favorable	0.48
	Thr	Stabilizing	Favorable	0.74
	Arg	Stabilizing	No change	0.06

After that, all 82 amino acid substitutions were analyzed, an effect of amino acid substitution on substrate binding affinities using mCSM-lig (106). As a result, only 7 amino acid substitutions {[Gly78 (G78N)], [Leu154 (L154Q)], [Tyr174 (Y174D)], [Gly316 (G316W and G316S)], [Ala318 (A318Q)] and [Ala319 (A319T)]} can increase substrate binding affinities, especially when considering BCAAs as a substrate (Table 3-10). Among all seven amino acid substitutions, G316S shows the highest rate of substrate binding affinities toward all substrates, followed by A318Q, Y174D, and A319T, respectively. On the other hand, G78N and L154Q showed a slight change in substrate binding affinities from wild-type. Interestingly, the different substituted amino acids at a similar position (G316W) increase binding affinities when using BCAAs and co-substrates as a substrate. However, the binding affinities toward BCKAs, KIV, and KIC, are lower than wild-type, indicating the change in this substitution's catalytic properties.

Table 3-10 Predicted effect of amino acid substitutions on substrate binding affinities [originally from (42)]

Amino acid substitutions	Change in substrate binding affinities from the original amino acid residue					
	KIV	**KIC**	**KMV**	**Val**	**Leu**	**Ile**
G78N	-0.059	0.006	-0.016	0.063	0.061	0.1
L154Q	0.031	0.106	-0.01	0.00	0.001	0.145
Y174D	0.366	0.383	0.401	0.473	0.552	0.48
G316W	-0.056	-0.011	0.016	0.037	0.248	0.081
G316S	0.638	0.716	0.749	0.824	1.034	0.888
A318Q	0.572	0.63	0.657	0.737	0.854	0.779
A319T	0.159	0.205	0.252	0.299	0.493	0.299

The values were calculated as the logarithmic change of binding affinity from the original amino acid residue; the positive and negative values indicate an increase and decrease in binding affinity, respectively.

Taking the prediction effect of amino acid substitutions on substrate binding affinity (Table 3-10) and protein stability (Table 3-9), it is clear that G316S increases protein stability and substrate binding affinities toward all substrates (especially BCAAs). Indeed, G316S was the best-candidate amino acid substitution for further *in vivo* and *in vitro* investigation. Noteworthy, G316W shows an increase in protein stability and is interested in changing substrate binding affinities. Thus, these two amino acid substitutions of Bat2 (G316S and G316W) that show an increase in substrate binding affinities and protein stability from wild type were appropriately selected for *in vivo* experiments.

3.3.2. *In vivo* investigation of BCAT variants

3.3.2.1. Construction of the yeast transformants harboring BCAT-variants

S. cerevisiae harbors two BCAT isoforms, Bat1 in the mitochondria and Bat2 in the cytosol (41, 61). Both scBCATs play an essential role in BCAA metabolism. These two BCAT isoforms have 77% identity in primary amino acid sequences. By checking amino acid sequence alignment between Bat1 and Bat2 in detail, I found that G316 of Bat2 is conserved with G333 of Bat1 (Fig. 3-12).

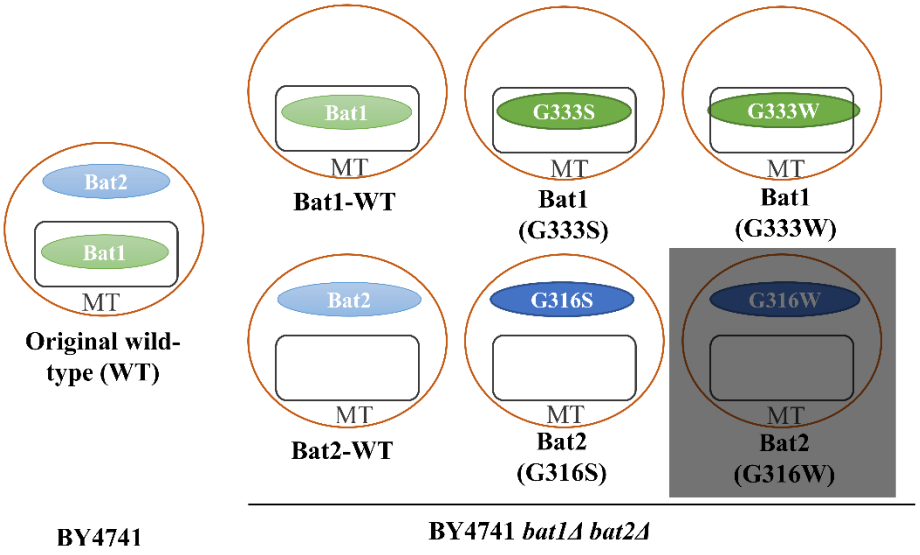

Fig. 3-16 Schematic of the yeast transformant strains constructed to investigate an effect of amino acid substitutions on Bat1 and Bat2. The yeast transformants named original wild-type; WT indicates BY4741 (empty vector; EV). In contrast, the yeast transformants named Bat1-WT, Bat1-G333S, and Bat1-G333W indicate BY4741*bat1*Δ*bat2*Δ (Bat1), BY4741*bat1*Δ*bat2*Δ (Bat1^{G333S}), and BY4741*bat1*Δ*bat2*Δ (Bat1^{G333W}), respectively. Meanwhile, the yeast transformants named Bat2-WT, Bat2-G316S, and Bat2-G316W indicate BY4741*bat1*Δ*bat2*Δ (Bat2), BY4741*bat1*Δ*bat2*Δ (Bat2G316S), and BY4741*bat1*Δ*bat2*Δ (Bat2^{G316W}), respectively. The rectangle represents mitochondria (MT) in which Bat1 is localized. The blank space in the circle represents cytosol in which Bat2 is localized. Grey-box represents strain that cannot grow.

Thus, I constructed both Bat1 and Bat2 variants with the same amino acid substitution: Bat1-variants [bearing amino acid substitution from Gly333 to Ser333 and Gly333 to Trp333 (G333S and G333W)] and Bat2-variants [bearing amino acid substitution from G316 to Ser316 and Gly316 to Trp316 (G316S and G316W)] (Fig. 3-16). I examined the effect of these amino acid substitutions by altering the laboratory strain (BY4741*bat1*Δ*bat2*Δ, the strain lacking both Bat1 and Bat2) and transforming it with the plasmid expressing either Bat1-series [wild-type

of Bat1 (Bat1-WT) and Bat1-variants' (G333S and G333W)] or Bat2-series [wild-type of Bat2 (Bat2-WT) and Bat2-variants' (G316S and G316W)]. These variants harbored only one BCAT isoform in their cells to eliminate the redundancy effect of Bat1 and Bat2 on yeast cells. Indeed, the control strains used in this study were Bat1-WT, Bat2-WT, and the original wild-type (WT) [BY4741 (bearing both Bat1 and Bat2), transformed with an empty vector]. Unfortunately, Bat2-G316W cannot grow. Thus, I used the other seven transformant strains [WT, Bat1-WT, Bat1-variants (Bat1-G333S and Bat1-G333W), Bat2-WT, and Bat2-variant (Bat2-G316S)] for further experiments (Fig. 3-16).

3.3.2.2. Growth phenotype and expression of BCAT variants

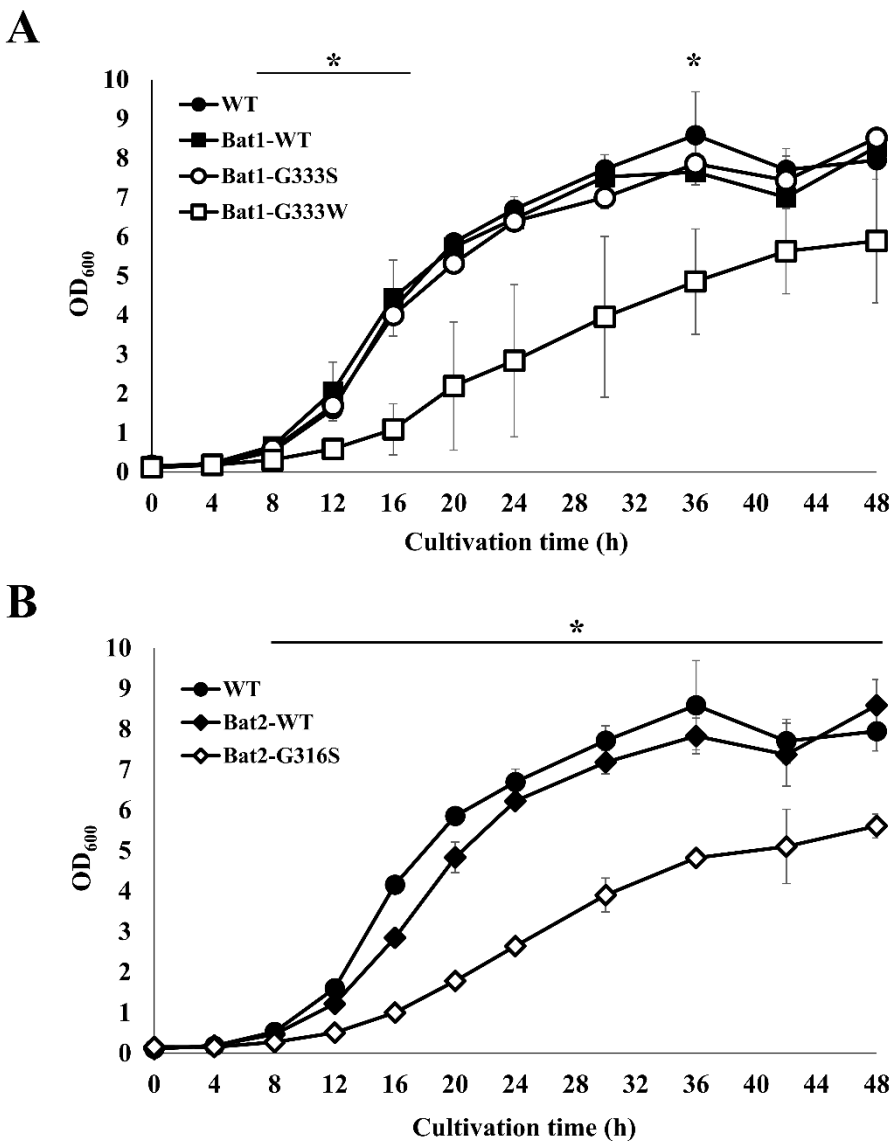

Fig. 3-17 Growth phenotype of BCAT variants. The yeast transformant named WT indicates BY4741 (empty vector; EV). In contrast, the yeast transformants named Bat1-WT, Bat1-G333S, and Bat1-G333W indicate BY4741*bat1*Δ*bat2*Δ (Bat1), BY4741*bat1*Δ*bat2*Δ ($Bat1^{G333S}$), and BY4741*bat1*Δ*bat2*Δ ($Bat1^{G333W}$), respectively. Meanwhile, the yeast transformants named Bat2-WT and Bat2-G316S indicate BY4741*bat1*Δ*bat2*Δ (Bat2) and BY4741*bat1*Δ*bat2*Δ ($Bat2^{G316S}$), respectively. (A) growth phenotypes of Bat1-WT (filled rectangle), Bat1-G333S (open circle), and Bat1-G333W (open rectangle). (B) growth phenotypes of Bat2-WT (filled diamond) and Bat2-G316S (open diamond). WT (filled circle) was used as an original strain for comparison in the Bat1 and Bat2 series. Yeast cells were cultivated in the SD medium. Each point represents the mean with standard deviations from three independent experiments. Differences where $p < 0.05$ (*) of Bat1-G333W and Bat2-G316S versus WT were significant when verified by the student's t-test [originally from (42)].

Bat1 and Bat2 of *S. cerevisiae* are involved in the production of BCHA and impact yeast cell growth, especially in minimal media, since they correspond to the biosynthesis of vital amino acids, BCAAs (62, 71). Therefore, I first investigated the growth phenotype of yeast cells that expressed scBCAT variants in minimal media by monitoring OD_{600} values over time (Fig 3-17). In practice, strains Bat1-WT and Bat1-G333S displayed the growth phenotype as same as WT. In contrast, strain Bat1-G333W exhibited a significantly slower growth phenotype compared to Bat1-WT and WT (Fig. 3-16A). Meanwhile, strain Bat2-G316S showed a significantly slower growth phenotype than Bat2-WT and WT (Fig. 3-17B).

Next, the expression of BCAT proteins ($Bat1^{WT}$, $Bat1^{G333S}$, $Bat1^{G333W}$, $Bat2^{WT}$, and $Bat2^{G316S}$) in *S. cerevisiae* cells was confirmed by western blot using a GFP tag fused to the C-terminus of BCATs ($Bat1^{WT}$-GFP, $Bat1^{G333S}$-GFP, $Bat1^{G333W}$-GFP, $Bat2^{WT}$-GFP, and $Bat2^{G316S}$-GFP), based on plasmid pRS416-*BAT1* and pRS415-*BAT2* fused to GFP [construct from the previous study (62)]. The western blot results demonstrated that both wild-type BCATs ($Bat1^{WT}$ and $Bat2^{WT}$) and variant BCATs ($Bat1^{G333S}$, $Bat1^{G333W}$, and $Bat2^{G316S}$) were expressed in *S. cerevisiae* strain BY4741*bat1*Δ*bat2*Δ (Fig. 3-18).

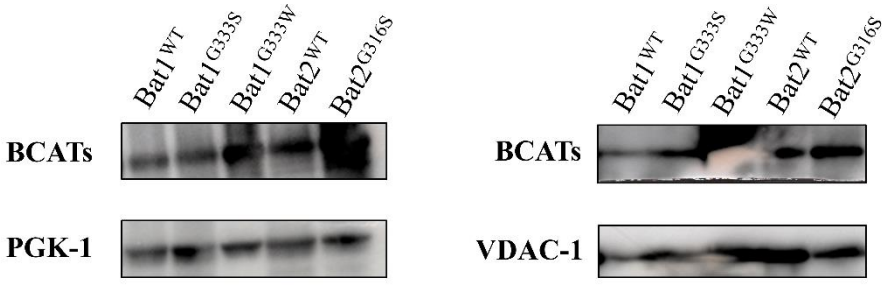

Fig. 3-18 Western blotting analysis of the BCAT variants expressing transformants. The two membranes (left and right) indicate protein extracts prepared from two independent colonies, grown in SD+His/Met medium for 72 h. $Bat1^{WT}$, $Bat1^{G333S}$, and $Bat1^{G333W}$ indicate BY4741*bat1*Δ*bat2*Δ (Bat1-GFP), BY4741*bat1*Δ*bat2*Δ ($Bat1^{G333S}$-GFP), and BY4741*bat1*Δ*bat2*Δ ($Bat1^{G333W}$-GFP), respectively. Meanwhile, the yeast transformants named $Bat2^{WT}$ and $Bat2^{G316S}$ indicate BY4741*bat1*Δ*bat2*Δ (Bat2-GFP) and BY4741*bat1*Δ*bat2*Δ ($Bat2^{G316S}$-GFP), respectively. PGK-1 and VDAC-1 (Porin) proteins demonstrated loading control.

3.3.2.3. Production of BCHA from BCAT variants

My previous study revealed that the growth defected phenotype of the yeast cells lacking Bat1 is related to changes in metabolites production (71). According to the growth defected phenotype of BCAT-variants from the previous section, it was likely that those variants exhibited the change in metabolites of BCAT, specifically branched-chain higher alcohols (BCHAs) and branched-chain amino acids (BCAAs). Hence, I examined the production of BCHAs (isobutanol, isoamyl alcohol, and active amyl alcohol) in the fermentation broth after cultivation with the yeast strains for three days (Fig. 3-19). Briefly, strain Bat1-G333S and Bat1-G333W exhibited a higher amount of BCHAs, isobutanol, and isoamyl alcohol, than WT and Bat1-WT. Surprisingly, all BCHA contents (isobutanol, isoamyl alcohol, and active amyl alcohol) of Bat1-G333W (131 ± 43, 79 ± 11, and 13 ± 1 mg/L, respectively) were greatly increased from Bat1-WT (16 ± 3, 15 ± 2, and 4 ± 1 mg/L, respectively) and WT (7 ± 1, 10 ± 2, and 3 ± 1 mg/L, respectively) (Fig 3-18A). Meanwhile, BCHA contents (isobutanol, isoamyl alcohol, and active amyl alcohol) of strain Bat2-G316S (122 ± 4, 81 ± 2, and 16 ± 1 mg/L, respectively) also exhibited the greatest increase from Bat2-WT (45 ± 2, 45 ± 2, and 14 ± 1 mg/L, respectively) and (7 ± 1, 10 ± 2, and 3 ± 1 mg/L, respectively) (Fig. 3-18B). The yeast transformant strains in this study that exhibited the highest BCHA productivity were Bat1-G333W and -Bat2G316S, respectively, for Bat1- and Bat2-variant. The productivity of these two transformant strains was: 18.7-folded (Bat1-G333W) and 17.4-folded (Bat2-G316S), 7.9-folded (Bat1-G333W) and 8.1-folded (Bat2-G316S), and 4.3-folded (Bat1-G333W) and 4.6-folded (Bat2-G316S) compared to WT strain, respectively for isobutanol, isoamyl alcohol, and active amyl alcohol.

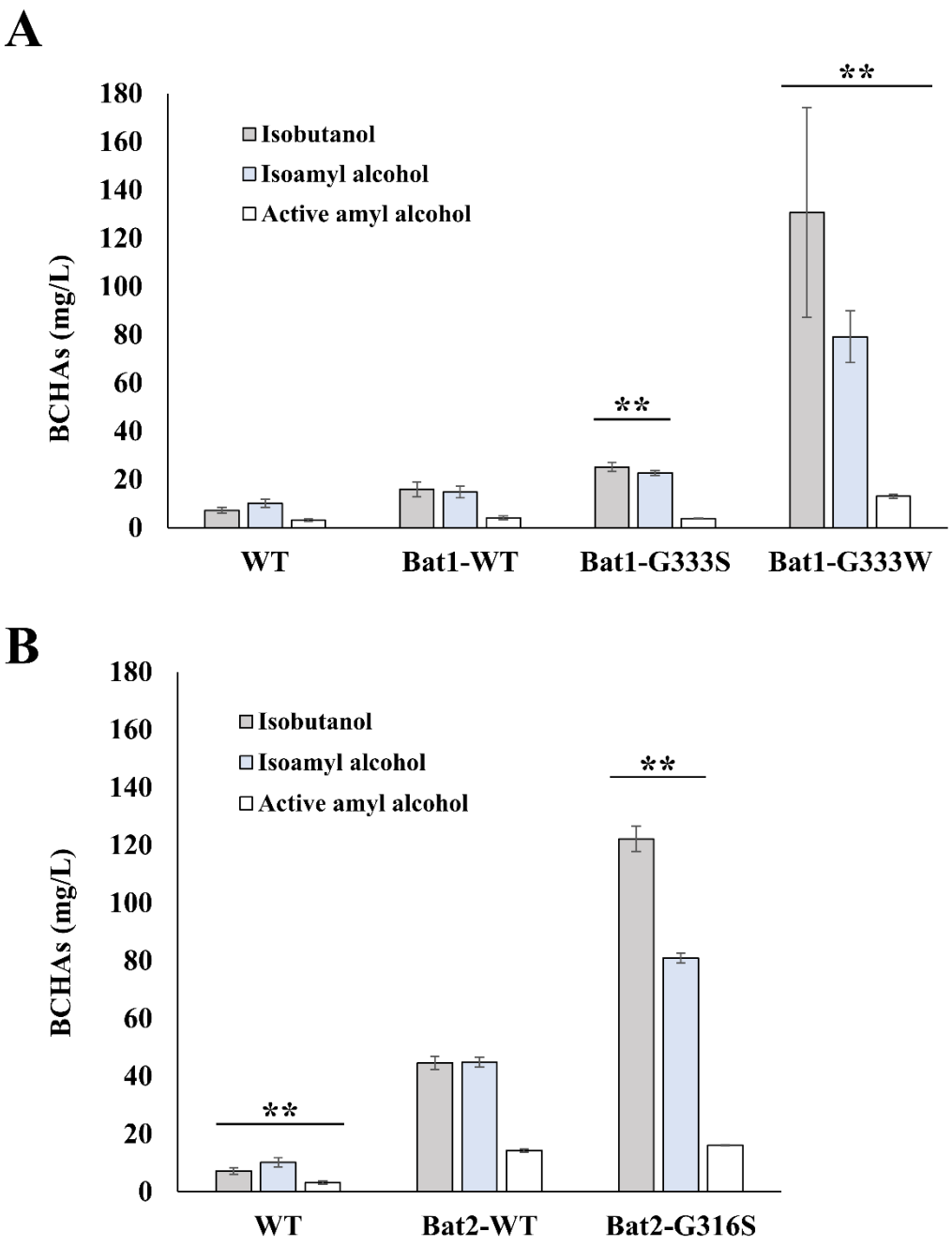

Fig. 3-19 Production of BCHAs from the yeast transformants. The yeast transformants named original wild-type; WT indicates BY4741 (empty vector; EV). In contrast, the yeast transformants named Bat1-WT, Bat1-G333S, and Bat1-G333W indicate BY4741*bat1*Δ*bat2*Δ (Bat1), BY4741*bat1*Δ*bat2*Δ (Bat1^{G333S}), and BY4741*bat1*Δ*bat2*Δ (Bat1^{G333W}), respectively. Meanwhile, the yeast transformants named Bat2-WT and Bat2-G316S indicate BY4741*bat1*Δ*bat2*Δ (Bat2) and BY4741*bat1*Δ*bat2*Δ (Bat2^{G316S}), respectively. (A) BCHA contents of Bat1-WT, Bat1-G333S, and Bat1-G333W. (B) BCHA contents of Bat2-WT and Bat2-G316S. WT was used as an original strain for comparison in both Bat1- and Bat2-series. Yeast cells were cultivated in the SD medium for three days. The supernatants from each cultured

broth were used to measure BCHA contents by GC-MS. Each point represents the mean with standard deviations from three independent experiments. Differences where $p < 0.01$ (**) versus controls (Bat1-WT or Bat2-WT) were significant when verified by the non-repeated measured ANOVA followed by the Bonferroni correction [originally from (42)].

3.3.2.4. Production of BCAAs from BCAT variants

Another important metabolite from BCAT is BCAA. Thus, I next measured the BCAA contents of the transformant cell (Fig 3-20). Unlike the BCHA content, the BCAA content of all Bat1- and Bat2-variants were changed from their wild-type and original wild-type. Strain Bat1-G333S (7.5 ± 0.4, 5.6 ± 0.6, and 3.7 ± 0.4 µmol/g-dry cell weight, respectively for Val, Leu, and Ile) had lower Leu and Ile contents than Bat1-WT (8.4 ± 0.2, 7.2 ± 0.8, and 4.6 ± 0.4 µmol/g-dry cell weight, respectively for Val, Leu, and Ile) and WT (8.0 ± 0.9, 6.7 ± 0.8, and 4.4 ± 0.5 µmol/g-dry cell weight, respectively for Val, Leu, and Ile). Meanwhile, all BCAA contents of strain Bat1-G333W (4.4 ± 1.0, 4.7 ± 0.1, and 3.3 ± 0.3 µmol/g-dry cell weight, respectively for Val, Leu, and Ile) were lower than those of Bat1WT and WT (Fig. 3-20A). Leu and Ile contents of Bat2-G316S (5.9 ± 0.4, 5.7 ± 0.3, and 4.0 ± 0.4 µmol/g-dry cell weight, respectively for Val, Leu, and Ile) were higher than those of Bat2-WT (5.0 ± 0.2, 4.2 ± 0.3, and 2.9 ± 0.2 µmol/g-dry cell weight, respectively for Val, Leu, and Ile). However, these contents of Bat2-G316S were still lower than those of WT.

It should be noted that the *in vivo* difference between strain Bat2-WT and WT, including growth defected phenotype, lower in BCAA contents and higher in BCHA contents than WT strain were well-studied in the previous studies (62, 71). The changes in BCAA contents of the Bat1- and Bat2-variants indicated a change in enzymatic properties of those variant enzymes from the wild-type, which is mandatory for further examination by *in vitro* enzymatic study.

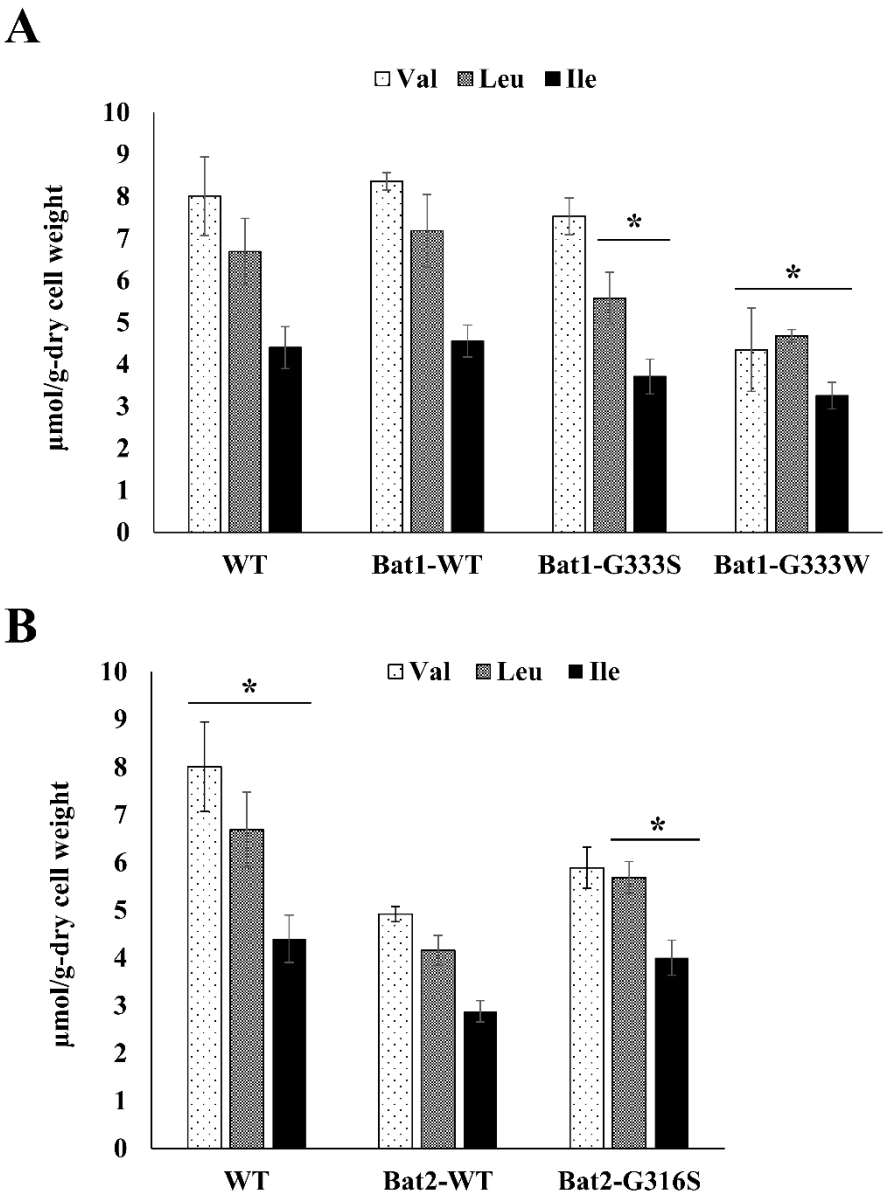

Fig. 3-20 Production of BCAAs from the yeast transformants. The yeast transformants named original wild-type; WT indicates BY4741 (empty vector; EV). In contrast, the yeast transformants named Bat1-WT, Bat1-G333S, and Bat1-G333W indicate BY4741*bat1*Δ*bat2*Δ (Bat1), BY4741*bat1*Δ*bat2*Δ (Bat1G333S), and BY4741*bat1*Δ*bat2*Δ (Bat1G333W), respectively. Meanwhile, the yeast transformants named Bat2-WT and Bat2-G316S indicate BY4741*bat1*Δ*bat2*Δ (Bat2) and BY4741*bat1*Δ*bat2*Δ (Bat2G316S), respectively. (A) BCAA contents of Bat1-WT, Bat1-G333S, and Bat1-G333W. (B) BCHA contents of Bat2-WT and Bat2-G316S. WT was used as an original strain for comparison in both Bat1- and Bat2-series. Intracellular BCAA contents were analyzed from the yeast cells cultured in an SD medium for two days. Each point represents the mean with standard deviations from three independent experiments. Differences where $p < 0.05$ (*) versus controls (Bat1-

WT or Bat2-WT) were significant when verified by the non-repeated measured ANOVA followed by the Bonferroni correction [originally from (42)].

3.3.3. *In vitro* investigation of BCAT variants

3.3.3.1. Construction, expression, and purification of the yeast recombinant-BCATs

I next attempted to purify the recombinant variant BCATs from *E. coli* BL21 (DE3) cells using Ni Sepharose 6 Fast Flow column as same as the wild-type BCATs (Bat1ΔN16^{WT} and Bat2^{WT}). Notably, the recombinant variant of Bat1 (Bat1^{G333S}) was truncated (without amino acid residues 1-16) as same as the Bat1 wild-type. As a result, I finally purified Bat1ΔN16^{WT}, Bat2^{WT}, Bat1ΔN16^{G333S}, and Bat2^{G316S} from E. coli BL21 (DE3) cells (Fig. 3-21).

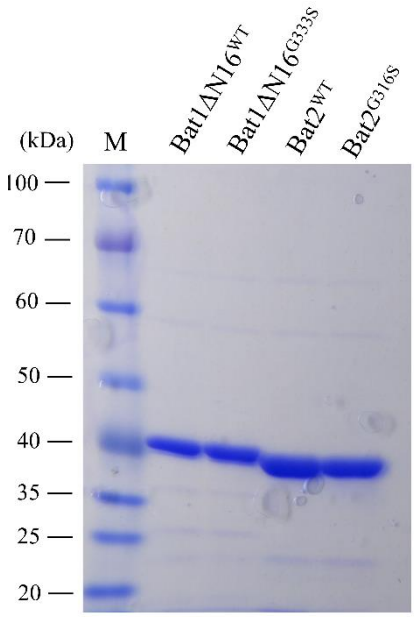

Fig. 3-21 SDS-polyacrylamide gel electrophoresis of the purified recombinant BCATs. Lane M: Molecular mass standards, Bat1ΔN16^{WT}, Bat1ΔN16^{G333S}, Bat2^{WT}, and Bat2^{G316S}: recombinant Bat1 (without amino acid residues 1-16 at N-terminus), G333S variant of recombinant Bat1 (without amino acid residues 1-16 at N-terminus), recombinant Bat2, and G316S variant of the recombinant Bat2 [originally from (42)].

3.3.3.2. Effects of amino acid substitutions in BCATs on the enzymatic activity

Next, I measured the enzymatic activity of BCAT variants (Bat1ΔN16^{G333S} and Bat2^{G316S}) versus wild-type BCATs (Bat1ΔN16^{WT} and Bat2^{WT}) using all substrates [BCKAs (KIV, KIC, and KMV) and BCAAs (Val, Leu, and Ile)] to trigger both forward (biosynthesis of BCAA, using BCKA as the substrate) and reverse reactions (degradation of BCAA, using BCKA as the substrate) of BCATs (Table 3-11). When BCKAs (KIV, KIC, and KMV) were used as substrates for BCAA synthesis (i.e., for monitoring the forward reaction of BCAT), Bat1ΔN16^{G333S} exhibited higher apparent K_m values (2.73 mM, 1.57 mM, and 0.548 mM for KIV, KIC, and KMV, respectively) than did Bat1ΔN16^{WT} (Km = 0.298, 0.323, and 0.218 mM for KIV, KIC, and KMV, respectively). Bat2^{G316S} also showed apparent K_m values toward BCKAs (1.73, 0.681, and 0.308 mM for KIV, KIC, and KMV, respectively) that were higher than the apparent K_m values of Bat2^{WT} (0.180, 0.212, and 0.150 mM for KIV, KIC, and KMV, respectively). Also, the apparent k_{cat} values of Bat1ΔN16^{G333S} (2.05, 4.95, and 1.46 s-1 for KIV, KIC, and KMV, respectively) and Bat2^{G316S} (1.79, 5.42, and 2.01 s-1 for KIV, KIC, and KMV, respectively) were lower than those of Bat1ΔN16^{WT} (9.55, 15.40, and 4.73 s^{-1} for KIV, KIC, and KMV, respectively) and Bat2^{WT} (8.05, 11.59, and 5.48 s-1 for KIV, KIC, and KMV, respectively). Therefore, the apparent k_{cat}/K_m values of Bat1ΔN16^{G333S} (0.751, 3.15, and 2.66 $mM^{-1}\cdot s^{-1}$ for KIV, KIC, and KMV, respectively) and Bat2^{G316S} (1.03, 7.96, and 6.53 $mM^{-1}\cdot s^{-1}$ for KIV, KIC, and KMV, respectively) were significantly lower than those of Bat1ΔN16^{WT} (32.1, 47.7, and 21.7 $mM^{-1}\cdot s^{-1}$ for KIV, KIC, and KMV, respectively) and Bat2^{WT} (44.7, 54.7, and 36.5 $mM^{-1}\cdot s^{-1}$ for KIV, KIC, and KMV, respectively).

Using BCAAs as a substrate for monitoring the reverse reaction of BCAT, we found that Bat1ΔN16^{G333S} and Bat2^{G316S} also displayed a similar trend in their forward reactions, which reduced the catalytic properties compared with Bat1ΔN16^{WT} and Bat2^{WT}, respectively. The apparent K_m values of Bat1ΔN16^{G333S} (7.70, 3.08, and 4.23 mM for Val, Leu, and Ile, respectively) and Bat2^{G316S} (13.3, 3.89, and 3.40 mM for Val, Leu, and Ile, respectively) were significantly higher than those of Bat1ΔN16^{WT} (0.454, 0.285, and 0.220 mM for Val, Leu, and Ile, respectively) and Bat2^{WT} (0.511, 0.189, and 0.119 mM for Val, Leu, and Ile, respectively). Similarly, both Bat1ΔN16^{G333S} and Bat2^{G316S} exhibited the apparent k_{cat} values (Bat1ΔN16^{G333S}: 0.834, 0.701, and 0.769 s^{-1} for Val, Leu, and Ile, respectively; Bat2^{G316S}: 1.40, 1.61, and 1.80 s^{-1} for Val, Leu, and Ile, respectively) that were significantly lower than those of Bat1ΔN16^{WT} (3.37, 3.51, and 3.74 s^{-1} for Val, Leu, and Ile, respectively) and Bat2^{WT} (2.71, 2.30, and 2.61 s^{-1} for Val, Leu, and Ile, respectively). The significantly higher apparent K_m and lower k_{cat} values of BCAT variants eventually led to a major reduction in apparent k_{cat}/K_m values of Bat1ΔN16^{G333S} (0.108, 0.228, and 0.182 $mM^{-1}\cdot s^{-1}$ for Val, Leu, and Ile, respectively) and Bat2^{G316S} (0.106, 0.414, and 0.529 $mM^{-1}\cdot s^{-1}$ for Val, Leu, and Ile, respectively) compared to the corresponding values for Bat1ΔN16^{WT} (7.42, 12.3, and 17.0 $mM^{-1}\cdot s^{-1}$ for Val, Leu, and Ile, respectively) and Bat2^{WT} (5.30, 12.2, and 21.9 $mM^{-1}\cdot s^{-1}$ for Val, Leu, and Ile, respectively).

In conclusion, all of the kinetic parameters of the BCAT variants (Bat1ΔN16^{G333S} and Bat2^{G316S}) showed an increase in the K_m values with a decrease in the k_{cat} and k_{cat}/K_m values relative to their wild-type enzymes (Bat1ΔN16^{WT} and Bat2^{WT}), indicating that the catalytic activities of the BCAT variants were reduced.

Table 3-11 Kinetic parameters of wild-type (Bat1 and Bat2) and variant BCATs (Bat1^{G333S} and Bat2^{G316S}) [originally from (42)]

Substrates	Enzymes	K_m (mM)	k_{cat} (s^{-1})	k_{cat}/K_m ($mM^{-1} \cdot s^{-1}$)
KIV	Bat1ΔN16^{WT}	0.298 ± 0.100	9.55 ± 1.92	32.1
	Bat1ΔN16^{G333S}	2.73 ± 3.24	2.05 ± 1.70	0.751
	Bat2^{WT}	0.180 ± 0.0444	8.05 ± 1.02	44.7
	Bat2^{G316S}	1.73 ± 0.826	1.79 ± 0.521	1.03
KIC	Bat1ΔN16^{WT}	0.323 ± 0.101	15.4 ± 2.92	47.7
	Bat1ΔN16^{G333S}	1.57 ± 0.505	4.95 ± 0.945	3.15
	Bat2^{WT}	0.212 ± 0.0610	11.6 ± 1.82	54.7
	Bat2^{G316S}	0.681 ± 0.189	5.42 ± 0.615	7.96
KMV	Bat1ΔN16^{WT}	0.218 ± 0.111	4.73 ± 1.29	21.7
	Bat1ΔN16^{G333S}	0.548 ± 0.455	1.46 ± 0.435	2.66
	Bat2^{WT}	0.150 ± 0.0594	5.48 ± 1.04	36.5
	Bat2^{G316S}	0.308 ± 0.134	2.01 ± 0.282	6.53
Val	Bat1ΔN16^{WT}	0.454 ± 0.123	3.37 ± 0.37	7.42
	Bat1ΔN16^{G333S}	7.70 ± 7.37	0.834 ± 0.319	0.108
	Bat2^{WT}	0.511 ± 0.111	2.71 ± 0.23	5.30
	Bat2^{G316S}	13.3 ± 3.44	1.40 ± 0.17	0.106
Leu	Bat1ΔN16^{WT}	0.285 ± 0.0679	3.51 ± 0.31	12.3
	Bat1ΔN16^{G333S}	3.08 ± 1.42	0.701 ± 0.102	0.228
	Bat2^{WT}	0.189 ± 0.0600	2.30 ± 0.24	12.2
	Bat2^{G316S}	3.89 ± 1.06	1.61 ± 0.15	0.414
Ile	Bat1ΔN16^{WT}	0.220 ± 0.102	3.74 ± 0.59	17.0
	Bat1ΔN16^{G333S}	4.23 ± 5.39	0.769 ± 0.312	0.182

$Bat2^{WT}$	0.119 ± 0.0389	2.61 ± 0.24	21.9
$Bat2^{G316S}$	3.40 ± 1.14	1.80 ± 0.20	0.529

The values are the means and standard deviations of results from three independent experiments.

CHAPTER IV: DISCUSSION

4.1. Bat1 and Bat2 shared a major primary transaminase function with minor differences

In the yeast *Saccharomyces cerevisiae*, a popular model organism for studying higher eukaryotes, branched-chain amino acid aminotransferases (scBCATs) are encoded by the *BAT1* and *BAT2* genes (61). Even though *BAT1* and *BAT2* are paralogous genes that share 77% amino acid identity, they exhibit different expression mechanisms and transcriptional regulation throughout the cell growth process (63, 64). Additionally, scBCATs coordinate Leu and TCA cycle metabolism to control TORC1 signaling, which in turn controls cell growth (110). Several investigations have also indicated the differences in the physiological and metabolic roles between Bat1 and Bat2 in yeast cells (62, 63, 65). However, no study has examined the relationship between enzymes' functions, conformational structures, and enzymatic properties of scBCATs. In the present study, I used molecular docking to analyze and compare the chemical difference between Bat1 and Bat2. I demonstrated substrates binding to holoenzyme (Bat1-PLP and Bat2-PLP), which is a crucial step for enzymatic study and directly affects the kinetic parameters of the enzyme (43). In addition, *in vitro* enzymatic assay experiments were performed to clarify the relationship between the structural and function of scBCATs or the difference between Bat1 and Bat2. Due to the limitation of each approach, a link between the computational and the conventional approaches will be needed for the enzymatic study to expand our understanding of the activities within the cells.

The preliminary structural analysis between Bat1 and Bat2 (superimposition of the structure and pocket analysis) revealed that their primary structural conformation was not different even though those amino acid sequences among them showed some differences in the protein's primary structure (Fig. 3-2 to 3-4). Accordingly, the fundamental catalytic function of those two scBCATs acquires the same among Bat1 and Bat2; corresponding with the substrate binding analysis that revealed the similarity in the utilization of important amino acid residues for substrate binding and recognition in the active site of Bat1 and Bat2: Tyr and Arg residues [(Tyr88, Tyr159, Arg161) of Bat1, which is corresponded to (Tyr71, Tyr142, and Arg166) of Bat2] (see also section 3.1.3.4). Moreover, the *in vitro* enzymatic activity assay of Bat1 and Bat2 exhibited a similar majority trend, i.e., BCKAs were the better substrate than BCAAs for both Bat1 and Bat2, and both BCATs utilized KIC with the highest rate among those BCKA substrates (Fig. 3-14). Those results consequently supported that Bat1 and Bat2 primary transamination functions were similar. In fact, *BAT1* and *BAT2* were reported to be the paralogous genes that arise from the ancestor, branched-chain amino acid aminotransferase of *Kluyveromyces lactis* (*KlBAT1*), by a whole-genome duplication event (122). Even though previous studies reported the differences in metabolic preferences of Bat1 and Bat2 (Bat1

prefers anabolism; Bat2 prefers catabolism) (62, 63, 65), the *in vitro* enzymatic activities of Bat1 and Bat2 revealed there was no difference between substrate preferences among Bat1 and Bat2 (Fig. 3-14). Therefore, the difference in metabolic roles of Bat1 and Bat2 relied on the difference in cellular localization, expression in the cell growth stage, and transcriptional regulation (61, 63, 64). Additionally, mitochondria were well-known as the central biosynthetic organelles (123).

Interestingly, Bat1 and Bat2 had minor differences in their conformational pocket (Fig 3-3 and 3-4), amino acid utilization for substrate binding (Fig. 3-7 to 3-10 and Table 3-5), enzymatic activity toward native substrates (Fig. 3-14), and substrate specificities toward non-native substrates (Table 3-7 and 3-8). In practice, pocket δ, δ', and ε showed a difference in pKd value (ligandability) (Fig. 3-3 and Table 3-2). Arg161 of Bat1 (corresponded with Arg144 of Bat2), Tyr159 of Bat1 (corresponded with Tyr142 of Bat2), Tyr207 of Bat2, and PLP were shown to have a difference in substrate binding/recognition characteristics (section 3.1.3.3). The minor differences in substrate utilization from *in vitro* enzymatic activity assay were also shown (Fig. 3-14): Bat1 can utilize KIC and BCAAs at a higher rate than Bat2. Moreover, substrate specificity toward non-native substrates differed between Bat1 and Bat2 (Tables 3-7 and 3-8). Indeed, those minor differences in the catalytic character of Bat1 and Bat2 were likely related to the minor difference in structure (conformational pocket of Bat1 and Bat2) and utilization of amino acid residues for substrate-binding of Bat1 and Bat2. However, the structural and substrate binding character of Bat1 and Bat2 did not largely affect the primary transaminase function of Bat1 and Bat2, which related to the similar trend of Bat1 and Bat2 enzymatic activity toward the native substrates (Fig. 3-14).

4.2. Proposed BCHA overproduction mechanism of BCAT variants

BCAT drives the transamination step of the Ehrlich pathway for branched-chain higher alcohol (BCHA) production. scBCATs have two BCAT isoforms, mitochondrial BCAT (Bat1) and cytosolic BCAT (Bat2). Bat1 and Bat2 are dynamically impacted branched-chain amino acid (BCAA) metabolic pathways in biosynthesis and degradation of BCAAs, leading to BCHA synthesis. In this present study, I engineered scBCATs, both Bat1 and Bat2, by applying *in silico* rational design approaches to design specific amino acid substitution. Then, I investigated the effect of the Bat1 and Bat2 variants on cell growth and production of metabolites (BCAAs and BCHAs) using the laboratory yeast strains (BY4741) that express Bat1 and Bat2 variants (*in vivo* study). Finally, I investigated the effect of amino acid substitution on variant enzymatic properties (*in vitro* study). Notably, the parental yeast strains used in this study, BY4741*bat1*Δ*bat2*Δ (BY4741 strain lacking both Bat1 and Bat2), originally had an auxotrophic phenotype in cultural media without BCAAs (41, 56). Remarkably, all media used for BY4741*bat1*Δ*bat2*Δ expressed wild-type, and variants of Bat1 and Bat2 are

minimal media without BCAA supplementation. Thus, BCAA produced from a functional Bat1 or Bat2 is crucial for the cell growth of those transformants. Moreover, the phenotypes in terms of cell growth, BCAA production, and BCHA production of BY4741*bat1*Δ*bat2*Δ cells expressed wild-type Bat1 (background strain equivalent to *bat2*Δ cells) and wild-type Bat2 (background strain equivalent to *bat1*Δ cells) were consistent with the previous studies (62, 71). Hence, it is safely concluded that this study's expressed BCATs (Bat1, $Bat1^{G333S}$, $Bat1^{G333W}$, Bat2, and $Bat2^{G333S}$) are functional.

The yeast cells expressing Bat1 ($Bat1^{G333S}$ and $Bat1^{G333W}$) and Bat2 ($Bat2^{G316S}$) variants produced BCHAs higher than the cells expressing wild-type Bat1 and Bat2 (Fig. 3-19). The variants' enzymatic activity was reduced from wild-type Bat1 and Bat2 (Table 3-11). In practice, the apparent kinetic parameters of all variants ($Bat1^{G333S}$ and $Bat2^{G316S}$) showed the lower apparent k_{cat} and higher in apparent K_m values than those of wild-type Bat1 and Bat2. The apparent k_{cat}/K_m values of BCAT variants were lower than those of wild-type Bat1 and Bat2, especially k_{cat}/K_m values toward BCKAs (synthesis of BCAAs), accordingly decreasing in BCAA contents compared to the original wild-type (Fig. 3-20). Hence, higher production of BCHAs by BCAT variants was likely a consequent effect of a reduction in the catalytic activity of BCAT variants. The *in vitro* results also indicate that scBCATs (wild-type Bat1 and Bat2) prefer synthesizing BCAAs (using BCKA as the substrates) under certain conditions. However, those k_{cat}/K_m toward BCKAs of BCAT variants ($Bat1^{G333S}$ and $Bat2^{G316S}$) were significantly lower than wild-types (Bat1 and Bat2) which benefits BCHA production from variants. Hence, using the reductive catalytic activity BCAT variants directly reduces the competitive reaction of BCHA production, which is the BCAA biosynthesis.

My recent study proposed that in the yeast cells lacking Bat1, the elevated level of BCKAs, generated from mitochondria and outflux from mitochondria to cytosol, take responsibility for increasing BCHA levels (71). Indeed, it is assumably that the elevated pool of BCKAs also happened with a higher amount of BCKA pool in yeast cells expressed reductive catalytic activity BCAT variants. Moreover, BCAAs have been known to feedback-inhibit the enzymes in their biosynthetic pathway (39, 40), which also affects the pool of BCKAs and consequently affects the biosynthesis of BCHAs. The reductive catalytic activity of BCAT variants also has a chance to indirectly reduce feedback inhibition from BCAAs, which is consistent with the lower BCAA contents of BCAT variants than wild-type (Fig. 3-20). With the above descriptions, BCKAs were greatly accumulated in BCAT variants and further utilized for BCHAs.

4.3. Proposed model for reductive catalytic ability in Bat1^{G333S}, Bat1^{G333W}, and Bat2^{G316S}

According to the *in vitro* enzymatic activities of Bat1- and Bat2-variants, the apparent K_m values toward all substrates (BCAAs and BCKAs) of BCAT variants were significantly higher than those in wild-type Bat1 and Bat2. Additionally, the apparent k_{cat} values of BCAT variants are significantly lower than those of wild-type Bat1 and Bat2 (Table 3-11). These results indicated that the ability to bind with substrates and convert substrates to a product of variant enzymes was reduced from wild-type Bat1 and Bat2. *In silico* analyzing the structure of Bat2^{G316S} compared to wild-type Bat2 structure (Fig. 4-1A and B), Ser316 residue showed an additional interaction (with Met241 residue) that did not exist in the original Bat2 structure. Met241 is located nearby Asn242. This Asn242 residue was reported to directly interact with the pyridoxal 5'-phosphate (PLP) cofactor in human BCAT (Fig. 4-3) (121). Thus, another additional interaction between Ser316-Met241 is likely to impact catalytic engines of Bat2^{G316S}. Moreover, residue316 of Bat2 is located nearby the phosphate group of PLP (4.5 angstroms) (Fig. 4-2A and B). This phosphate group of PLP is the catalytic center where transamination reactions occur (60). Ser has a larger and bulkier side chain than an original amino acid (Gly), with a molecular mass of 75.0666 and 105.093 g·mol^{-1}, respectively for Gly and Ser (124). This bulkier side chain of Ser easily blocks or affects substrate binding and interaction with the phosphate group of PLP. Hence, the phenomena above are likely to affect the enzymatic properties of amino acid substitution from Gly to Ser in BCAT variants. Noteworthy, Ser316 and Met241 residues of Bat2 were conserved with Ser333 and Met258 residues of Bat1 (Fig. 3-12).

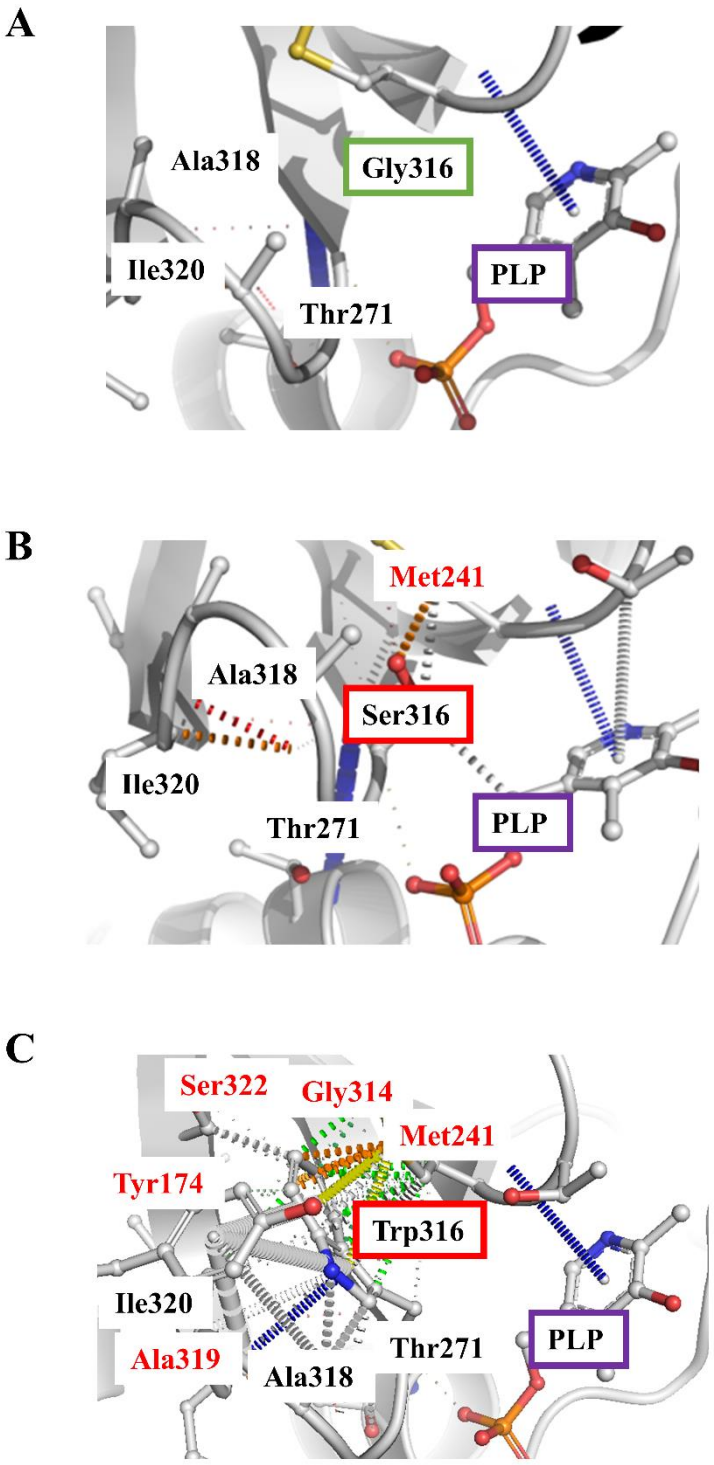

Fig. 4-1 Schematic interatomic interaction between amino acid residues at position 316 in Bat2^{WT} (A), Bat2^{G316S} (B), and Bat2^{G316W} (C). Gly316, Ser316, and Trp316 are shown in the green, red, and red boxes, respectively. The amino acid residues that interact with Ser316 and Trp316 but do not interact with Gly316 are shown with the red fonts [originally from (42)].

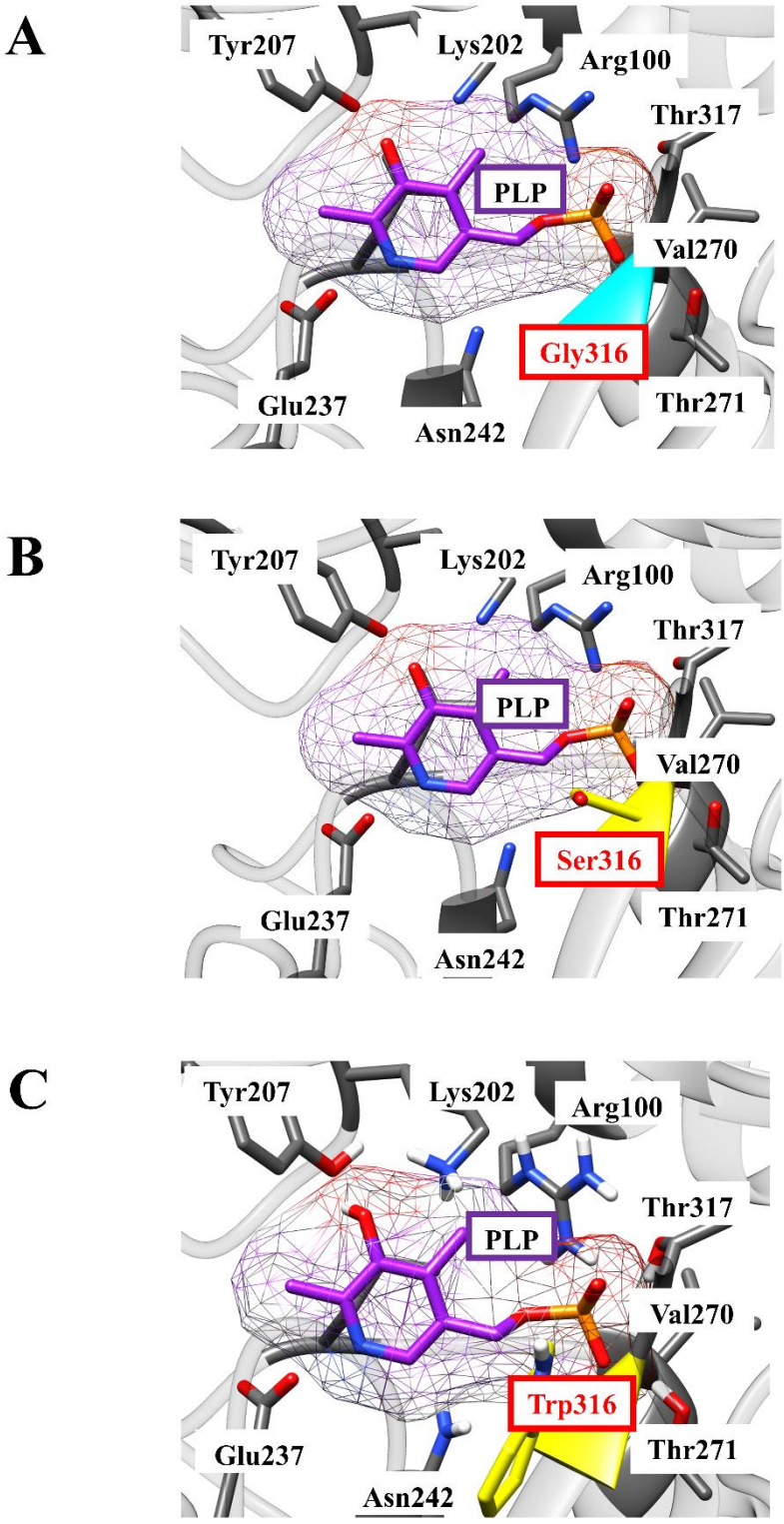

Fig. 4-2 Schematic active center of Bat2^{WT} (A), Bat2^{G316S} (B), and Bat2^{G316W} (C). Gly316 in Bat2^{WT} is marked in the cyan color. Ser316 and Trp316 in Bat2^{G316S} and Bat2^{G316W}, respectively, are marked in yellow color. The distance between Ser316 or Trp316 and the phosphate group of PLP (orange-red end) is around 4.5 angstroms (measured from UCSF Chimera) [originally from (42)]

In fact, *in vitro* enzymatic properties (apparent K_m, k_{cat}, and k_{cat}/K_m) resembled Bat1^{G333S} and Bat2^{G316S}, indicating an effect of Ser substitution on enzymatic properties of Bat1^{G333S} and Bat2^{G316S} was similar, which is reducing catalytic activity of BCAT. However, *in vivo* results of the yeast cell-expressed Bat2^{G316S} [showing growth defected phenotype and exhaustive in productivity of BCHAs (Fig. 3-17B and 3-19B)] were opposite from the cells expressed Bat1^{G333S} [no growth defected phenotype and not much enhanced the BCHA productivity (Fig. 3-17A and 3-19A)]. Those differences *in vivo* phenomena could be argued from the differences between Bat1 and Bat2 in localization, expression, and transcriptional regulation (61, 63, 125). The growth phenotypic and metabolite (BCAAs and BCHAs) production background differences between yeast cells expressed one BCAT [Bat1 in mitochondria (*bat2*Δ cells) and Bat2 in cytosol (*bat1*Δ cells)] also well studied (62, 71). In practice, yeast cells that expressed only Bat2 in the cytosol (*bat1*Δ cells) initially exhibited a growth defect phenotype along with enhancing the BCHA content compared to yeast cells that expressed only Bat1 in mitochondria (*bat2*Δ cells) (62, 65, 71). Accordingly, those differences among Bat1 and Bat2 are responsible for the *in vivo* phenotypic differences between yeast cells expressed Bat1^{G333S} and Bat2^{G316S}, particularly, Ser substitution (G316S) on Bat2 has more impact on *in vivo* phenotypes of the yeast cells than Ser substitution (G333S) at the identical amino acid residues on Bat1.

The yeast cells expressed Bat^{G333W} highly increased in BCHA contents, especially isobutanol and isoamyl alcohol contents, compared to the wild-type Bat1, original wild-type, and Bat1^{G333S} (Fig. 3-19A). The extensive increase in BCHA contents of Bat1^{G333W} is consistent with largely decreased BCAA contents from wild-type Bat1 and original wild-type (Fig. 3-20A). Moreover, yeast cells expressed Bat1^{G333W} also showed the lowest growth phenotype compared to the yeast cells expressed Bat1G333S and wild-type Bat1 (Fig. 3-17A). The fact that Ser and Trp acquire the difference in categorization, polar-uncharged and non-polar, respectively for Ser and Trp; along with differences in acidity (pKa) {[2.21 (carboxyl group) and 9.15 (amino group) for Ser] and [2.38 (carboxyl group) and 9.39 (amino group) for Trp]} and molecular mass (105.093 and 204.229 $g \cdot mol^{-1}$, respectively for Ser and Trp) (124). The *in silico* investigation of an amino acid substitution on protein structure revealed that Trp substitution at position 316 had an additional intramolecular interaction with the other residues (Tyr174, Gly314, Ala319, and Ser322) from Ser substitution at position 316 (Fig 4-1B and 4-1C). Notably, those residues mentioned above were located within the substrate-binding area (within the five-angstrom surrounding substrate) and indirectly interacted with substrates (Table 3-5). Importantly, all of those residues (Tyr174, Gly314, Ala319, and Ser322 of Bat2) are conserved with Bat1 (Tyr191, Gly331, Ala336, and Ser339 of Bat1) (Fig. 3-12). This Trp substitution leads to the more reductive catalytic activity of Bat1^{G333W} than Bat1^{G333S}, consequently impacting cell growth and metabolite production (especially BCHAs). Besides, relinquishing Bat1 is the well-known effective approach to overproducing BCHA (38, 65). Nonetheless, this study showed that the yeast cells that expressed functional-Bat1 variant (Bat1^{G333W}) could highly increase the productivity of BCHAs, especially isobutanol, compared to either the original wild-type or the cells lacking Bat1.

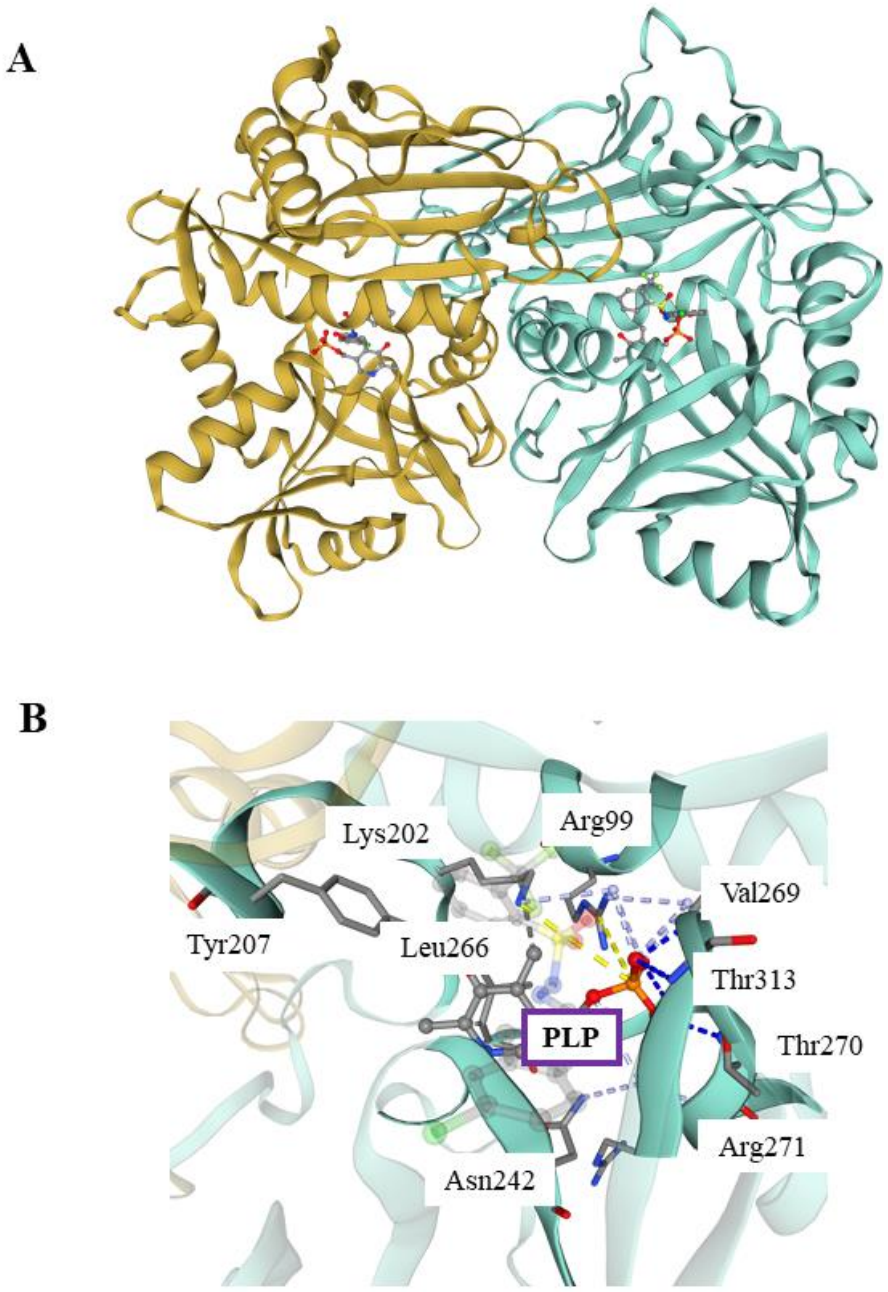

Fig. 4-3 Crystal structure of human cytosolic branched-chain amino acid aminotransferase (hBCATc). The structure was obtained from SWISS-MODEL with SMTL ID: 2abj.1. (A) ribbon representative structure (chain A, yellow and chain B, blue-green) and (B) PLP-interactive residues [originally from (42)].

4.4. Relationship between growth defected phenotype and catalytic properties of BCAT variants

The yeast cells that expressed Bat1^{G333W} and Bat2^{G316S} had growth defected phenotype cultured in minimal synthetic media without BCAA supplemented compared to the original wild-type (BY4741) or yeast cells expressed wild-type Bat1 and Bat2 (Fig. 3-17). Those growth phenotypes of BCAT variants (Bat1^{G333W} and Bat2^{G316S}) were related to metabolite production. In practice, the yeast cells that expressed Bat1^{G333W} produced BCHAs better than wild-type ones, but they also exhibited lower BCAA contents than wild-type ones. In the BY4741 background strain, BCAAs are required for cell growth (62, 71). Compared with the yeast cells expressed Bat1^{G333S}, they can grow as well as wild-type along with metabolite productions were not critically changed from those of wild-type. Moreover, it was revealed that a high level of BCHAs also has toxicity to yeast cells, similar to ethanol which affects the plasma membrane and inhibits protein translation initiation (126, 127). Accordingly, these two factors will likely affect the growth phenotype of yeast cells expressed Bat1^{G333W} and Bat2^{G316S}.

Oppositely from Bat2^{G316S}, the yeast cell-expressed Bat2^{G316W} cannot grow in minimal media without BCAA supplemented (data not shown). As previously discussed, the different effects of Ser substitution on Bat1 (Bat1^{G333S}) and Bat2 (Bat2^{G316S}), practically, Ser substitution on Bat2 (Bat2^{G316S}) showed more effect on growth phenotype and metabolite production than Bat1 (Bat1^{G333S}), which is consistent with the background difference between Bat1 and Bat2 localization, expression, and transcriptional regulation. Trustworthy, Trp substitution is supposed to be more effective on Bat2 (Bat2^{G316W}) than Bat1 (Bat1^{G333W}), which is a consequence of lower BCAAs and higher in BCHAs productivity. In addition to the BCAA requirement for BY4741 background strain, those factors severely affect the yeast cells expressed Bat2^{G316W}.

4.5. Argument between *in silico* and *in vitro* investigation of BCAT variants and BCHA productivity from BCAT variants

In this study, Bat1 (Bat1^{G333S}) and Bat2 (Bat2^{G316S}) variants showed a decrease in catalytic activity compared to wild-type Bat1 and Bat2 (Table 3-11). However, the binding affinity toward substrates was increased based on *in silico* analysis (Table 3-10). The fact that *in silico* simulations, especially the calculation of substrate binding affinity (mCSM-lig), mainly used in this study are static and roughly determine the properties of variant BCATs based on a binding affinity of the substrate, which is one of the modern methods to clarify or predict their biological performance of variant enzyme (128). Nevertheless, enzyme catalytic way more dynamic; movement of amino acids, the vibration of the backbone, or conformational fluctuation are integrated to attain their catalytic function (129–131). Molecular dynamics simulation and QM/MM studies were used to clarify a catalytic

mechanism of histidine decarboxylase, one of the PLP-dependent enzymes in the recent study (132). Beyond substrate binding, the unbinding of product is also crucial for enzymatic function. In the previous study, studying ligands (substrates or products of enzymes) unbinding was reported to affect enzyme turnover positively (133). Therefore, complementing static simulations with the dynamic simulations, including molecular dynamic simulation, QM/MM study, and unbinding kinetics of ligand, would benefit understanding the enzyme dynamics, eventually obtaining the engineered enzymes that improve catalytic activity for biotechnological application.

In terms of BCHA productivity, yeast cells expressed Bat1^{G333W} (18.7-folded higher than the original wild-type) and Bat2^{G316S} (17.4-folded higher than the original wild-type) were the highest BCHA production strains in this study compared to the other strains that expressed wild-type or variants of Bat1 and Bat2, respectively (Fig. 3-19). The previous study reported a 13.1-folded increase in isobutanol production from parental strain using the engineered BY4741 [deleted Bat1 and overexpressed BCKA biosynthetic (*ILV*) genes] when cultured in synthetic complete (SC) media with 10% glucose (65). Surprisingly, I achieved 18.7-folded (Bat1^{G333S}) and 17.4-folded (Bat2^{G316S}) isobutanol productivity, respectively, for the yeast cells expressed Bat1^{G333W} and Bat1^{G316S} using the variant of Bat1 and Bat2 without further engineering the other enzymes; additionally, the fermentation media in this study was synthetic dextrose (SD) media with 2% glucose. Besides, isoamyl alcohol contents in those cells expressed Bat1^{G333W} and Bat^{G316S} also increased along with isobutanol. My present study introduced the novel approach to overproducing BCHAs using the engineered BCATs (Bat1 and Bat2) to change the catalytic activity (altering catalytic ability) from wild-type. Along with using variants Bat1 and Bat2, further study can perform to enhance the production of BCHAs by integrating with the previous successful approaches: engineering the other enzymes (by overexpressing *ILV* genes), compartmentalization of the BCHA biosynthetic engines (KDCs and ADHs) into mitochondria, increasing glucose or nutrient content in fermentation media and changing cultured media (65, 76, 77).

In conclusion, I succeeded in clarifying the presence of multiple ligand-bindable pockets in the Bat1 and Bat2 conformations and the dissimilarities in locations and cavity properties between them by computational structure analysis. I also identified the potential and essential residues, such as Arg, Tyr, and Thr, for substrate binding, recognition, and stabilization in the yeast BCATs. This fundamental knowledge of Bat1 and Bat2 will promote understanding of the catalytic mechanisms in BCATs and inform further investigations related to modifying the substrate specificities and the engineering of BCATs in other species. Moreover, I also successfully constructed the engineered Bat1 and Bat2. Applying *in silico* analysis, I designed and constructed amino acid substitution at Gly333 and Gly316 residues of Bat1 and Bat2, respectively, from Gly to Ser and Gly to Trp. Those BCAT variants were responsible for a significant increase of BCHAs, the valuable compounds in industry.

ACKNOWLEDGEMENTS

Importantly, I would like to give a sincere and deep thank you to Prof. Hiroshi Takagi, my supervisor and the principal investigator (PI) at Laboratory of Applied Stress Microbiology, for his kind assistance and advice throughout my study. I also would like to express my grateful thank you to my advisors: Assoc. Prof. Yukio Kimata and Assoc. Prof. Shosuke Yoshida for their suggestion, discussion, and evaluation from my master's degree until my doctor's degree. Meanwhile, I would like to thank Assoc. Prof. Daisuke Watanabe, Assist. Prof. Akira Nishimura and Assist Prof. Ryo Nasuno in Takagi-lab for their assistance in my experiment, different points of view, suggestions, and comments which kindly helped me with this succession. Additionally, I would like to thank the important postdoctoral fellows who always supported my study (Dr. Yoichi Toyokawa and Dr. Isogai Shota) for their valuable assistance, experimental training, and fruitful discussion throughout my study. Moreover, I would like to express my deep thank to my collaborators: Prof. Vithaya Ruangpornvisuti and Mr. Nontawat Ploysongsri (from Department of Chemistry at Chulalongkorn University) and Prof. Maitreya Dunham and Dr. Christopher Large (from Department of Genome Sciences at University of Washington), for their great effort in the successful collaborative works.

In addition, I would like to give additional thanks to Takagi lab members'; especially Ms. Yoko Torisawa (lab assistant), Ms. Yukiko Sugimoto (lab technician), and Ms. Yuki Kimata (postdoctoral fellow), who always assisted and helped my student life go smoothly. Also, my special thanks to Dr. Supapid Eknikom (my Thai senior in Takagi-lab), Ms. Phuong Thi Huong, Ms. Mohd Fauzee Yasmin Nabiah, and Ms. Nguyen Thi Mai Phuong (my great friends in Takagi-lab) and Mr. Thanet Pakpuwadon (my great Thai friend in NAIST) who always supporting and spending a splendid and wonderful time together in NAIST. Importantly, I would like to thank the Japanese Government Scholarship (Monbukagakusho) for financially supporting my studying at NAIST. Moreover, I would like to thank my family and my friends in Thailand (especially Mr. Ponlavit Subpradit, Mr. Nontawat Ploysongsri, and Ms. Krittaporn Yoocharoen) for being an important part of my success. Finally, I would like to thank my girlfriend (Ms. Kittima Paktranon), who always stood by me, supported, and cheered me up throughout my study.

Jirasin Koonthongkaew

REFERENCES

1. Nykänen, L., Nykänen, I. (1977). Production of esters by different yeast strains in sugar fermentations. J Inst Brew 83, 30–31.

2. Ehrlich, F. (1907). Über die Bedingungen der Fuselölbildung und über ihren Zusammenhang mit dem Eiweißaufbau der Hefe. Berichte der Dtsch Chem Gesellschaft 40, 1027–1047.

3. Hazelwood, L.A., Daran, J.M., Van, Maris, A.J.A., Pronk, J.T., Dickinson, J.R. (2008). The Ehrlich pathway for fusel alcohol production: a century of research on Saccharomyces cerevisiae metabolism. Appl Environ Microbiol 74, 2259–2266.

4. Lambrechts, M.G., Pretorius, I.S. (2000). Yeast and its importance to wine aroma-a review. South African J Enol Vitic 21, 97–129.

5. Kim, S., Thiessen, P.A., Bolton, E.E., Chen, J., Fu, G., Gindulyte, A., Han, L., He, J., He, S., Shoemaker, B.A. (2016). PubChem substance and compound databases. Nucleic Acids Res 44, D1202–D1213.

6. Atsumi, S., Hanai, T., Liao, J.C. (2008). Non-fermentative pathways for synthesis of branched-chain higher alcohols as biofuels. Nature 451, 86–89.

7. Mainguet, S.E., Liao, J.C. (2010). Bioengineering of microorganisms for C3 to C5 alcohols production. Biotechnol J 5, 1297–1308.

8. Wang, B.W., Shi, A.Q., Tu, R., Zhang, X.L., Wang, Q.H., Bai, F.W. (2012) Branched-Chain Higher Alcohols. Biotechnology in China III: Biofuels and Bioenergy 128, 101–118.

9. Connor, M.R., Liao, J.C. (2009). Microbial production of advanced transportation fuels in non-natural hosts. Curr Opinion in Biotechnology 20, 307–315.

10. Peralta-Yahya, P.P., Keasling, J.D. (2010). Advanced biofuel production in microbes. Biotechnol J 5, 147–162.

11. Cheng, J., Jiang, C. (2007). Analysis on process technology and market situation of isobutyl alcohol worldwide. Chem Ind 25, 28–31.

12. Amerine, A.M. (1980). The Technology of wine making. 4th ed. (AVI Technical Books Inc.), Westport, CT, USA.

13. Ashida, S., Ichkawa, E., Suginami, K., Imayasu, S. (1987). Isolation and application of mutants producing sufficient isoamyl acetate, a sake flavor component. Agric Biol Chem 51, 2061–2065.

14. Taira, J., Tsuchiya, A., Furudate, H. (2012). Initial volatile aroma profiles of young and aged awamori shochu determined by GC/MS/pulsed FPD. Food Sci Technol Res 18, 177–181.

15. Pires, E.J., Teixeira, J.A., Brányik, T., Vicente, A.A. (2014). Yeast: the soul of beer's aroma—a review of flavour-active esters and higher alcohols produced by the brewing yeast. Appl Microbiol Biotechnol 98, 1937–1949.

16. Wang, Y.P., Wei, X., Guo, X.W., Xiao, D.G. (2020). Effect of the deletion of genes related to amino acid metabolism on the production of higher alcohols by *Saccharomyces cerevisiae*. Biomed Res Int 2020, 6802512.

17. Dan, T., Ren, W., Liu, Y., Tian, J., Chen, H., Li, T., Liu, W. (2019). Volatile flavor compounds profile and fermentation characteristics of milk fermented by *Lactobacillus delbrueckii* subsp. bulgaricus. Front Microbiol 10, 2183.

18. Molimard, P., Spinnler, H.E. (1996). Review: Compounds Involved in the Flavor of Surface Mold-Ripened Cheeses: Origins and Properties. J Dairy Sci 79, 169–184.

19. Zhou, T., Feng, Y., Thomas-Danguin, T., Zhao, M. (2021). Enhancement of saltiness perception by odorants selected from Chinese soy sauce: A gas chromatography/olfactometry-associated taste study. Food Chem 335, 127664.

20. Watanabe, M., Fukuda, K., Asano, K., Ohta, S. (1990). Mutants of bakers' yeasts producing a large amount of isobutyl alcohol or isoamyl alcohol, flavour components of bread. Appl Microbiol Biotechnol 34, 154–159.

21. Ayres, EE. (1929). Amyl alcohols from the pentanes. Ind Eng Chem 21, 899–904.

22. Olson, E.S., Sharma, R.K., Aulich, T.R. (2004). Higher-alcohols biorefinery. Appl Biochem Biotechnol 115, 913–932.

23. Atsumi, S., Wu, T.Y., Eckl, E.M., Hawkins, S.D., Buelter, T., Liao, J.C. (2010). Engineering the isobutanol biosynthetic pathway in *Escherichia coli* by comparison of three aldehyde reductase/alcohol dehydrogenase genes. Appl Microbiol Biotechnol 85, 651–657.

24. Blombach, B., Eikmanns, B.J. (2011). Current knowledge on isobutanol production with *Escherichia coli*, *Bacillus subtilis* and *Corynebacterium glutamicum*. Bioeng Bugs 2, 346–350.

25. Blombach, B., Riester, T., Wieschalka, S., Ziert, C., Youn, J.W., Wendisch, V.F., Eikmanns, B.J. (2011). *Corynebacterium glutamicum* tailored for efficient isobutanol production. Appl Environ Microbiol 77, 3300–3310.

26. Hohmann, S. (2002). Osmotic stress signaling and osmoadaptation in yeasts. Microbiol Mol Biol Rev 66, 300–372.

27. Porro, D., Gasser, B., Fossati, T., Maurer, M., Branduardi, P., Sauer, M., Mattanovich, D. (2011). Production of recombinant proteins and metabolites in yeasts: when are these systems better than bacterial production systems? Appl Microbiol Biotechnol 89, 939–948.

28. Schoch, C.L., Ciufo, S., Domrachev, M., Hotton, C.L., Kannan, S., Khovanskaya, R., Leipe, D., Mcveigh, R., O'Neill, K., Robbertse, B., Sharma, S., Soussov, V., Sullivan, J.P., Sun, L., Turner, S., Karsch-Mizrachi, I. (2020). NCBI Taxonomy: a comprehensive update on curation, resources and tools. Database.

29. Feldmann, H. (2011). Yeast: molecular and cell biology. (John Wiley & Sons), Weinheim, Baden-Württemberg, Germany.

30. Moyad, M.A., Robinson, L.E., Kittelsrud, J.M., Reeves, S.G., Weaver, S.E., Guzman, A.I., Bubak, M.E. (2009). Immunogenic yeast-based fermentation product reduces allergic rhinitis-induced nasal congestion: a randomized, double-blind, placebo-controlled trial. Adv Ther 26, 795–804.

31. Goffeau, A., Barrell, B.G., Bussey, H., Davis, R.W., Dujon, B., Feldmann, H., Galibert, F., Hoheisel, J.D., Jacq, C., Johnston, M., Louis, E.J. (1996). Life with 6000 Genes. Science 274, 546–567.

32. Goffeau, A., Aert, R., Agostini-Carbone, M.L., Ahmed, A., Aigle, M., Alberghina, L., Albermann, K., Albers, M., Aldea, M., Alexandraki, D., Aljinovic, G., Allen, E., Alt-Mörbe, J., André, B., Andrews, S., Ansorge, W., Antoine, G., Anwar, R., Aparicio, A., Araujo, R., Arino, J., Arnold, F., Arroyo, J., Aviles, E., Backes, U., Baclet, M.C., Badcock, K., Bahr, A., Baladron, V., Ballesta, J.P.G., Bankier, A.T., Banrevi, A., Bargues, M., Baron, L., Barreiros, T., Barrell, B.G., Barthe, C., Barton, A.B., Baur, A., Bécam, A.M., Becker, A., Becker, I., Beinhauer, J., Benes, V., Benit, P., Berben, G., Bergantino, E., Bergez, P., Berno, A., Bertani, I., Biteau, N., Bjourson, A.J., Blöcker, H., Blugeon, C., Bohn, C., Boles, E., Bolle, P.A., Bolotin-Fukuhara, M., Bordonné, R., Boskovic, J., Bossier, P., Botstein, D., Bou, G., Bowman, S., Boyer, J., Brandt, P., Brandt, T., Brendel, M., Brennan, T., Brinkman, R., Brown, A., Brown, A.J.P., Brown, D., Brückner, M., Bruschi, C.V., Buhler, J.M., Buitrago, M.J., Bussereau, F., Bussey, H., Camasses, A., Carcano, C., Carignani, G., Carpenter, J., Casamayor, A., Casas, C., Castagnoli, L., Cederberg, H., Cerdan, E., Chalwatzis, N., Chanet, R., Chen, E., Chéret, G., Cherry, J.M., Chillingworth, T., Christiansen, C., Chuat, J.C., Chung, E., Churcher, C., Churcher, C.M., Clark, M.W., Clemente, M.L., Coblenz, A., Coglievina, M., Coissac, E., Colleaux, L., Connor, R., Contreras, R., Cooper, J., Copsey, T., Coster, F., Coster, R., Couch, J., Crouzet, M., Cziepluch, C., Daignan-Fornier, B., Dal Paro, F., Dang, D.V., D'Angelo, M., Davies, C.J., Davis, K., Davis, R.W., De Antoni, A., Dear, S., Dedman, K., Defoor, E., De Haan, M., Delaveau, T., Del Bino, S., Delgado, M., Delius, H., Delneri, D., Del Rey, F., Demolder, J., Démolis, N., Devlin, K., de

Wergifosse, P., Dietrich, F.S., Ding, H., Dion, C., Dipaolo, T., Doignon, F., Doira, C., Domdey, H., Dover, J., Du, Z., Dubois, E., Dujon, B., Duncan, M., Durand, P., Düsterhöft, A., Düsterhus, S., Eki, T., El Bakkoury, M., Eide, L.G., Entian, K.D., Eraso, P., Erdmann, D., Erfle, H., Escribano, V., Esteban, M., Fabiani, L., Fabre, F., Fairhead, C., Fartmann, B., Favello, A., Faye, G., Feldmann, H., Fernandes, L., Feroli, F., Feuermann, M., Fiedler, T., Fiers, W., Fleig, U.N., Flöth, M., Fobo, G.M., Fortin, N., Foury, F., Francingues-Gaillard, M.C., Franco, L., Fraser, A., Friesen, J.D., Fritz, C., Frontali, L., Fukuhara, H., Fulton, L., Fuller, L.J., Gabel, C., Gaillardin, C., Gaillon, L., Galibert, F., Galisson, F., Galland, P., Gamo, F.J., Gancedo, C., Garcia-Cantalejo, J.M., García-Gonzalez, M.I., Garcia-Ramirez, J.J., García-Saéz, M., Gassenhuber, H., Gatius, M., Gattung, S., Geisel, C., Gent, M.E., Gentles, S., Ghazvini, M., Gigot, D., Gilliquet, V., Glansdorff, N., Gómez-Peris, A., Gonzaléz, A., Goulding, S.E., Granotier, C., Greco, T., Grenson, M., Grisanti, P., Grivell, L.A., Grothues, D., Gueldener, U., Guerreiro, P., Guzman, E., Haasemann, M., Habbig, B., Hagiwara, H., Hall, J., Hallsworth, K., Hamlin, N., Hand, N.J., Hanemann, V., Hani, J., Hankeln, T., Hansen, M., Harris, D., Harris, D.E., Hartzell, G., Hatat, D., Hattenhorst, U., Hawkins, J., Hebling, U., Hegemann, J., Hein, C., Hennemann, A., Hennessy, K., Herbert, C.J., Hernandez, K., Hernando, Y., Herrero, E., Heumann, K., Heuss-Neitzel, D., Hewitt, N., Hiesel, R., Hilbert, H., Hilger, F., Hillier, L., Ho, C., Hoenicka, J., Hofmann, B., Hoheisel, J., Hohmann, S., Hollenberg, C.P., Holmstrøm, K., Horaitis, O., Horsnell, T.S., Huang, M.E., Hughes, B., Hunicke-Smith, S., Hunt, S., Hunt, S.E., Huse, K., Hyman, R.W., Iborra, F., Indge, K.J., Iraqui Houssaini, I., Isono, K., Jacq, C., Jacquet, M., Jacquier, A., Jagels, K., Jäger, W., James, C.M., Jauniaux, J.C., Jia, Y., Jier, M., Jimenez, A., Johnson, D., Johnston, L., Johnston, M., Jones, M., Jonniaux, J.L., Kaback, D.B., Kallesøe, T., Kalman, S., Kalogeropoulos, A., Karpfinger-Hartl, L., Kashkari, D., Katsoulou, C., Kayser, A., Kelly, A., Keng, T., Keuchel, H., Kiesau, P. (1997). The Yeast Genome Directory. Nature 387, 5.

33. Kurtzman, C.P., Fell, J.W., Boekhout, T. (2011). The yeasts: a taxonomic study. (Elsevier), London, UK.

34. Pronk, J.T., Yde Steensma, H., Vav Dijken, J.P. (1996). Pyruvate Metabolism in *Saccharomyces cerevisiae*. Yeast 12, 1607–1633.

35. Parapouli, M., Vasileiadis, A., Afendra, A.S., Hatziloukas, E. (2020). *Saccharomyces cerevisiae* and its industrial applications. AIMS Microbiology 6, 1.

36. Kasavi, C., Finore, I., Lama, L., Nicolaus, B., Oliver, S.G., Toksoy Oner, E., Kirdar, B. (2012). Evaluation of industrial *Saccharomyces cerevisiae* strains for ethanol production from biomass. Biomass and Bioenergy 45, 230–238.

37. Elke, N. (2008). Progress in Metabolic Engineering of *Saccharomyces cerevisiae*. Microbiol Mol Biol Rev 72, 379–412.

38. Park, S.H., Kim, S., Hahn, J.S. (2014). Metabolic engineering of *Saccharomyces cerevisiae* for the production of isobutanol and 3-methyl-1-butanol. Appl Microbiol Biotechnol 98, 9139–9147.

39. Ryan, E.D., Kohlhaw, G. (1974). Subcellular Localization of Isoleucine-Valine Biosynthetic Enzymes in Yeast. J Bacteriol 120, 631–637.

40. Baichwal, V.R., Cunningham, T.S., Gatzek, P.R., Kohlhaw, G.B. (1983). Leucine biosynthesis in yeast. Curr Genet 7, 369–377.

41. Kispal, G., Steiner, H., Court, D.A., Rolinski, B., Lill, R. (1996). Mitochondrial and cytosolic branched-chain amino acid transaminases from yeast, homologs of the myc oncogene-regulated Eca39 protein. J Biol Chem 271, 24458–24464.

42. Jirasin, K., Nontawat, P., Yoichi, T., Vithaya, R., Hiroshi, T., Haruyuki, A. (2022). Improvement of Fusel Alcohol Production by Engineering of the Yeast Branched-Chain Amino Acid Aminotransaminase. Appl Environ Microbiol 88, e00557-22.

43. Berg, J.M., Tymoczko, J.L., Stryer, L. (2002). Amino Acid Biosynthesis Is Regulated by Feedback Inhibition. Biochemistry. (WH Freeman), New York, USA.

44. Ljungdahl, P.O., Daignan-Fornier, B. (2012). Regulation of amino acid, nucleotide, and phosphate metabolism in *Saccharomyces cerevisiae*. Genetics 190, 885–929.

45. Natarajan, K., Meyer, M.R., Jackson, B.M., Slade, D., Roberts, C., Hinnebusch, A.G., Marton, M.J. (2001). Transcriptional Profiling Shows that Gcn4p Is a Master Regulator of Gene Expression during Amino Acid Starvation in Yeast. Mol Cell Biol 21, 4347–4368.

46. Thireos, G., Penn, M.D., Greer, H. (1984). 5'untranslated sequences are required for the translational control of a yeast regulatory gene. Proc Natl Acad Sci 81, 5096–5100.

47. van Dijken, J.P., Scheffers, W.A. (1986). Redox balances in the metabolism of sugars by yeasts. FEMS Microbiol Rev 1, 199–224.

48. Boulton, R., Singleton, V., Bisson, L., Kunkee, R. (2013). Principles and practices of winemaking. (Springer Science & Business Media), New York, USA.

49. Vollbrecht, D., Radler, F. (1973). The formation of higher alcohols by amino acid auxotrophic mutants of *Saccharomyces cerevisiae*. I. The conversion of amino acids to higher alcohols (author's transl). Arch Mikrobiol 94, 351–358.

50. Ribéreau-Gayon, P., Dubourdieu, D., Donèche, B., Lonvaud, A. (2006). Handbook of enology, Volume 1: The microbiology of wine and vinifications. (John Wiley & Sons), Weinheim, Baden-Württemberg, Germany.

51. Lilly, M., Bauer, F.F., Styger, G., Lambrechts, M.G., Pretorius, I.S. (2006). The effect

of increased branched-chain amino acid transaminase activity in yeast on the production of higher alcohols and on the flavour profiles of wine and distillates. FEMS Yeast Res 6, 726–743.

52. Styger, G., Jacobson, D., Prior, B.A., Bauer, F.F. (2013). Genetic analysis of the metabolic pathways responsible for aroma metabolite production by *Saccharomyces cerevisiae*. Appl Microbiol Biotechnol 97, 4429–4442.

53. Grishin, N.V., Phillips, M.A., Goldsmith, E.J. (1995). Modeling of the spatial structure of eukaryotic ornithine decarboxylases. Protein Sci 4, 1291–1304.

54. Okada, K., Hirotsu, K., Sato, M., Hayashi, H., Kagamiyama, H. (1997). Three-Dimensional Structure of *Escherichia coli* Branched-Chain Amino Acid Aminotransferase at 2.5 Å Resolution1. J Biochem 121, 637–641.

55. Davoodi, J., Drown, P.M., Bledsoe, R.K., Wallin, R., Reinhart, G.D., Hutson, S.M. (1998). Overexpression and characterization of the human mitochondrial and cytosolic branched-chain aminotransferases. J Biol Chem 273, 4982–4989.

56. Prohl, C., Kispal, G., Lill, R. (2000). Branched-chain-amino-acid transaminases of yeast *Saccharomyces cerevisiae*. Methods in Enzymology 324, 365–75.

57. Hutson, S. (2001). Structure and Function of Branched Chain Aminotransferases. Progress in Nucleic Acid Research and Molecular Biology, Academic Press 70, 175–206.

58. Toney, M.D. (2011). Pyridoxal phosphate enzymology. Biochim Biophys Acta - Proteins Proteomics 1814, 1405–1406.

59. Dolphin, D., Poulson, R., Avramovic, O. (1986). Coenzymes and Cofactors, Volume 1: Vitamin B6 Pyridoxal Phosphate: Chemical, Bio-chemical and Medical Aspects, (Wiley), New York.

60. Eliot, A.C., Kirsch, J.F. (2004). Pyridoxal phosphate enzymes: Mechanistic, structural, and evolutionary considerations. Annu Rev Biochem 73, 383–415.

61. Eden, A., Simchen, G., Benvenisty, N. (1996). Two yeast homologs of ECA39, a target for c-Myc regulation, code for cytosolic and mitochondrial branched-chain amino acid aminotransferases. Journal of Biological Chemistry. 271, 20242–20245.

62. Takpho, N., Watanabe, D., Takagi, H. (2018). Valine biosynthesis in *Saccharomyces cerevisiae* is regulated by the mitochondrial branched-chain amino acid aminotransferase Bat1. Microb Cell 5, 293–299.

63. Colón, M., Hernández, F., López, K., Quezada, H., González, J., López, G., Aranda, C., González, A. (2011). *Saccharomyces cerevisiae* Bat1 and Bat2 Aminotransferases Have Functionally Diverged from the Ancestral-Like *Kluyveromyces lactis* Orthologous

Enzyme. PLoS One 6, e16099.

64. González, J., López, G., Argueta, S., Escalera-Fanjul, X., El Hafidi, M., Campero-Basaldua, C., Strauss, J., Riego-Ruiz, L., González, A. (2017). Diversification of Transcriptional Regulation Determines Subfunctionalization of Paralogous Branched Chain Aminotransferases in the Yeast *Saccharomyces cerevisiae*. Genetics 117, 300290.

65. Hammer, S.K., Avalos, J.L. (2017). Uncovering the role of branched-chain amino acid transaminases in *Saccharomyces cerevisiae* isobutanol biosynthesis. Metab Eng 44, 302–312.

66. Picotti, P., Clément-Ziza, M., Lam, H., Campbell, D.S., Schmidt, A., Deutsch, E.W., Röst, H., Sun, Z., Rinner, O., Reiter, L., Shen, Q., Michaelson, J.J., Frei, A., Alberti, S., Kusebauch, U., Wollscheid, B., Moritz, R.L., Beyer, A., Aebersold, R. (2013). A complete mass-spectrometric map of the yeast proteome applied to quantitative trait analysis. Nature 494, 266–270.

67. Li, W., Wang, J.H., Zhang, C.Y., Ma, H.X., Xiao, D.G. (2017). Regulation of *Saccharomyces cerevisiae* genetic engineering on the production of acetate esters and higher alcohols during Chinese Baijiu fermentation. J Ind Microbiol Biotechnol 44, 949–960.

68. Ofuonye, E., Kutin, K., Stuart, D.T. (2013). Engineering *Saccharomyces cerevisiae* fermentative pathways for the production of isobutanol. Biofuels 4, 185–201.

69. Zhang, C.Y., Qi, Y.N., Ma, H.X., Li, W., Dai, L.H., Xiao, D.G. (2015). Decreased production of higher alcohols by *Saccharomyces cerevisiae* for Chinese rice wine fermentation by deletion of Bat aminotransferases. J Ind Microbiol Biotechnol 42, 617–625.

70. Zhang, A., Li, Y., Gao, Y., Jin, H. (2016). Increasing isobutanol yield by double-gene deletion of *PDC6* and *LPD1* in *Saccharomyces cerevisiae*. Chinese J Chem Eng 24, 1074–1079.

71. Koonthongkaew, J., Toyokawa, Y., Ohashi, M., Large, C.R.L., Dunham, M.J., Takagi, H. (2020). Effect of the Ala234Asp replacement in mitochondrial branched-chain amino acid aminotransferase on the production of BCAAs and fusel alcohols in yeast. Appl Microbiol Biotechnol 104, 7915–7925.

72. Takagi, H. (2019). Metabolic regulatory mechanisms and physiological roles of functional amino acids and their applications in yeast. Biosci Biotechnol Biochem 83, 1449–1462.

73. Magee, P.T., de Robichon-Szulmajster, H. (1968). The Regulation of Isoleucine-Valine Biosynthesis in *Saccharomyces cerevisiae*. Eur J Biochem 3, 502–506.

74. Takpho, N., Watanabe, D., Takagi, H. (2018). High-level production of valine by expression of the feedback inhibition-insensitive acetohydroxyacid synthase in *Saccharomyces cerevisiae*. Metab Eng 46, 60–67.

75. Kohlhaw, G.B. (2003). Leucine Biosynthesis in Fungi: Entering Metabolism through the Back Door. Microbiol Mol Biol Rev 67, 1–15.

76. Hammer, S.K., Zhang, Y., Avalos, J.L. (2020). Mitochondrial Compartmentalization Confers Specificity to the 2-Ketoacid Recursive Pathway: Increasing Isopentanol Production in *Saccharomyces cerevisiae*. ACS Synth Biol 9, 546–555.

77. Avalos, J.L., Fink, G.R., Stephanopoulos, G. (2013). Compartmentalization of metabolic pathways in yeast mitochondria improves the production of branched-chain alcohols. Nat Biotechnol 31, 335–341.

78. Wang, X.L., Li, C.J., Xing, Y., Yang, Y.H., Jia, J.P. (2015). Hypervalinemia and hyperleucine-isoleucinemia caused by mutations in the branched-chain-amino-acid aminotransferase gene. J Inherit Metab Dis 38, 855–861.

79. Knerr, I., Colombo, R., Urquhart, J., Morais, A., Merinero, B., Oyarzabal, A., Pérez, B., Jones, S.A., Perveen, R., Preece, M.A., Rogers, Y., Treacy, E.P., Mayne, P., Zampino, G., MacKinnon, S., Wassmer, E., Yue, W.W., Robinson, I., Rodríguez-Pombo, P., Olpin, S.E., Banka, S. (2019). Expanding the genetic and phenotypic spectrum of branched-chain amino acid transferase 2 deficiency. J Inherit Metab Dis 42, 809–817.

80. Korendovych, I.V. (2018). Rational and semirational protein design. In Methods in Molecular Biology. (Humana Press Inc), pp. 15–23.

81. Butler, C.F., Peet, C., Mason, A.E., Voice, M.W., Leys, D., Munro, A.W. (2013). Key mutations alter the cytochrome P450 BM3 conformational landscape and remove inherent substrate bias. J Biol Chem 288, 25387–25399.

82. Reetz, M.T., Carballeira, J.D., Vogel, A. (2006). Iterative saturation mutagenesis on the basis of B factors as a strategy for increasing protein thermostability. Angew Chemie 118, 7909–7915.

83. Holland, J.T., Harper, J.C., Dolan, P.L., Manginell, M.M., Arango, D.C., Rawlings, J.A., Apblett, C.A., Brozik, S.M. (2012). Rational Redesign of Glucose Oxidase for Improved Catalytic Function and Stability. PLoS One 7, e37924.

84. Shota, I., Tomonori, M., Hiroyuki, I., Jirasin, K., Yoichi, T., Akira, N., Xiao,Y., Romas, K., Hiroshi, T., Julia, P.M. (2022). High-Level Production of Lysine in the Yeast *Saccharomyces cerevisiae* by Rational Design of Homocitrate Synthase. Appl Environ Microbiol 87, e00600–21.

85. Brackenridge, D.A., McGuffin, L.J. (2021). Proteins and Their Interacting Partners: An

Introduction to Protein–Ligand Binding Site Prediction Methods with a Focus on FunFOLD3FunFOLD3 BT - Targeted Protein Degradation: Methods and Protocols. In Cacace, AM, Hickey, CM, Békés, M (eds.). (Springer US, New York), NY, pp. 43–58.

86. Schwede, T., Kopp, J., Guex, N., Peitsch, M.C. (2003). SWISS-MODEL: an automated protein homology-modeling server. Nucleic Acids Res 31, 3381–3385.

87. Laskowski, R.A., MacArthur, M.W., Moss, D.S., Thornton, J.M. (1993). {\it PROCHECK}: a program to check the stereochemical quality of protein structures. J Appl Crystallogr 26, 283–291.

88. Laskowski, R.A., Jabłońska, J., Pravda, L., Vařeková, R.S., Thornton, J.M. (2018). PDBsum: Structural summaries of PDB entries. Protein Sci 27, 129–134.

89. Xu, Y., Wang, S., Hu, Q., Gao, S., Ma, X., Zhang, W., Shen, Y., Chen, F., Lai, L., Pei, J. (2018). CavityPlus: a web server for protein cavity detection with pharmacophore modelling, allosteric site identification and covalent ligand binding ability prediction. Nucleic Acids Res 46, W374–W379.

90. Panjkovich, A., Daura, X. (2014). PARS: a web server for the prediction of Protein Allosteric and Regulatory Sites Bioinformatics 30, 1314–5.

91. Mistry, J., Bateman, A., Finn, R.D. (2007). Predicting active site residue annotations in the Pfam database. BMC Bioinformatics 8, 298.

92. Pettersen, E.F., Goddard, T.D., Huang, C.C., Couch, G.S., Greenblatt, D.M., Meng, E.C., Ferrin, T.E. (2004). UCSF Chimera--a visualization system for exploratory research and analysis. J Comput Chem 25, 1605–1612.

93. Frisch, M.J., Trucks, G.W., Schlegel, H.B., Scuseria, G.E., Robb, M.A., Cheeseman, J.R., Scalmani, G., Barone, V., Mennucci, B., Petersson, G.A. (2009). Gaussian 09; Gaussian, Inc., CT, Wallingford.

94. Becke, A.D. (1996). Density-functional thermochemistry. IV. A new dynamical correlation functional and implications for exact-exchange mixing. J Chem Phys 104, 1040–1046.

95. Lee, C., Yang, W., Parr, R.G. (1988). Development of the Colle-Salvetti correlation-energy formula into a functional of the electron density. Phys Rev B Condens Matter 37, 785–789.

96. Hehre, W.J., Ditchfield, R., Pople, J.A. (1972). Self—Consistent Molecular Orbital Methods. XII. Further Extensions of Gaussian—Type Basis Sets for Use in Molecular Orbital Studies of Organic Molecules. J Chem Phys 56, 2257.

97. Trott, O., Olson, A.J. (2010). AutoDock Vina: improving the speed and accuracy of docking with a new scoring function, efficient optimization, and multithreading. J

Comput Chem 31, 455–461.

98. Sanner, M.F. (1999). Python: A programming language for software integration and development. J Mol Graph Model 17, 57–61.

99. Laskowski, R.A., Swindells, M.B. (2011). LigPlot^{+}: multiple ligand-protein interaction diagrams for drug discovery. J Chem Inf Model 51, 2778–2786.

100. Ashkenazy, H., Erez, E., Martz, E., Pupko, T., Ben-Tal, N. (2010). ConSurf 2010: calculating evolutionary conservation in sequence and structure of proteins and nucleic acids. Nucleic Acids Res 38, W529–W533.

101. Sievers, F., Higgins, D.G. (2018). Clustal Omega for making accurate alignments of many protein sequences. Protein Sci 27, 135–145.

102. Shapovalov, M.V., Dunbrack, R.L. (2011). A Smoothed Backbone-Dependent Rotamer Library for Proteins Derived from Adaptive Kernel Density Estimates and Regressions. Structure 19, 844–858.

103. Wang, J., Wang, W., Kollman, P.A., Case, D.A. (2006). Automatic atom type and bond type perception in molecular mechanical calculations. J Mol Graph Model 25, 247–260.

104. Jubb, H.C., Higueruelo, A.P., Ochoa-Montaño, B., Pitt, W.R., Ascher, D.B., Blundell, T.L. (2017). Arpeggio: A Web Server for Calculating and Visualising Interatomic Interactions in Protein Structures. J Mol Biol 429, 365–371.

105. Parthiban, V., Gromiha, M.M., Schomburg, D. (2006). CUPSAT: prediction of protein stability upon point mutations. Nucleic Acids Res 34, W239–W242.

106. Pires, D.E.V., Blundell, T.L., Ascher, D.B. (2016). mCSM-lig: quantifying the effects of mutations on protein-small molecule affinity in genetic disease and emergence of drug resistance. Sci Rep 6, 1–8.

107. Inoue, H., Nojima, H., Okayama, H. (1990). High efficiency transformation of Escherichia coli with plasmids. Gene 96, 23–28.

108. Burke, D., Dawson, D., Stearns, T. (2000). Methods in Yeast Genetics: A Cold Spring Harbor Laboratory Course Manual (2000 Edition). (Cold Spring Harb Lab Press Sch), Plainview, NY.

109. St-Jacques AD, Eyahpaise M-ÈC, Chica RA. Computational Design of Multisubstrate Enzyme Specificity. Acs Catalysis 9, 5480-5485.

110. Kingsbury, J.M., Sen, N.D., Cardenas, M.E. (2015). Branched-Chain Aminotransferases Control TORC1 Signaling in *Saccharomyces cerevisiae*. PLoS Genet 11, e1005714–e1005714.

111. Yennawar, N., Dunbar, J., Conway, M., Hutson, S., Farber, G. (2001). The structure of

human mitochondrial branched-chain aminotransferase. Acta Crystallogr D Biol Crystallogr 57, 506–515.

112. Yennawar, N.H., Islam, M.M., Conway, M., Wallin, R., Hutson, S.M. (2006). Human mitochondrial branched chain aminotransferase isozyme: Structural role of the CXXC center in catalysis. J Biol Chem 281, 39660–39671.

113. Goto, M., Miyahara, I., Hayashi, H., Kagamiyama, H., Hirotsu, K. (2003). Crystal structures of branched-chain amino acid aminotransferase complexed with glutamate and glutarate: true reaction intermediate and double substrate recognition of the enzyme. Biochemistry 42, 3725–3733.

114. Taylor, R.T., Jenkins, W.T. (1966). Leucine Aminotransferase: II. PURIFICATION AND CHARACTERIZATION. J Biol Chem 241, 4396–4405.

115. Nakai, T., Nakagawa, N., Maoka, N., Masui, R., Kuramitsu, S., Kamiya, N. (2005). Structure of P-protein of the glycine cleavage system: implications for nonketotic hyperglycinemia. Embo j 24, 1523–1536.

116. Peter Guthrie, J. (1996). Short strong hydrogen bonds: can they explain enzymic catalysis? Chem Biol 3, 163–170.

117. Rosenberg, M.M., Redfield, A.G., Roberts, M.F., Hedstrom, L. (2016). Substrate and Cofactor Dynamics on Guanosine Monophosphate Reductase Probed by High Resolution Field Cycling 31P NMR Relaxometry. J Biol Chem 291, 22988–22998.

118. Rosenberg, M.M., Yao, T., Patton, G.C., Redfield, A.G., Roberts, M.F., Hedstrom, L. (2020). Enzyme–Substrate–Cofactor Dynamical Networks Revealed by High-Resolution Field Cycling Relaxometry. Biochemistry 59, 2359–2370.

119. Sperringer, J.E., Addington, A., Hutson, S.M. (2017). Branched-Chain Amino Acids and Brain Metabolism. Neurochem Res 42, 1697–1709.

120. Schoondermark-Stolk, S.A., Tabernero, M., Chapman, J., Ter Schure, E.G., Verrips, C.T., Verkleij, A.J., Boonstra, J. (2005). Bat2p is essential in *Saccharomyces cerevisiae* for fusel alcohol production on the non-fermentable carbon source ethanol. FEMS Yeast Res 5, 757–766.

121. Hu, L.Y., Boxer, P.A., Kesten, S.R., Lei, H.J., Wustrow, D.J., Moreland, D.W., Zhang, L., Ahn, K., Ryder, T.R., Liu, X., Rubin, J.R., Fahnoe, K., Carroll, R.T., Dutta, S., Fahnoe, D.C., Probert, A., Roof, R.L., Rafferty, M.F., Kostlan, C.R., Scholten, J.D., Hood, M., Ren, X.D., Schielke, G.P., Su, T.Z., Taylor, C.P., Mistry, A., McConnell, P., Hasemann, C., Ohren, J. (2006). The design and synthesis of human branched-chain amino acid aminotransferase inhibitors for treatment of neurodegenerative diseases. Bioorg Med Chem Lett 16, 2337–2340.

122. Kellis, M., Birren, B.W., Lander, E.S. (2004). Proof and evolutionary analysis of ancient genome duplication in the yeast *Saccharomyces cerevisiae*. Nature 428, 617–624.

123. Chandel, N.S. (2015). Evolution of mitochondria as signaling organelles. Cell Metab 22, 204–206.

124. Dawson, R.M.C., Elliott, D.C., Elliott, W.H., Jones, K.M. (2002). Data for biochemical research. (Vol. 3), Clarendon Press, London.

125. González, J., López, G., Argueta, S., Escalera-Fanjul, X., el Hafidi, M., Campero-Basaldua, C., Strauss, J., Riego-Ruiz, L., González, A. (2017). Diversification of Transcriptional Regulation Determines Subfunctionalization of Paralogous Branched Chain Aminotransferases in the Yeast *Saccharomyces cerevisiae*. Genetics 207, 975–991.

126. González-Ramos, D., van den Broek, M., van Maris, A.J.A., Pronk, J.T., Daran, J.M.G. (2013). Genome-scale analyses of butanol tolerance in *Saccharomyces cerevisiae* reveal an essential role of protein degradation. Biotechnol Biofuels 6, 1–18.

127. Taylor, E.J., Campbell, S.G., Griffiths, C.D., Reid, P.J., Slaven, J.W., Harrison, R.J., Sims, P.F.G., Pavitt, G.D., Delneri, D., Ashe, M.P. (2010). Fusel alcohols regulate translation initiation by inhibiting eIF2B to reduce ternary complex in a mechanism that may involve altering the integrity and dynamics of the eIF2B body. Mol Biol Cell 21, 2202–2216.

128. Marques, S.M., Bednar, D., Damborsky, J. (2019). Computational Study of Protein-Ligand Unbinding for Enzyme Engineering. Front Chem 6, 650.

129. Agarwal, P.K. (2005). Role of protein dynamics in reaction rate enhancement by enzymes. J Am Chem Soc 127, 15248–15256.

130. Agarwal, P.K. (2006). Enzymes: An integrated view of structure, dynamics and function. Microb Cell Fact 5, 1–12.

131. Eisenmesser, E.Z., Bosco, D.A., Akke, M., Kern, D. (2002). Enzyme dynamics during catalysis. Science 295, 1520–1523.

132. Fernandes, H.S., Ramos, M.J., Cerqueira, N.M.F.S.A. (2017). The Catalytic Mechanism of the Pyridoxal-5′-phosphate-Dependent Enzyme, Histidine Decarboxylase: A Computational Study. Chem – A Eur J 23, 9162–9173.

133. Shlomi, R., Michael, U., Joseph, K. (2014). Role of substrate unbinding in Michaelis–Menten enzymatic reactions. Proc Natl Acad Sci 111, 4391–4396.